Title
Cryo-electron microscopy studies of microtubules and microtubule associated proteins: tubulin acetylation, engineered kinesins, yeast microtubules, and PRC1

Author
Howes, Stuart Craig

Publication Date
2015

Peer reviewed|Thesis/dissertation

Cryo-electron microscopy studies of microtubules and microtubule associated proteins: tubulin acetylation, engineered kinesins, yeast microtubules, and PRC1

By

Stuart Craig Howes

A dissertation submitted in partial satisfaction of the

requirements for the degree of

Doctor of Philosophy

in

Biophysics

in the

Graduate Division

of the

University of California, Berkeley

Committee in charge:
Professor Eva Nogales, Chair
Professor David Drubin
Professor Rebecca Heald
Professor Ahmet Yildiz

Fall 2015

Abstract

Cryo-electron microscopy studies of microtubules and microtubule associated proteins: tubulin acetylation, engineered kinesins, yeast microtubules, and PRC1

By

Stuart Craig Howes

Doctor of Philosophy in Biophysics

Professor Eva Nogales, Chair

Microtubules (MTs) are an essential component of the eukaryotic cytoskeleton formed by the polymerization of tubulin into hollow, cylindrical polymers and are involved in a diverse array of cellular functions. The diversity of MT functionality is achieved in part by the specialization of MTs for certain activities through the accumulation of post-translational modifications (PTMs), and the binding of MT associated proteins (MAPs) that help organize and regulate the MT network. I used cryo-electron microscopy (cryo-EM) to directly visualize these important biological assemblies in their native states. The first part of my work was to determine a role for the acetylation of tubulin. This PTM is unique in that it is located on the luminal surface of the MT, away from the exterior of the MT where MAPs bind. I sought to gain insight into the function of acetylation by looking for structural changes in MTs that occur upon acetylation. No significant changes were observed in protofilament distributions or MT helical lattice parameters. Furthermore, no clear differences in tubulin structure were detected when comparing subnanometer reconstructions of deacetylated or acetylated MTs. Our results indicate that the effect of acetylation must be highly localized and directly affect interactions with proteins that bind to the luminal surface. I also wanted to understand how the enzyme that carries out this modification, αTAT1, gains access to the lumen of the MT. I found that αTAT1 interacts with the outside of the MT, possibly serving as a funneling mechanism to deliver the enzyme to the lumen through lattice defects or transient openings in the MT wall. My data show that αTAT1 does not rely on open ends of MTs to access the lumen.

I also visualized the structures of engineered kinesins on MTs. The motors had been modified to directly test design principles of biological motors as well as respond to external light stimulation. By changing the length of the lever arm it was possible to alter the velocity of these motors. The cryo-EM reconstructions confirmed the geometry of the engineered lever arms. Incorporation of a light sensitive (LOV) domain into the lever arm made the motor photoactivatable. However, the LOV domain introduced greater flexibility into the engineered domain, preventing us from visualizing the full lever arm.

Yeast tubulin mutants offer the possibility to directly test molecular mechanisms of dynamic instability. I performed near atomic resolution reconstructions of WT and mutant yeast microtubules to understand the structural basis for the mutant phenotypes. I found that, unlike in mammalian MTs, the tubulin dimer size in WT yeast MTs is the same for dynamic lattice and those stabilized with drugs or GMPCPP. These yeast lattices are all expanded. However, the lattice compacts with the addition of the plus-end tracking protein, Bim1, or when it is assembled with GTPγS. The greatest differences for the mutant tubulin were seen outside of the microtubule lattice

where the length and curvature of tubulin oligomers in solution were greater. All yeast oligomers were longer and straighter than those formed by mammalian tubulin.

Finally, the atomic level details about the interaction between PRC1, a MT crosslinker that stabilizes antiparallel MT arrays, and MTs was determined. The reconstruction shows that the spectrin domain of PRC1 binds using a loop that remained disordered in previous crystal structures. The binding site of PRC1 on MTs overlaps with that used by motor proteins at the intra-dimer interface. Using cryo-EM to examine MTs in their natural state at near atomic resolution has provided important information about their function and how they interact with MAPs.

Table of Contents

Acknowledgements

Many people have helped me during the course of my doctoral work, and I am extremely grateful to all of them. None have helped quite as much as my advisor Eva Nogales. Her mentorship and advising have been instrumental in my PhD training. She always found something constructive to say and do, even in the most challenging situations, and for that I cannot express my gratitude strongly enough. Her seemingly limitless energy and enthusiasm for doing great science are remarkable. Eva also created a wonderful laboratory environment that I was privileged to join.

The people of the Nogales lab, both past and present, have all in some way helped me. In particular, I would like to thank Gregory Alushin for teaching the basics of microtubules and electron microscopy. I could not have asked for a teacher with a greater depth of understanding and his exacting direction served me well from the very beginning and long after he left. Gabriel Lander and Rui Zhang both helped me solve computational issues and taught me many things that made my data processing more efficient. Tom Houweling provided endless entertainment and superb computer support, often far beyond our needs. Patricia Grob, as well as Gigi Kemalyan and Steve Hill, maintained the electron microscopes and made sure all the associated equipment was available and working. Much less data would have been collected without them. Patricia also provided many hours of microscope hardware explanation and troubleshooting advice. Her years of experience made my research much easier without having to go through the same learning curve. My biochemistry education was significantly enriched by help and guidance from Jie Fang who helped me purify my proteins and optimize protocols for better experiments. My error bars would have been a lot bigger without her. And finally Teresa Tucker who was always there to put bad days in perspective while making sure administrative tasks were simply always done. The permanent staff all made working in the lab much easier and allowed me to focus on the research.

I also owe a huge debt of gratitude to my co-authors and collaborators. Firstly, the Drubin-Barnes laboratory here at UC Berkeley, in particular Georjana Barnes, Nathaniel Krefman and Itziar Ibarlucea for help purifying yeast tubulin. This was a huge task that I did not have the biochemical knowledge to undertake successfully myself. Splitting the labor with them was a great pleasure, and our long back-to-back days of purification will always be remembered fondly. Zev Bryant, Muneaki Nakamura and Lu Chen from Stanford University were great collaborators that opened my mind to forward-engineering proteins, rather than the reverse engineering that is typical of structural biologists. They are amazing scientist and the interactions with them will always be treasured. Luke Rice and Elizabeth Geyer at UT Southwestern provided a steady supply of precious yeast tubulin, saving me weeks of purifications. Their willingness to answer questions and provide suggestions when experiments were not working helped tremendously and will always be remembered. Tarun Kapoor and Shih-Chieh Ti (Jeff) at Rockefeller University also provided valuable insights during our time working together. I am also grateful to Erik Jonsson and Ronald Vale of UC San Francisco for the monomeric kinesin protein and expression plasmid. A simple thing, but that kinesin has become an integral part of our microtubule studies. I wonder sometimes how we ever did without it.

I would also like to thank the members of my thesis committee, David Drubin, Rebecca Heald, and Ahmet Yildiz for their excellent feedback and advice.

Last but certainly not least, I would like to thank my family for their unwavering support.

List of Abbreviations

2D	Two dimensional
3D	Three dimensional
AMPPNP	Adenosine 5′-(β,γ-imido)triphosphate
CH	Calponin homology
EB	End binding
EM	Electron microscopy
FMN	Flavin mononucleotide
FSC	Fourier shell correlation
GDP	Guanosine diphosphate
GMPCPP	Guanylyl-(α, β)-methylene-diphosphonate
GTP	Guanosine triphosphate
GTPγS	Guanosine 5'-O-[γ-thio]triphosphate
HDAC6	Histone deacetylase 6
IHRSR	Iterative helical real space reconstruction
IPTG	Isopropyl β-D-1-thiogalactopyranoside
MAP	Microtubule associated protein
MT	Microtubule
NCD	Non-claret disjunctional, a kinesin
PTM	Post-translational modification
SIRT2	Sirtuin 2
SNR	Signal-to-noise ratio
TB	Terrific broth
YT	Yeast extract and Tryptone

List of Figures

List of Tables

1 Chapter 1: Introduction

1.1 Microtubule assembly and dynamic instability

Microtubules are an essential component of the eukaryotic cytoskeleton formed by the polymerization of tubulin into hollow, cylindrical polymers. They play a pivotal role in organizing the cellular contents (de Forges, Bouissou, & Perez, 2012; Desai & Mitchison, 1997; Mitchison & Kirschner, 1984; Nédélec, Surrey, & Karsenti, 2003) and forming the mitotic spindle, a microtubule based structure crucial to cell division (Walczak & Heald, 2008; Ward, Roque, Antony, & Nédélec, 2014). They also provide mechanical stability to cells (Brangwynne et al., 2006). Central to microtubule functionality is the ability to reorganize the microtubule network during the cell cycle and in response to environmental cues.

The microtubule network contributes to the ease of reorganization by having an inherent instability built into the polymer. In the absence of any external factors, there is a constant flux of tubulin between the polymerized microtubule and soluble form as microtubules stochastically switch between polymerizing and depolymerizing states. This behavior is termed dynamic instability. Tubulin at sufficiently high concentration (i.e. above the critical concentration) and with a supply of GTP will spontaneously nucleate to form microtubules. These microtubules will

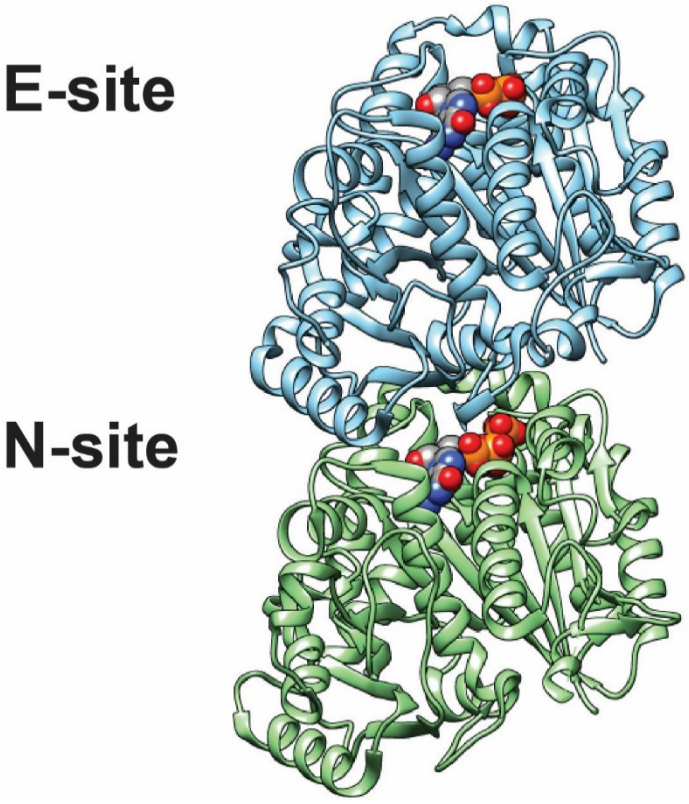

Figure 1-1 Nucleotide binding sites of the tubulin heterodimer
Tubulin binds a GTP molecule at the N-site (nonexchangeable) that plays a structural role. The E-site (exchangeable) is occupied by GTP when the heterodimer is in solution. The GTP at the E-site undergoes hydrolysis within the MT lattice. Structure of GDP-bound tubulin, PDB ID: 3JAS from Zhang et al., 2015.

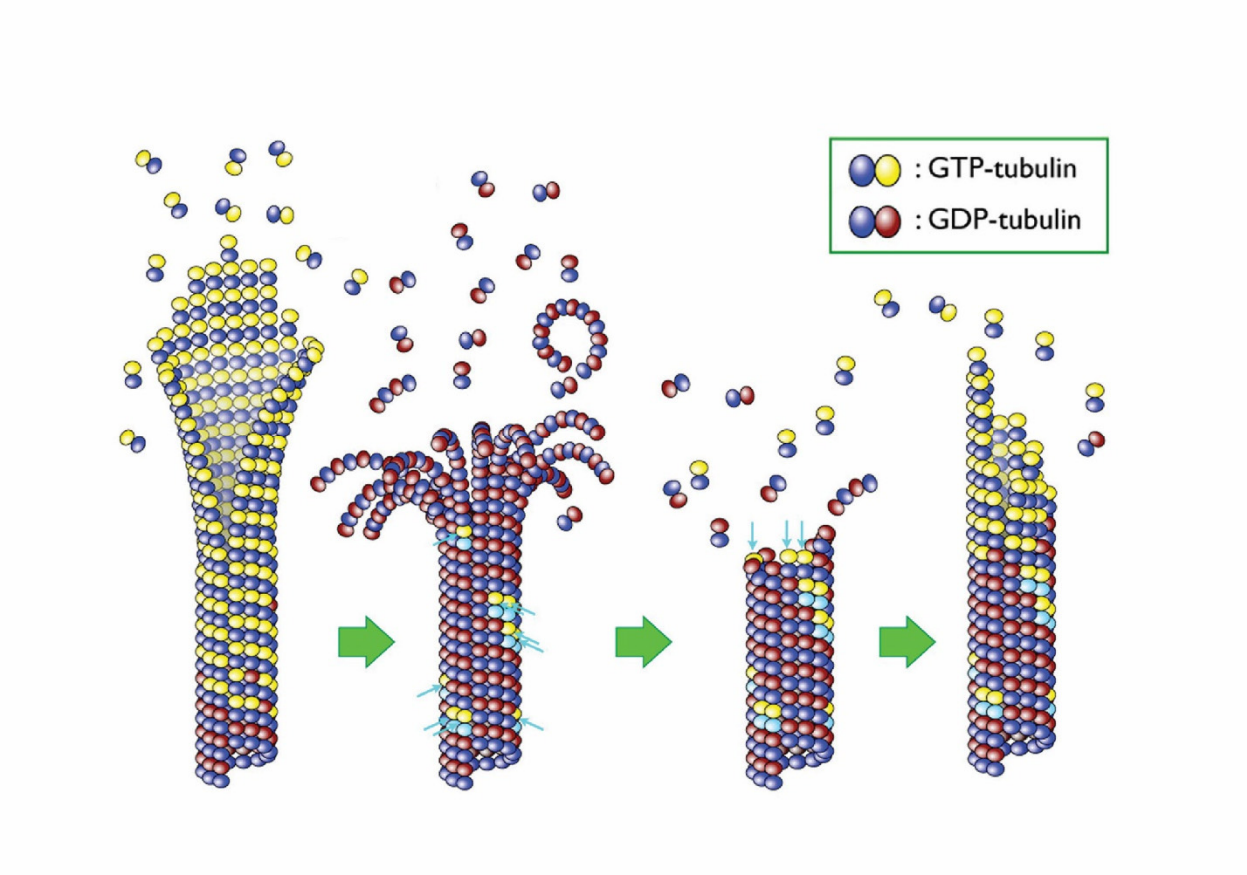

Figure 1-2 Microtubule dynamic instability
Microtubules cycle between growing and shrinking phases. Adapted from Horio & Murata, 2014.

then continue to grow until the soluble tubulin concentration approaches the critical concentration. Once the soluble tubulin concentration is near the critical concentration, the total mass of polymerized tubulin will remain constant. However, individual microtubules will continue to grow and shrink, switching between the two states. This constant flux of tubulin between the polymer and the solution will continue as long as there is available GTP (Desai & Mitchison, 1997; Mitchison & Kirschner, 1984). The growth phase can even persist for some microtubules for a short while after the soluble pool of tubulin has been diluted below the critical concentration.

Tubulin is a heterodimer of α- and β-tubulin whose structure was first solved using 2D electron crystallography (Löwe, Li, Downing, & Nogales, 2001; Nogales, Wolf, & Downing, 1998). Each tubulin monomer binds one GTP molecule (see Figure 1-1). The GTP bound to α-tubulin, at the nonexchangeable site (N-site), plays a structural role and is never hydrolyzed (Geahlen & Haley, 1979; Löwe et al., 2001). This GTP binds during the biogenesis of tubulin and remains there for the life of the tubulin heterodimer. The GTP bound to β-tubulin, at the exchangeable site (E-site) makes the heterodimer competent for polymerization. Once within the lattice, the β-tubulin GTP is hydrolyzed, resulting in a compaction of the lattice (Alushin et al., 2014; Zhang, Alushin, Brown, & Nogales, 2015). When the microtubule switches from a growing to shrinking phase, the stress within the lattice caused by this compaction is released, resulting in fast depolymerization.

During polymerization, tubulin molecules pack into a regular arrangement. Longitudinal association of tubulin molecules, in a head-to-tail manner, forms polar protofilaments that then bind together laterally to form a left-handed helical polymer. When these protofilaments associate there is a slight offset with respect to each other along the axis of the microtubule. Microtubules form with a varying number of protofilaments, generally ranging from 11 to 15, though 13 is typical. The size of the offset depends on how many protofilaments are in the microtubule. The closure of protofilaments into a cylinder usually results in a discontinuity of the helical packing, termed the seam. This makes the microtubule a pseudo-helical polymer.

The molecular mechanisms that underlie the switch from a growth phase to a shrinking phase, or the reverse, are not fully understood (Bowne-Anderson, Zanic, Kauer, & Howard, 2013; Howard & Hyman, 2003), but the GTP-cap model is generally used to explain microtubule behavior. Tubulin is added at the growing microtubule end in the GTP-bound state. Once inside the lattice hydrolysis occurs, but at a rate slower than the addition of new tubulin. Through decreasing soluble tubulin concentration and molecular fluctuations, the hydrolysis within the lattice will at some point catch up to the tip of the microtubule, where the structural changes caused by hydrolysis will trigger the switch from a polymerization state to depolymerization (see Figure 1-2). The strain resulting from the hydrolysis of GTP is stored in the lattice until the microtubule depolymerizes, making depolymerization a much more rapid event, and is often termed catastrophe. It is thought that residual GTP within the lattice (marked by blue arrows in Figure 1-2) are necessary for the rescue event, where microtubules switch from depolymerizing to polymerizing states.

The dynamic instability of microtubules make them well suited to performing various functions within the cell. The cell can easily harness this behavior and direct it towards productive activities that coordinate with the rest of the cellular functions. Much of our understanding of the workings of tubulin has come from extensive *in vitro* experiments. Production of recombinant tubulin in heterologous expression systems has been impossible until very recently (Minoura et al., 2013). This has limited the options available for obtaining the necessary tubulin. The sources of tubulin employed are discussed next.

1.2 Tubulin sources and purification

The central importance of microtubules has led to extensive research to understand the molecular origins of dynamic instability in numerous *in vitro* studies. For the overwhelming majority of these experiments, the tubulin was sourced from brain tissue. Brain tubulin is heterogeneous in terms of protein isoforms and post-translational modifications, however tubulin is near 25% of the total protein content (Hiller & Weber, 1978). This makes purification relatively straightforward using cycles of polymerization, pelleting, washing, and depolymerization to isolate the tubulin. The convenience of this source and its high yields have made it the obvious choice for most studies.

However, reliance on brain tubulin has precluded the study of highly disruptive mutants by site-directed mutagenesis, as any lethal mutation would make the organism inviable. Instead milder phenotypes from temperature and drug sensitive mutants, as well as sex specific mutations have been used to probe different parts of the protein (Fackenthal, Hutchens, Turner, & Raff, 1995; Machin, Lee, & Barnes, 1995; Schatz, Solomon, & Botstein, 1988; Thomas, Neff, & Botstein, 1985). Efforts to produce recombinant tubulin (Minoura et al., 2013) and purify tubulin from different sources (Davis, Sage, Wilson, & Farrell, 1993; Drummond et al., 2011; Sackett, Werbovetz, & Morrissette, 2010; Widlund et al., 2012), while successful, have not provided the

yields necessary for widespread adoption. The genetic tractability of yeast has resulted in a large body of knowledge about yeast tubulin mutants and has provided important insights into microtubule functionality and dynamic instability. Previous researchers have used the limited quantities of yeast tubulin to perform important characterizations of yeast tubulin (Davis et al., 1993). The critical concentration at which soluble tubulin will spontaneously nucleate and form microtubules is roughly 1 μM for yeast tubulin compared to approximately 5 μM for mammalian tubulin. Furthermore, microtubules polymerized from yeast tubulin were generally less dynamic than mammalian microtubules and had lower GTPase activities (Davis et al., 1993). Obtaining tubulin from fungal sources using carefully designed overexpression systems have made purification from *Saccharomyces cerevisiae* (hereafter referred to as yeast) possible, even for tubulin that is lethal under normal circumstances (Ayaz, Ye, Huddleston, Brautigam, & Rice, 2012; Geyer et al., 2015; Johnson, Ayaz, Huddleston, & Rice, 2011). This removes the isoform variation normally found in brain tubulin and allows for the production of mutant tubulin. This method now yields sufficient quantities of yeast wild type and mutant tubulin for structural studies by x-ray crystallography and electron microscopy. The results of our investigations into the structural differences between yeast and mammalian microtubules are reported in Chapter 4. The tubulin from yeast also has the advantage of being less heterogeneous in terms of post-translational modifications. The roles of these modifications are discussed next.

1.3 Post-translational modifications of tubulin

The diverse functions of microtubules often requires specialization, which arises, in part, from the accumulation of post-translational modifications (PTMs) on the tubulin subunits, both in the soluble form and within the microtubule lattice. The modifications in turn influence the binding of MAPs (see section 1.4) and/or the dynamic instability parameters of the microtubules. Tubulin is known to undergo several types of PTMs, including detyrosination (removal of the C-terminal tyrosine), Δ2-tubulin generation (a non-reversible modification that results from the removal of the terminal tyrosine and glutamate residues), polyglutamylation, polyglycylation and acetylation (Janke & Bulinski, 2011). Most of the tubulin PTMs occur within its unstructured C-terminal tails (or E-hooks) that extend outwards on the surface of microtubules (see Figure 1-3). The C-terminal tails of tubulin are involved in interaction with most MAPs, either by themselves or in addition to the globular domain of tubulin, and specific PTMs have been shown to influence tubulin-MAP interactions.

Reversible acetylation of α-tubulin at lysine-40 (αK40) is unique in that it occurs on the luminal surface of the microtubule (Nogales, Whittaker, Milligan, & Downing, 1999). Acetylation of α-tubulin was first reported by L'Hernault and Rosenbaum (L'Hernault & Rosenbaum, 1983, 1985) when they observed that the α-tubulin in flagella was post-translationally modified, and mapped it to the ε-amino group of a single lysine residue (see Figure 1-4). A monoclonal antibody that recognizes acetylation of α-tubulin was initially generated by Piperno and colleagues (Piperno & Fuller, 1985) and later mapped to αK40 (LeDizet & Piperno, 1987; Piperno, LeDizet, & Chang, 1987). This reagent remains the only specific antibody that binds to acetylated tubulin. Other acetylation sites have been identified by enriching cell isolates using pan anti-acetylated lysine antibodies and mass spectrometry (Choudhary et al., 2009). However, acetylation of those sites is unlikely to be conserved (Akella et al., 2010; L'Hernault & Rosenbaum, 1985); many of these acetylation sites have not been confirmed *in vivo,* and their physiological relevance remains in question. An acetylation site on β-tubulin, which occurs at the tubulin dimer interface, has also been identified and shown to impact the polymerization kinetics of tubulin (Chu et al., 2011).

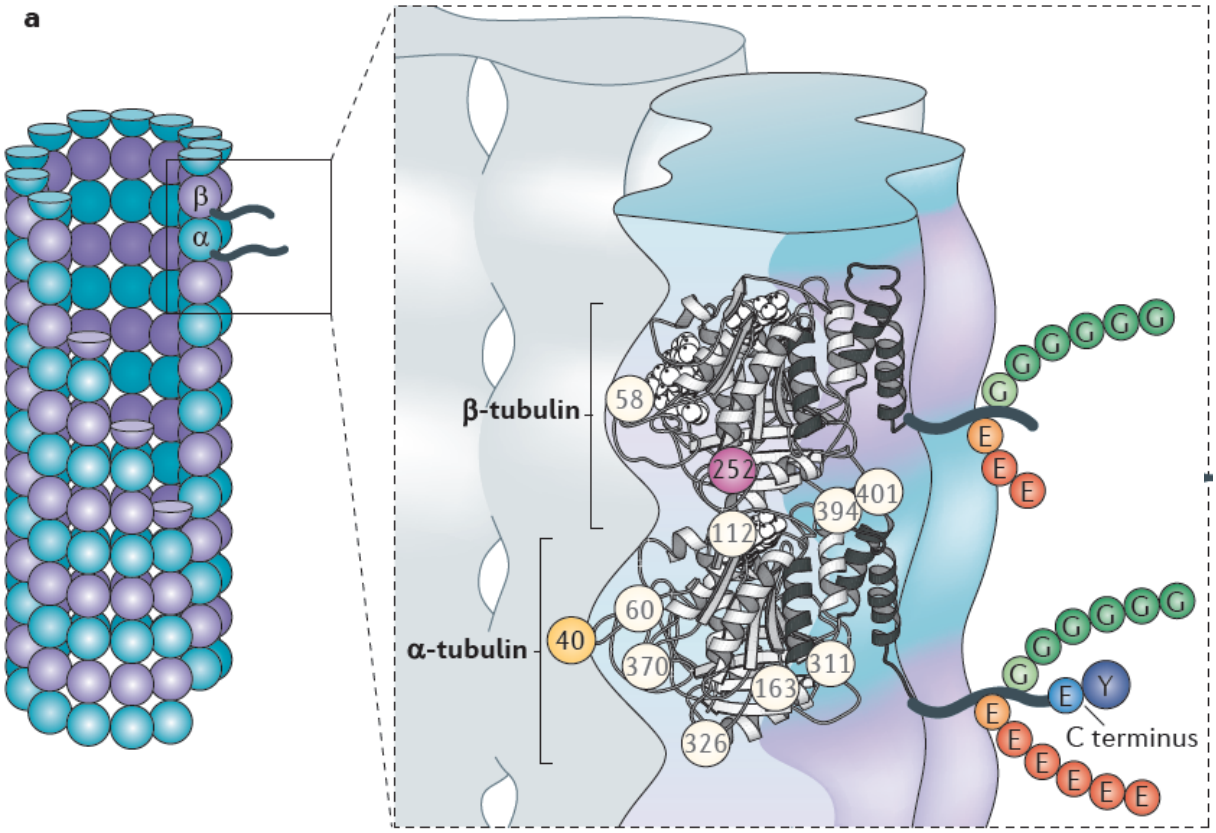

Figure 1-3 Post-translational modifications of tubulin
Tubulin is subjected to many modifications that occur primarily on the C-terminal tails. Acetylation occurs on the luminal surface of the microtubule where its role remains unclear. Adapted from Janke & Bulinski, 2011.

Determining the roles of the different tubulin post-translational modifications *in vivo* has been challenging due to the fact that PTMs rarely occur in isolation and the level of each modification is separately regulated by the cell (Quinones, Danowski, Devaraj, Singh, & Ligon, 2011). In fact, no clear role for αK40 acetylation has emerged despite the long time elapsed since its initial discovery. Acetylated microtubules in the cytoplasm are generally more stable than unmodified microtubules, in that they can withstand mild treatment with microtubule depolymerizing drugs such as nocodazole (De Brabander, Van de Veire, Aerts, Borgers, & Janssen, 1976) or colchicine (LeDizet & Piperno, 1986; Piperno et al., 1987). However, it has been shown that this modification does not directly influence tubulin polymerization or depolymerization kinetics *in vitro* (Maruta, Greer, & Rosenbaum, 1986).

Studies that have tracked the appearance of acetylated microtubules after release from nocodazole in interphase cells (Bulinski, Richards, & Piperno, 1988), showed that acetylation was restored before detyrosination, another major PTM that regulates interaction of microtubules with motors (Dunn et al., 2008; Y. Konishi & Setou, 2009; Peris et al., 2009) and plus-end binding proteins (Kumar & Wittmann, 2012; Mimori-Kiyosue, Shiina, & Tsukita, 2000; Perez, Diamantopoulos, Stalder, & Kreis, 1999). This result was confirmed for microtubules that specifically associate with the Golgi complex (Thyberg & Moskalewski, 1993). In the recovery of cilia of sea urchins after hypertonic salt treatment, microtubules were highly acetylated, both

within the axoneme and in the matrix/membrane associated tubulin fraction, before they reached mature levels of detyrosination (Stephens, 1992). However, acetylation is a late stage event in myogenesis (Fulvio, Azakir, Therrien, & Sinnreich, 2011). These studies suggest that acetylation is adapted to specific processes and that cells carefully control the acetylation levels depending on the microtubule structures being built. No direct link between αK40 acetylation and the binding of other proteins that are also predominantly located in stable, highly acetylated microtubule structures, such as cilia and axons, has been identified. Acetylated microtubules have also been

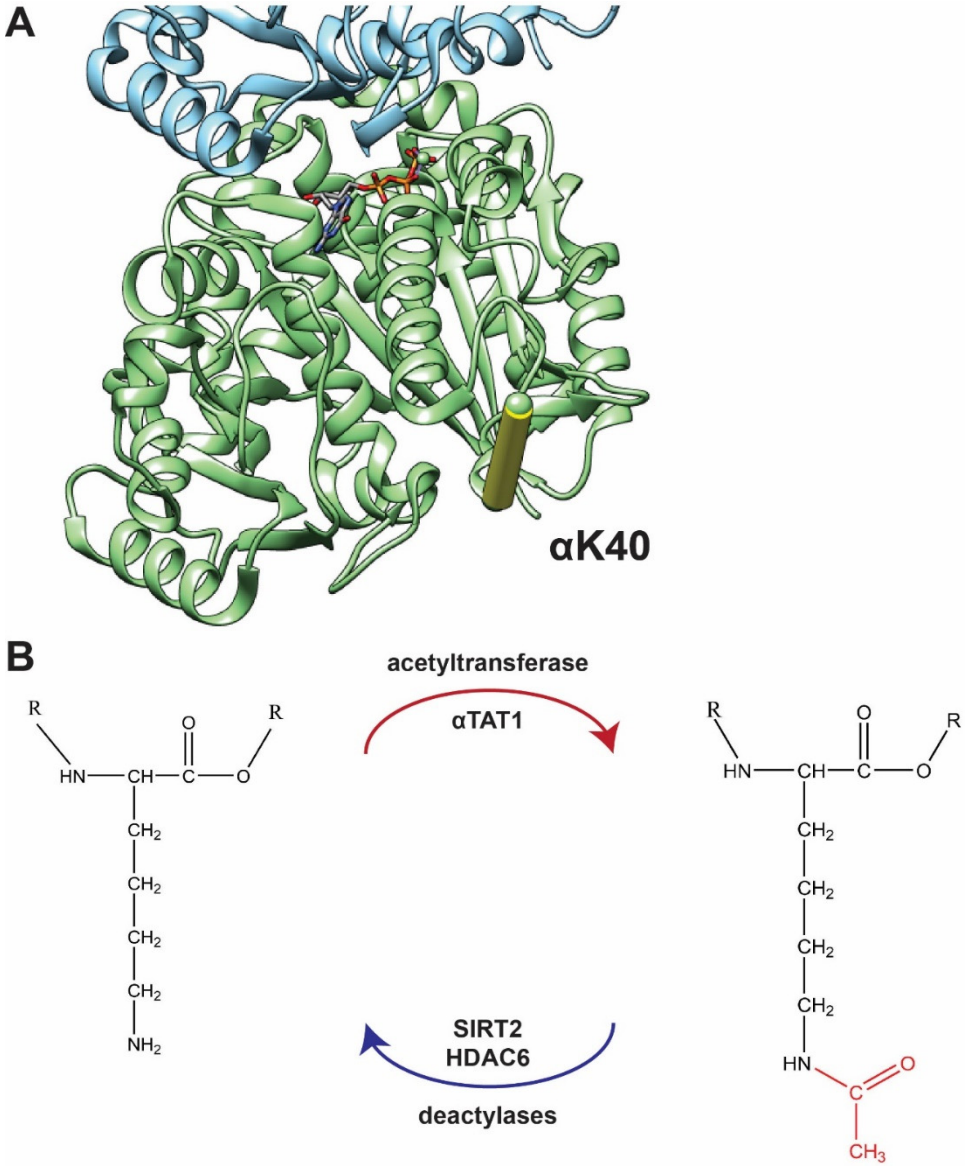

Figure 1-4 Acetylation of α-tubulin
A) View of α-tubulin from the lumen of the microtubule. The lysine modified by αTAT1 is on a flexible loop that is not resolved in crystal structures of tubulin, shown as yellow rod. **B**) Modification of the lysine residue by the addition of an acetyl-group to the ε-amino group.

identified in less stable structures, such as the microtubule network that assembles at the cleavage furrow to deposit new membrane during cytokinesis (Danilchik, Funk, Brown, & Larkin, 1998). Many other examples of diverse processes that correlate with acetylated microtubules are reported in the literature (Cai, McEwen, Martens, Meyhofer, & Verhey, 2009; Creppe et al., 2009; Friedman, Webster, Mastronarde, Verhey, & Voeltz, 2010; Reed et al., 2006; Serrador et al., 2004; Sudo & Baas, 2010), but the direct role of this tubulin modification remains unclear.

The enzymes responsible for the removal of the acetyl group from αK40 were identified first and were found to be homologues of histone deacetylases. Histone deacetylase 6 (HDAC6) and sirtuin 2 (SIRT2) both have deacetylase activity for αK40 (Hubbert et al., 2002; North, Marshall, Borra, Denu, & Verdin, 2003), and localize to the cytoplasm rather than the nucleus where histone deacetylases are generally restricted. Both proteins deacetylate multiple substrates and operate on the free tubulin heterodimer. Soon before the start of my graduate work, it was found that acetylation of αK40 is performed by αTAT1 (Akella et al., 2010; Shida, Cueva, Xu, Goodman, & Nachury, 2010), which also shows homology to histone acetyltransferases (Friedmann, Aguilar, Fan, Nachury, & Marmorstein, 2012; Kormendi, Szyk, Piszczek, & Roll-Mecak, 2012; Taschner, Vetter, & Lorentzen, 2012). Sequence alignments show that αTAT1 is related to the GCN5 superfamily of acetyltransferases (Taschner et al., 2012). However, it has a unique elements not found in other GCN5 acetyltransferases (Friedmann et al., 2012; Kormendi et al., 2012; Taschner et al., 2012) and a unique active site, as attempts to crystallize it with substrate (a peptide from α-tubulin containing K40) were unsuccessful, unlike histone acetyltransferases that could be crystallized with the substrate. The structure was finally solved with a synthetic peptide-acetyl-

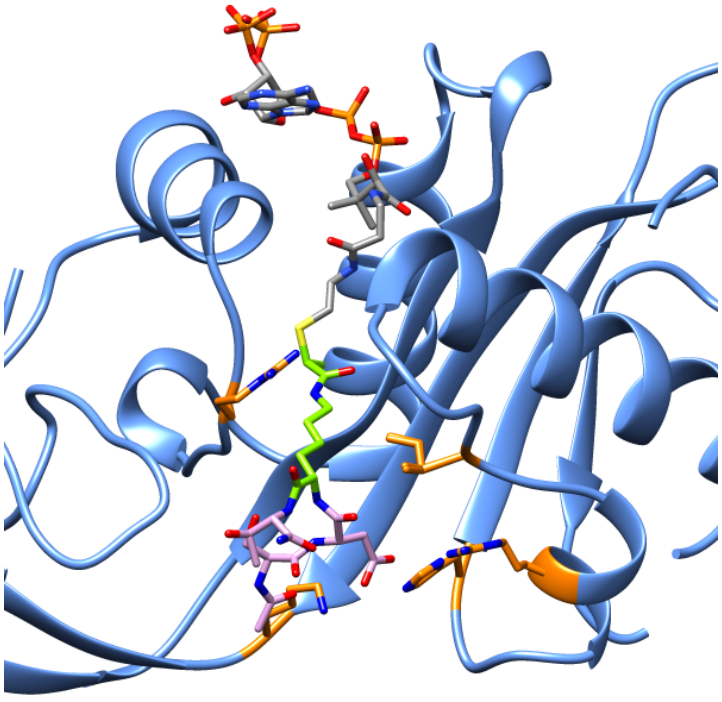

Figure 1-5 Structure and active site of αTAT1
αTAT1 shown in blue and residues important for acetylation activity shown in orange, peptide-CoA bisubstrate colored grey (CoA) and pink (peptide). Modified lysine shown in green. Residues important for tubulin binding shown in orange. Adapted from Taschner 2012 and Szyk, 2014.

CoA bisubstrate analog (Szyk et al., 2014) showing the interaction between the enzyme and this stretch of amino acids. The active site is shown in Figure 1-5 with the peptide modeled in pink. Mutational analyses have identified residues that are important for substrate binding (Taschner et al., 2012) and these are shown in orange.

Despite the lack of a clear role for acetylated microtubules, αTAT1 is well conserved across many phyla and correlates perfectly with the presence of cilia, hinting at an essential role in this structure (Shida et al., 2010). A notable exception to this conservation, is fungi. Tubulin from these organisms do not have a lysine residue near K40, and searches of their genome do not reveal obvious homologs to αTAT1. Depletion of αTAT1 was shown to impair primary cilium assembly and reduce touch response in *C. elegans* (Shida et al., 2010). Consistent with these results, in *Danio rerio*, reduced touch response was also reported in knockdown animals along with abnormal development (Akella et al., 2010). Changes in protofilament number of microtubules has also been reported as a result of αTAT1 knockout (Cueva, Hsin, Huang, & Goodman, 2012; Topalidou et al., 2012).

1.4 Microtubule associated proteins organize the cytoskeleton and cellular contents

Microtubule associated proteins regulate the microtubule network to stabilize or destabilize individual microtubules as necessary and to optimize their spatial arrangement. The diverse functions of microtubules are made possible through two major classes of proteins that bind the microtubule network, non-motor MAPs (or traditional MAPs) and motor proteins. Traditional MAPs bind along the length of microtubules and generally increase their stability (Bonnet et al., 2001) while other proteins, such as katanin will severe and destabilize microtubules (Díaz-Valencia et al., 2011). This allows the cell to reorganize the cytoskeleton as the cell progresses through the cell cycle, during migration or in response to external stimuli (Nakano et al., 2010). Microtubules are estimated to bind approximately 400 different proteins, emphasizing their importance to normal cell functionality (Chuong et al., 2004; Sakamoto et al., 2008).

Microtubule motors (i.e. kinesin and dynein) perform critical force generation and transport functions in eukaryotic cells (Vale, 2003). Through the hydrolysis of ATP they actively transport cargoes within cells. Kinesin motors are generally involved in moving cargo to the plus-end of microtubules (Lakämper & Meyhöfer, 2006), while dynein moves towards the minus end. The microtubule network is typically arranged such that the minus-end is near the cell nucleus and the plus-end is near the periphery of the cell. In neurons where the cell may have a very long axon, intracellular transport is critical and must cover impressively large distances. This has made it a useful model system for better understanding motor based transport, as any perturbation results in an readily measurable phenotype and have been useful for identifying and understanding defects in motor based transport (Levy et al., 2006).

Kinesins are a large class of motors that have been classified based on phylogenetic analysis (Hirokawa, Noda, Tanaka, & Niwa, 2009). Kinesin-14 motors, such as Non-claret disjunctional (Ncd), are minus-end directed motors and help to organize the mitotic spindle by sliding anti-parallel microtubule arrays (Fink et al., 2009). They are also involved in nuclear congression (Scheffler, Minnes, Fraisier, Paoletti, & Tran, 2015). Interestingly, they have been shown to lock parallel microtubules in place and contribute to the increased stability of these parts of the mitotic spindle (Fink et al., 2009). Ncd is thought to use a swinging lever arm mechanism that alters the geometry of the connection with the nucleotide binding domain to achieve motion in the opposite direction to other kinesins (Endres, Yoshioka, Milligan, & Vale, 2006; Wendt et al., 2002; Yun et al., 2003).

Non-motor MAPs complement the activity of motor proteins and tightly regulate the microtubule network. Some of these proteins act by binding directly to microtubule ends, either to the highly dynamic plus-end, like the conserved end binding (EB) proteins (Akhmanova & Steinmetz, 2010; Blake-Hodek, Cassimeris, & Huffaker, 2010), or to the minus-end (Goodwin & Vale, 2010; K. Jiang et al., 2014). These proteins then recruit other complexes to the end of the microtubule depending on the task required of that microtubule. Other microtubule regulators, such as MAP1 and MAP2/Tau, bind along the length of the microtubule lattice, thereby stabilizing it and helping to build parallel arrays, most notably in axons (Dehmelt & Halpain, 2005; Halpain & Dehmelt, 2006). Members of the MAP65 family, which includes human the protein regulating cytokinesis-1 (PRC1) and budding yeast Ase1, form antiparallel microtubule arrays in the region where microtubules from opposite spindle poles overlap, termed the spindle midzone, which also determines the location of cytokinesis (Fourniol et al., 2014; Kosetsu, de Keijzer, Janson, & Goshima, 2013; K.-Y. Lee, Esmaeili, Zealley, & Mishima, 2015; Portran et al., 2013; Stoppin-Mellet, Fache, Portran, Martiel, & Vantard, 2013; Subramanian et al., 2010). In addition to selectively binding and stabilizing antiparallel microtubules, PRC1 recruits other spindle organizing factors and is therefore an essential component of the mitotic spindle (Bieling, Telley, & Surrey, 2010; Subramanian et al., 2010). The binding of PRC1 to microtubules is the subject of Chapter 5.

1.5 Rationale and Goals

The diversity of microtubules and the proteins that they bind is reflected in the many projects I have worked on during my doctoral work. The identification of the tubulin acetyltransferase at the beginning of my graduate career provided the impetus for my first project. It was possible for the first time to prepare tubulin that was acetylated or deacetylated, rather than the mixture that is purified from brain. We reasoned that given most MAPs bind the outside of the microtubule, the modification on the luminal surface of the microtubule must somehow be propagated to the surface where they are recognized by MAPs. Another possibility, is that proteins specifically recognize the modification on the inside of the microtubule. We also reasoned that by using tubulin that was fully acetylated or deacetylated we might identify proteins the specifically respond to this modification and thereby learn about the role of acetylation, unfortunately this was not successful. Another aspect of this work was the question of how αTAT1 gained access to the lumen of the microtubule. The enzymatic preference that αTAT1 displays for microtubules over soluble tubulin heterodimers, and the fact that acetylation of free tubulin heterodimers has not been reported *in vivo*, suggest that it has a mechanism to gain access to the lumen of the microtubule. The results of this work are reported in Chapter 2.

At the conclusion of this project, I began work on yeast kinetochore proteins. I started to optimize constructs of yeast Ndc80 that might be used to visualize the interaction between Ndc80 and Dam1 on microtubules. My Ndc80 constructs did not decorate microtubules well, leading me to become involved in other projects. This included the structural characterization of engineered kinesin motors produced by the Bryant laboratory at Stanford University, described in Chapter 3. We were interested in directly testing the proposed mechanisms of biological motors by porting structural elements to different types of motors in order to gain new behaviors. The goal was to confirm that the engineered components were adopting the expected conformations.

The lack of progress getting Ndc80 and Dam1 to bind mammalian microtubules led us purify yeast tubulin in collaboration with the Drubin-Barnes laboratory, with the idea that these yeast proteins might decorate yeast microtubules better than mammalian microtubules. While this did

not solve the major hurdle, we noticed striking differences between yeast and mammalian microtubules. This work was greatly aided by the use of a direct electron detector that dramatically improved the resolution of our microtubule reconstructions and allowed us to visualize the lattice at near-atomic resolution. We became interested in understanding the how the subtle differences in the amino acid sequences were giving rise to large scale changes in the microtubule lattice. Yeast tubulin also opened up the possibility to look at tubulin mutants that might further our understanding of the molecular mechanisms underlying dynamic instability. This work is discussed in Chapter 4. Finally, our collaboration with Tarun Kapoor to look at mammalian tubulin mutants led to the observation that PRC1 bound the mutant microtubules with much lower affinity than WT mammalian microtubules. Our goal was to visualize the PRC1-tubulin interaction in atomic detail to see exactly how PRC1 bound the microtubule and gain some insight as to how it functions as an anti-parallel crosslinker. These results are discussed in Chapter 5.

2 Chapter 2: Tubulin acetylation and acetyltransferase binding

The ability to prepare acetylated or deacetylated microtubules *in vitro* for the first time enabled us to investigate whether tubulin acetylation on lysine residue 40 of α-tubulin (αK40) altered the architecture of microtubules or the conformation of tubulin. We imaged microtubules assembled from maximally acetylated or deacetylated tubulin using cryo-electron microscopy (cryo-EM). We were also interested in how αTAT1 gained access to the lumen of the microtubule. The results of these studies, many of which have been published (Howes, Alushin, Shida, Nachury, & Nogales, 2014) are presented here.

2.1 Cryo-EM visualization shows no significant effect of tubulin acetylation on microtubule structural parameters

Our starting hypothesis was that changes conferred by acetylation could either alter tubulin-tubulin contacts and microtubule lattice parameters, or otherwise propagate to the microtubule external surface where they could be recognized by MAPs. This was based on the reasoning that most proteins would likely have difficulty gaining access to the lumen of the microtubule, and the generality in the binding of MAPs and microtubule motors to the external surface of microtubules.

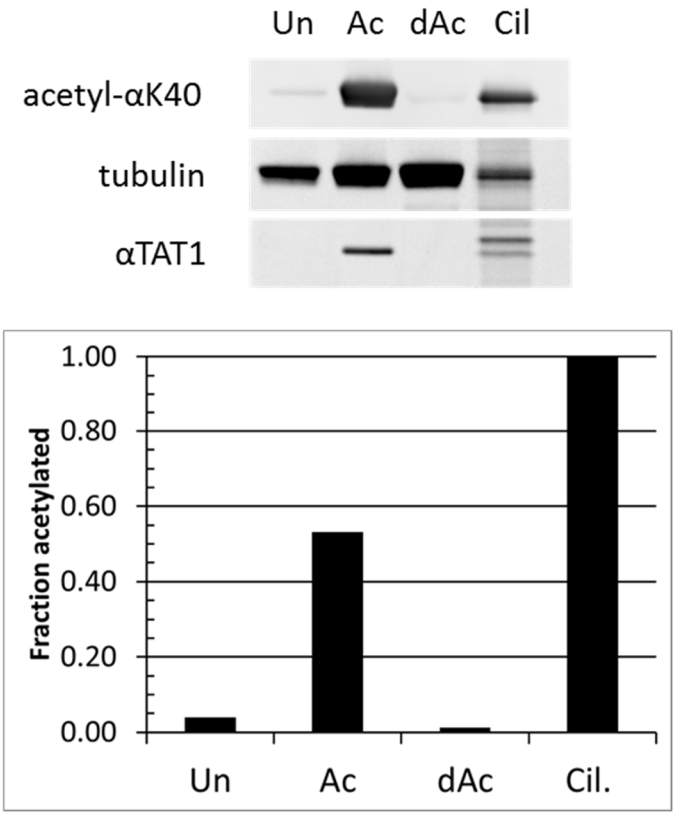

Figure 2-1 Modification of tubulin *in vitro*
Western blot of tubulin samples used to prepare EM grids after *in vitro* modification with αTAT1 or SIRT2 probed with an anti-acetylated tubulin antibody (top) and replicated lane stained with SYPRO (middle and bottom). Un = untreated, Ac = acetylated, dAc = deacetylated, Cil = ciliary tubulin. Quantification of Western blot shown below. Adapted from Howes, 2014.

Such changes in the microtubule lattice would provide the means for proteins that bind to the outside of microtubules to detect this modification. To determine what kind of effect tubulin acetylation has on microtubule structure, mammalian brain tubulin was modified *in vitro* to generate either maximal or minimal levels of acetylation (see section 7.4). These levels were determined using an antibody that specifically recognizes acetylated tubulin in Western blots (see Figure 2-1).

The modified tubulin was then assembled into either dynamic or taxol stabilized microtubules for analysis by cryo-electron microscopy. Similar amounts of tubulin polymerized for acetylated and deacetylated tubulin samples, based on the apparent abundance of microtubules in micrographs, and both types of samples showed a similar increase in the amount of assembled

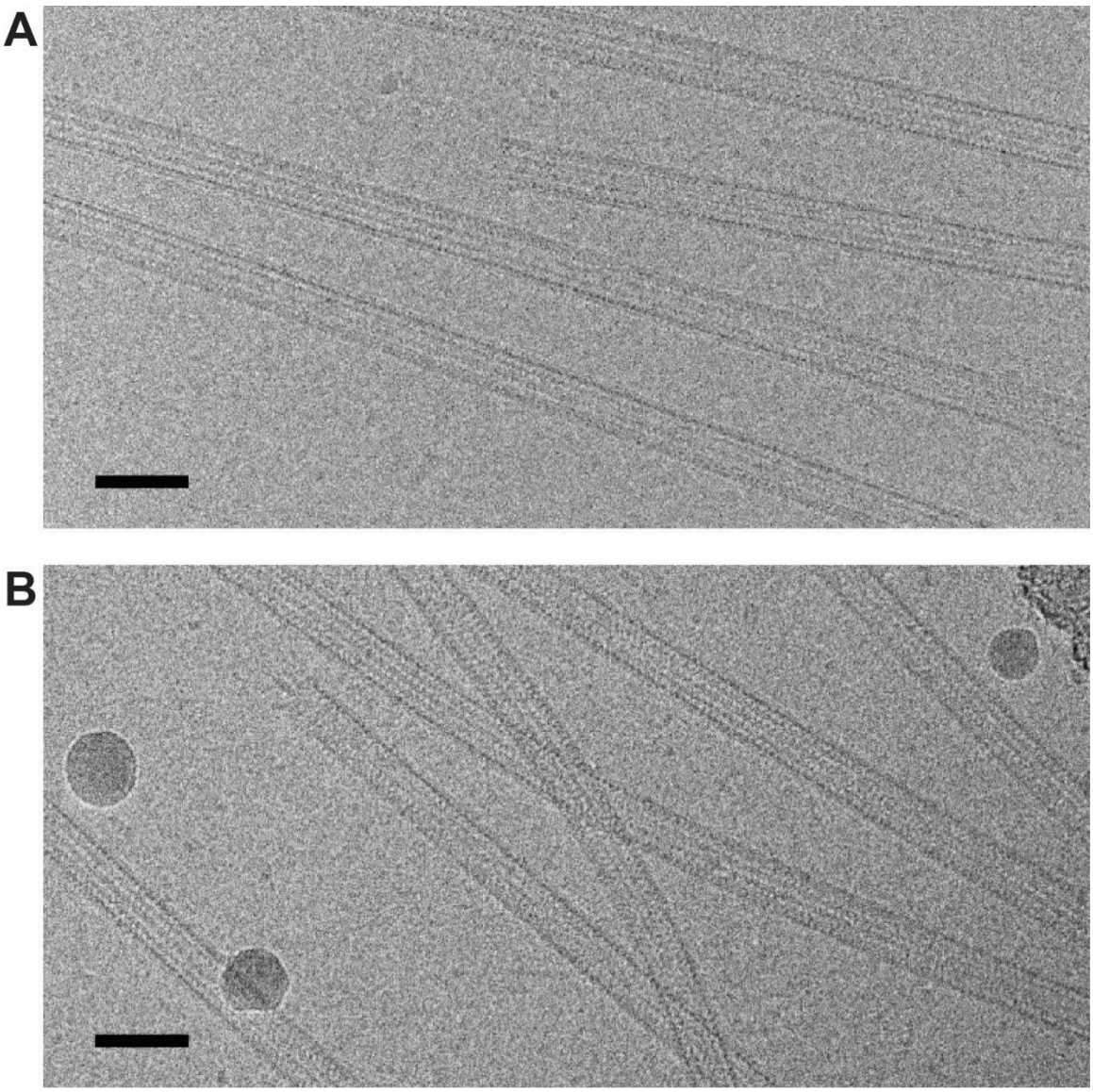

Figure 2-2 Raw micrographs of acetylated and deacetylated microtubules
Representative cryo-EM images of **A)** acetylated and **B)** deacetylated dynamic microtubules. No differences in gross morphology were observed. Scale bar = 50 nm. Adapted from Howes, 2014.

microtubules upon addition of taxol. Additionally, no obvious differences were seen in the gross morphology or curvature of the microtubules (see Figure 2-2).

We visualized acetylated and deacetylated microtubules with the ultimate goal of generating high-resolution 3D structures of the two types of polymers. A requirement for achieving high resolution is the reliable separation of α- and β-tubulin. In a raw micrograph, the low signal-to-noise ratio prevents discrimination of the two tubulin monomers, so any three dimensional processing would result in the averaging of α- and β-tubulin together. To prevent this averaging, we decorated the microtubules with a monomeric kinesin construct that had a glutamic acid to alanine mutation at position 236 that prevented ATP hydrolysis (hereafter referred to as kinesin). Besides being biochemically very stable and easy to work with, this mutant is also trapped the motor in the high-affinity state of microtubule binding, making decoration of microtubules relatively straightforward. The large kinesin density on the outside of the microtubule provides a strong signal for the tubulin heterodimer, ensuring that α- and β- subunits are not averaged together.

As a first indication of whether acetylation alters the packing of tubulin heterodimers within the microtubule, we examined the distribution of protofilament numbers in acetylated and deacetylated microtubules. Overlapping square boxes of 700 Å, spaced 80 Å apart, were masked from the raw images and grouped into 2D reference-free class averages using IMAGIC (van Heel, Harauz, Orlova, Schmidt, & Schatz, 1996). Particles belonging to class averages that appeared to contain high resolution information were further processed using EMAN2 multi-model refinement (Tang et al., 2007) against initial models of 12, 13, 14, and 15 protofilament microtubules (Sui & Downing, 2010) low-pass filtered to 20 Å resolution, and IHRSR (Egelman, 2007) to obtain the 3D reconstruction. The number of particles that matched each model was used to estimate the total number of microtubules of each protofilament number. The percentages of microtubule segments with different protofilament numbers are shown in Figure 2-3. Dynamic microtubules show a close

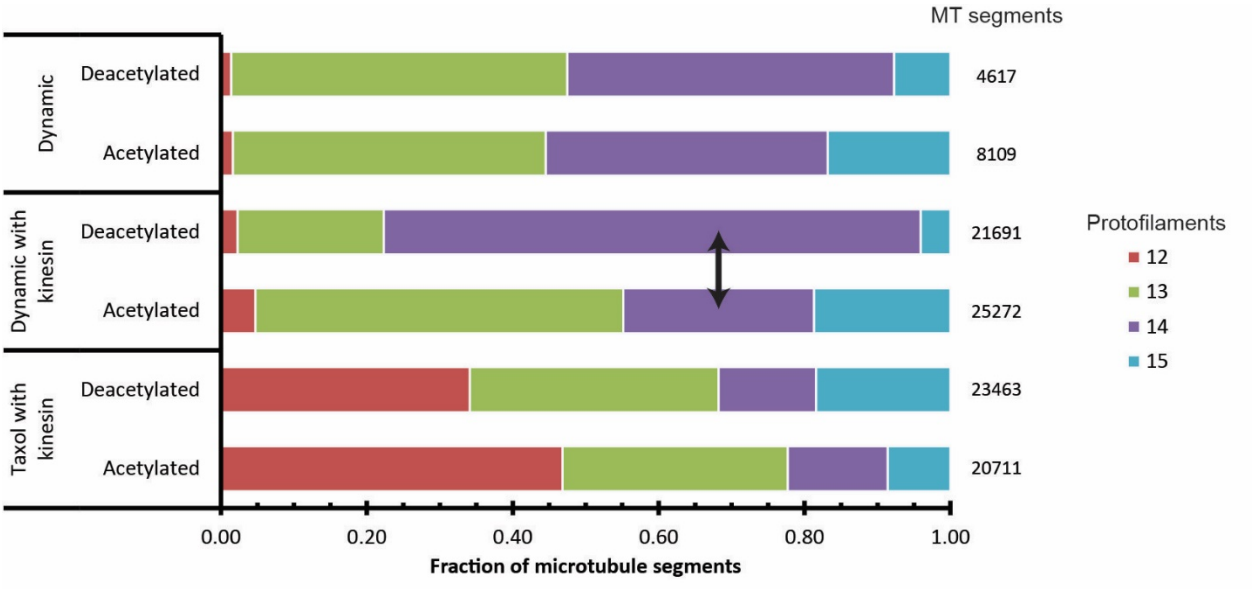

Figure 2-3 Protofilament distribution for acetylated and deacetylated microtubules
Protofilament number distribution of microtubules polymerized after acetylation or deacetylation into dynamic or taxol stabilized microtubules. Arrow shows largest observed change. Adapted from Howes, 2014.

to 50-50 % mixture of microtubules with predominantly 13 and 14 protofilaments, irrespective of the acetylation state of tubulin. The binding of kinesin affects protofilament numbers in acetylated microtubules very marginally, by slightly increasing the proportion of 13 protofilament microtubules. Interestingly, the binding of kinesin to deacetylated microtubules significantly reduces the number of 13 protofilament microtubules while increasing the number of 14 protofilament microtubules**.** Addition of both taxol and kinesin had the most severe effect in the spreading of protofilament number, dramatically increasing the fraction of 12 protofilament microtubules, a previously characterized effect of taxol (Andreu et al., 1992). Importantly, this effect was very similar for acetylated and deacetylated microtubules. These results indicate that taxol and kinesin have a much more significant effect on protofilament numbers than the acetylation state of tubulin. The abundance of 14 protofilaments in dynamic, deacetylated microtubules in the presence of kinesin is a curious result for which we do not have a clear interpretation. However, it seems to indicate that kinesin has an apparent destabilizing effect on 13 (but not 14) protofilament microtubules that are devoid of acetylation, perhaps by having lower affinity for the 13 protofilament lattice of the deacetylated tubulin. Considering that 13 protofilaments are likely the predominant microtubule architecture in the cell, our *in vitro* assay may reflect a higher affinity of kinesin for the 13 protofilament microtubule made of acetylated versus deacetylated tubulin, which would have biological implications for the effect of this modification on intracellular motility.

Previous experiments have shown that while the sensory dendrites of wild-type C. elegans touch receptor neurons contain microtubules of almost exclusively 15 protofilaments, mutants lacking the acetyltransferase have fewer microtubules, and protofilament numbers spread between 11 and 16 (Cueva et al., 2012; Topalidou et al., 2012). Given our *in vitro* results, it is likely that the change in protofilament number spread with acetylation state is not due to the direct effect of this modification on microtubule structure, but to the effect of the binding of specific MAPs, sensitive to the tubulin acetylation state. Given the proximity of αK40 to the lateral contacts between tubulin heterodimers, binding of a MAP in this region could have a constraining effect on the angle of the interaction, thus fixing the number of protofilaments.

To further investigate whether acetylation alters the packing of tubulin heterodimers within the microtubule, we next examined the helical lattice parameters for each of the microtubule conditions. Such parameters are obtained during the process of image analysis. Our 3D cryo-EM reconstruction of microtubules follows an iterative refinement process whereby estimates for the longitudinal (rise) and lateral (twist) spacing of tubulin subunits are optimized by improving the alignment of individual microtubule segments with respect to an evolving model (Egelman, 2007). This method is called iterative helical real space reconstruction (IHRSR). Firstly, a volume is reconstructed without any imposed symmetry that would contain multiple copies of the subunit, in this case αβ-tubulin. The underlying symmetry is then estimated using a least-squares fit to minimize the residuals when comparing voxels from symmetrically related copies of the subunit. These helical estimates (rise and twist) are then used to impose the symmetry on the volume. This increases the SNR and generally improves the resolution of the volume. This symmetrized volume is then used as a reference for another round of projection matching against the raw particles. Presumably, because the reference has improved, alignment of the raw particles can be improved. This cycle is repeated until there is not further improvement. Estimates for the rise and twist of a 14 protofilament microtubule at each iteration of the reconstruction are shown in Figure 2-4.

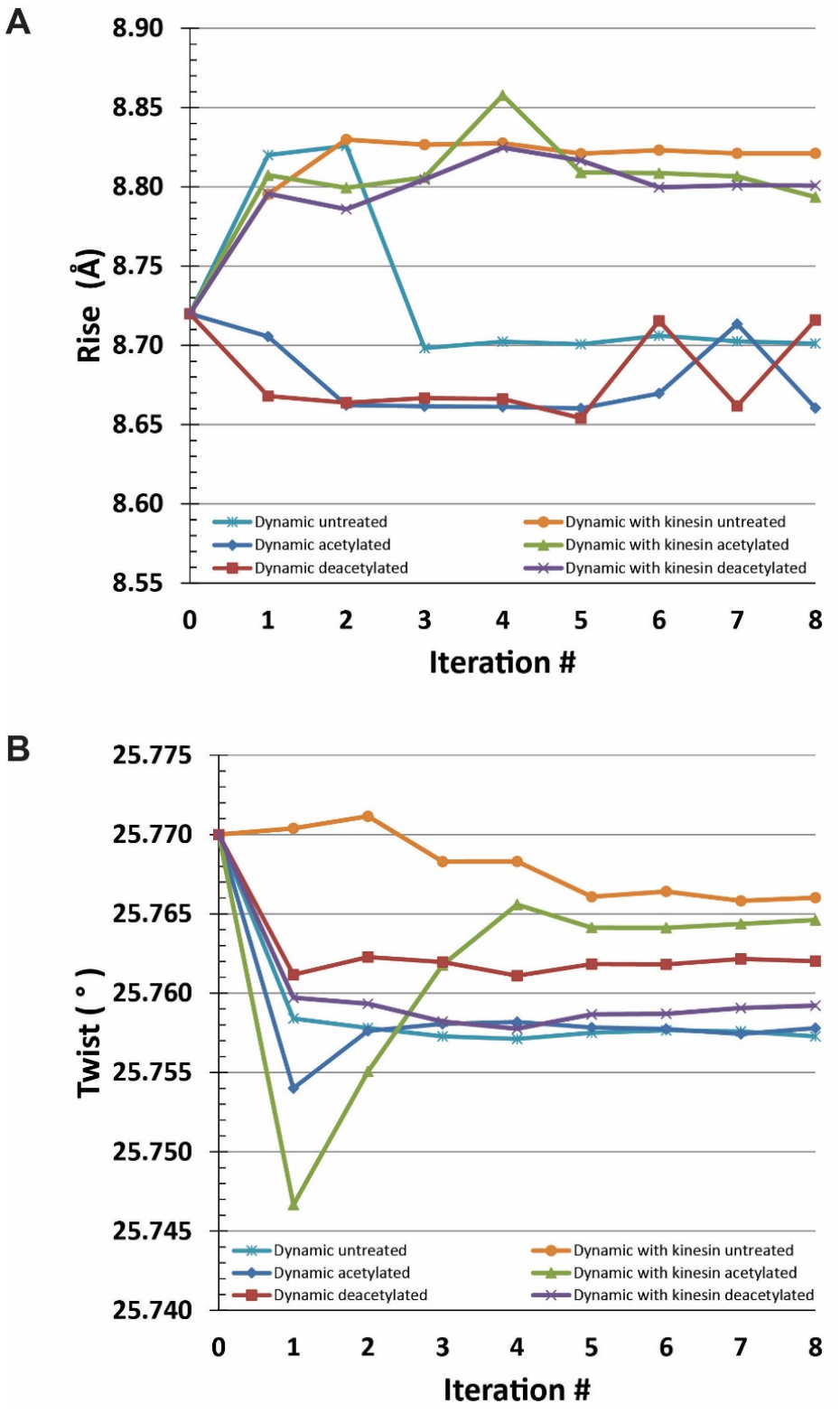

Figure 2-4 Refinement of acetylated and deacetylated helical parameters
Estimations for rise (A) and twist (B) of tubulin dimers in 14 protofilament microtubules shown at each iteration of refinement during the reconstruction process of dynamic microtubules assembled from untreated, acetylated and deacetylated tubulin, both in the presence or absence of kinesin. Adapted from Howes, 2014.

Final estimates for 13 and 14 protofilament microtubules are given in Table 1. We observed no influence of acetylation in the longitudinal or lateral spacing of the tubulin heterodimers. When we examined acetylated and deacetylated microtubules bound to kinesin, which serves as a marker of the tubulin heterodimer repeat (allowing one to discriminate α- and β -tubulin during the reconstruction) we saw a small but detectable increase in the longitudinal spacing of tubulin heterodimers of about 1-2%, irrespective of whether tubulin was acetylated or deacetylated. Our data shows remarkable structural similarity between the acetylated and deacetylated microtubule lattices, demonstrating that helical packing of tubulin heterodimers within the microtubules is not altered by the acetylation state of αK40. Previous computational models have suggested the formation of a salt bridge between neighboring α-tubulin subunits across protofilaments upon αK40 acetylation (Cueva et al., 2012). Our data shows that if this salt bridge forms, it must not alter the packing of tubulin heterodimers within the microtubule.

Table 1 Final helical parameter estimates for acetylated and deacetylated microtubules

	Untreated	Deacetylated	Acetylated	Untreated + kinesin	Deacetylated + kinesin	Acetylated + kinesin
13 protofilaments						
Rise	9.44	9.36	9.36	9.23	9.49	9.50
Twist	-27.68	-27.69	-27.69	-27.70	-27.70	-27.69
14 protofilaments						
Rise	8.70	8.72	8.88	8.82	8.80	8.79
Twist	-25.75	-25.76	-25.76	-25.77	-25.76	-25.77

2.2 Structures of tubulin in acetylated and deacetylated microtubules are indistinguishable

In order to investigate whether acetylation locally altered the structure of tubulin without modifying the lattice parameters, perhaps having an allosteric effect that would be propagated to the outside surface of the microtubule, we generated subnanometer resolution 3D cryo-EM structures of acetylated and deacetylated microtubules (see Figure 2-5). We carried out parallel reconstructions for coexisting 13 and 14-protofilament microtubules in each sample. The conclusions were the same for both types of microtubules, so we describe in detail the results for just one of them. We found that the reconstructions of 14-protofilament microtubules made of maximally acetylated or deacetylated tubulin look very similar to each other, as well as to previous reconstructions of mammalian brain tubulin (H. Li, DeRosier, Nicholson, Nogales, & Downing, 2002; Sui & Downing, 2010), which has been previously reported to be acetylated by about 5% (Eddé et al., 1990) but we find to correspond to 25-30% of the total. We isolated a single tubulin heterodimer from the acetylated and deacetylated microtubule structures, aligned them to each other, and calculated a difference map using Fourier space subtraction and amplitude correction. Figure 2-5B & C display the positive and negative difference densities in red and blue, respectively, with isosurfaces contoured at three standard deviations. No statistically significant changes in density are observed at this resolution.

Taxol stabilized microtubules were also prepared, imaged and reconstructed. The reconstructions obtained were of marginally lower resolution than those from dynamic microtubules, but also showed no differences between acetylated and deacetylated states. The

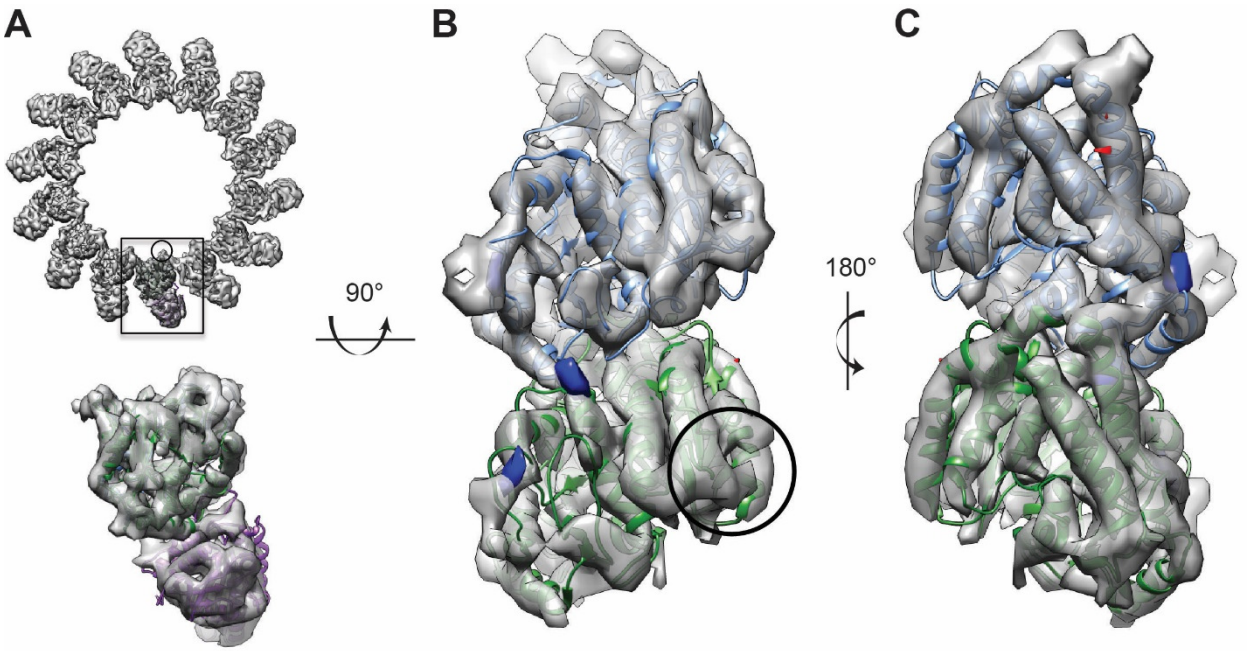

Figure 2-5 Acetylation state does not alter the structure of dynamic microtubules
A) End-on view of the deacetylated, dynamic microtubule reconstruction with the electron crystallographic structure of tubulin (1JFF) and kinesin (1BG2) docked in. **B**) Inside view (from the microtubule lumen) of the difference maps between acetylated and deacetylated reconstructions contoured at 3σ, with extra density in acetylated microtubules shown in blue and extra density in deacetylated microtubules shown in red. The differences are superimposed on the cryo-EM reconstruction of deacetylated microtubules shown as grey isosurface. The location of the loop containing the modified residue is indicated by the circle. **C**) Outside view, colors as in **B**). α-Tubulin shown in green, β-tubulin shown in blue and kinesin shown in purple in all panels. Adapted from Howes, 2014.

lower resolution of the taxol reconstructions is likely due to the increased flexibility caused by the presence of the drug (Felgner, Frank, & Schliwa, 1996), or the greater number of defects in these lattices, which would result in the depolymerization of a drug-free microtubule.

The data presented here indicate that acetylation of α-tubulin at K40 has no appreciable structural effect in overall microtubule assembly and architecture, or on tubulin structure as visualized at 8-9 Å resolution. Although we cannot discard the possibility that acetylation has a small effect on the structure/stability of the loop where αK40 resides, something which would only be detectable in structures closer to atomic resolution. Our analyses strongly suggest that the effect of acetylation must be small and local. We also cannot completely exclude the possibility that the modification might alter the local packing of the αK40 loop in a manner that would not persist if the microtubule was depolymerized and reformed. For these studies the tubulin was acetylated outside of the microtubule, then polymerized, which may give a different result to forming the microtubule then performing the acetylation. On the other hand, the remarkable structural similarity we observe between the acetylated and deacetylated microtubule samples could mean that this modification is invisible to the majority of proteins that bind the outside of the microtubule. We propose that the "biological readout" of this modification must require protein factors that directly recognize the acetyl group of the modified lysine or a small, local structural rearrangement near the site. Thus, it is likely that acetylation affects microtubule function by the

binding of proteins that gain access to the lumen of microtubules where the acetylation mark resides. Interestingly, the microtubule lumen appears not to be empty in the cell, as a number of electron tomographic studies have demonstrated the presence of luminal particles in neurons, astrocytes and stem cells (Bouchet-Marquis et al., 2007; Burton, 1984; Garvalov et al., 2006). The identity of these particles remains unknown, but intriguingly the greater abundance of luminal particles in neurons correlates with an increased degree of acetylation in this microtubule population. Furthermore, mutants lacking the acetyltransferase have much fewer luminal particles (Topalidou et al., 2012).

2.3 αTAT1 binding to microtubules is not influenced by accessibility to the lumen

Given that αTAT1 acts on the luminal surface of the microtubule and that its enzymatic activity is higher for assembled microtubules than for free tubulin heterodimers, it must be able to gain access to the inside of the microtubule to carry out its enzymatic activity. Thus αTAT1 represented the first protein strongly predicted to bind to the inside of microtubules. This raises the question of how it accesses the luminal surface. To test whether αTAT1 binding to microtubules is limited by accessibility to the acetylation site, we compared the results of co-sedimentation assays for two alternative tubulin polymer forms: taxol-stabilized microtubules, and vinblastine-induced coils. Vinblastine creates open, spiral polymers of tubulin where the luminal surface of the microtubule is fully exposed and prevents the formation of microtubules (Gigant et al., 2005; Nogales et al., 1995).

Surprisingly, no increase in αTAT1 binding was observed for this type of polymer with respect to binding to taxol-stabilized microtubules (Figure 2-6A). Because the structure of tubulin is different in the vinblastine-induced polymers (curved, versus the straight conformation within

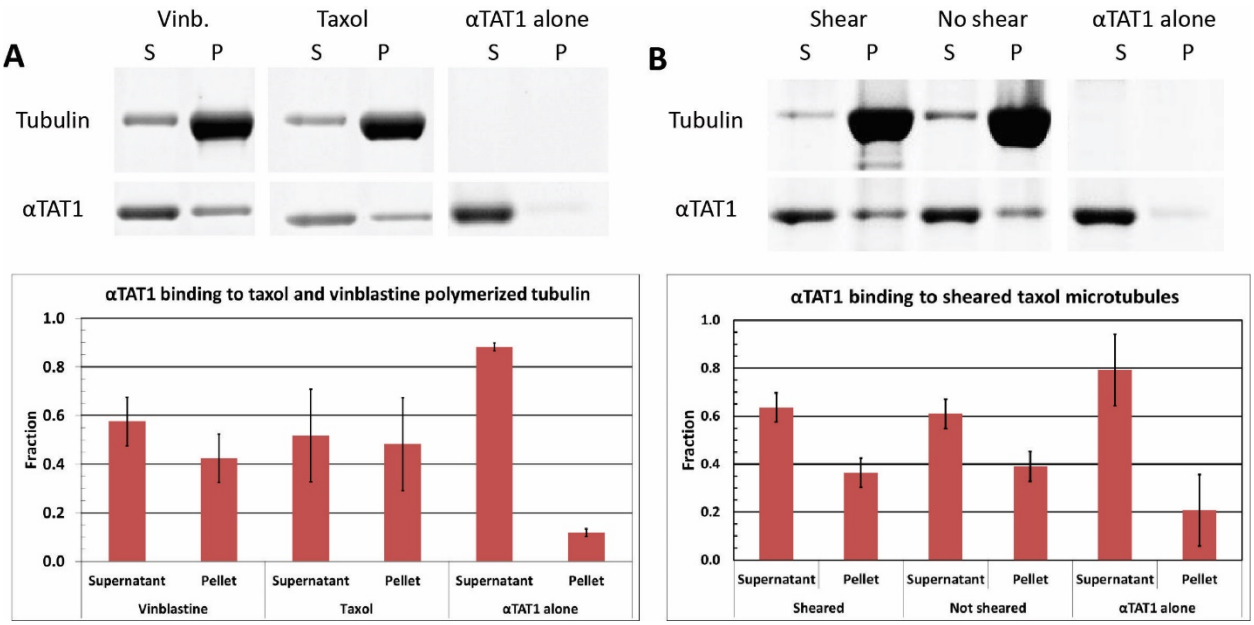

Figure 2-6 αTAT1 accessibility to its binding sites on tubulin polymers
SDS gel (top) and quantitation (bottom) of pelleting assays showing that **A)** αTAT1 binds similarly to tubulin polymers assembled with vinblastine (coils) or taxol (microtubules); **B)** Shearing microtubules to create more microtubule ends does not increase binding of αTAT1 to microtubules. Data from three independent co-sedimentation assays. Error bars show standard deviation. Adapted from Howes, 2014.

microtubules), a decrease in affinity could have compensated for the better accessibility. Thus, we carried out a second test in which taxol microtubules were sheared by passing them through a small diameter needle This shears long microtubules and creates more free ends, which should allow the enzyme to access the microtubule lumen more readily if access is gained through the microtubule ends. However, we did not observe any significant increase of αTAT1 binding to sheared microtubules compared to unsheared (Figure 2-6B). These results indicate that αTAT1 binding to taxol microtubules is not limited by accessibility to the microtubule lumen. All our pelleting assays show that a significant fraction of αTAT1 remains unbound, even when mixed with an excess of tubulin, indicating that the binding affinity of αTAT1 for microtubules is modest.

2.3.1 αTAT1 binds the exterior and interacts with the C-termini of tubulin

In an attempt to directly observe how αTAT1 binds microtubules, we polymerized dynamic microtubules in the presence of stoichiometric amounts of αTAT1. The structures obtained are shown in Figure 2-7A. We observed extensive microtubule bundling, mediated by a complex coat of protein around the microtubules. The size and granularity of this coat indicate that it likely involves both αTAT1 and tubulin assembled into curved structures, a type of arrangement previously observed for other microtubule binding proteins such as kinesin-13 (Tan, Asenjo, Mennella, Sharp, & Sosa, 2006). This result can only be explained if, irrespective of its binding to the lumen, αTAT1 binds also to the outside surface of the microtubule, where it could interact with unassembled tubulin and promote microtubule bundling. Such a "sandwich" of aTAT1 between tubulin structures could be obtained if the enzyme either had more than one tubulin binding site per molecule (e.g. one site could bind the globular part of the tubulin structure, while other could interact with the acidic C-tails of tubulin), or by oligomerization of the enzyme (e.g. dimers where

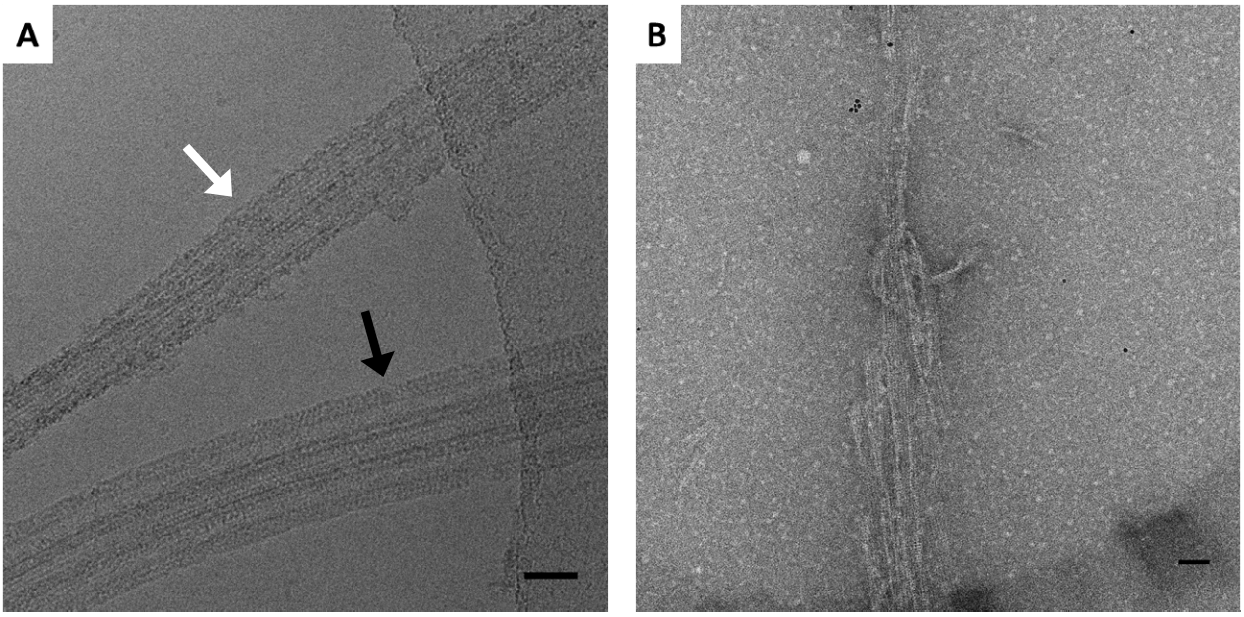

Figure 2-7 Effect of αTAT1 binding on microtubule assembly and bundling
A) Cryo-EM image showing that the presence of αTAT1 during the assembly of dynamic microtubules gives rise to large protein structures around the microtubule lattice (black arrow) and promotes bundling (white arrow). **B)** Negative stain EM image of microtubules copolymerized with αTAT1 in the presence of taxol at 1:5 αTAT1:tubulin molar ratio showing incomplete microtubule closure and numerous defects. Scale bar = 50 nm. Adapted from Howes, 2014.

each monomer binds identical regions in tubulin). Our gel filtration indicates that, while full length αTAT1 can dimerize, the truncated construct used in this study does not dimerize. Further study will be required to determine the molecular origin of the bundling and if there is any biological relevance for this *in vitro* observation.

We also studied the effect of adding taxol to acetylation reactions. Taxol is a potent microtubule stabilizer and results in there being very little soluble tubulin. Notice that in the presence of taxol there is little unassembled tubulin (as demonstrated in the co-sedimentation assays, e.g. Figure 2-6A). Microtubules formed with αTAT1:tubulin molar ratios from 1:3 to 1:10 had numerous defects and were often opened (Figure 2-7B). Taxol microtubules are known to open laterally (between and along the length of protofilaments) more often than dynamic microtubules (or perhaps, just as often, but while dynamic microtubules may depolymerize upon opening in the absence of other stabilizing proteins, taxol microtubules do not) and contain more discontinuities in the helical packing of tubulin dimers (Arnal & Wade, 1995). This effect was dramatically enhanced in the presence of the acetyltransferase, suggesting that its binding may sterically preclude re-closure. At the high excess molar ratio of 10:1 αTAT1:tubulin, microtubule assembly was inhibited entirely. Thus, excess of αTAT1 has a deleterious effect on microtubule assembly, perhaps by steric hindrance while bound to its luminal site. The destabilizing effect of αTAT1 that we see *in vitro* agrees with the decrease in microtubule stability observed upon overexpression of the enzyme in mammalian cells, even if the overexpressed enzyme is a catalytically dead mutant (Kalebic et al., 2013), again suggesting that it is the presence of the enzyme rather than the tubulin modification, that has an effect on microtubule stability.

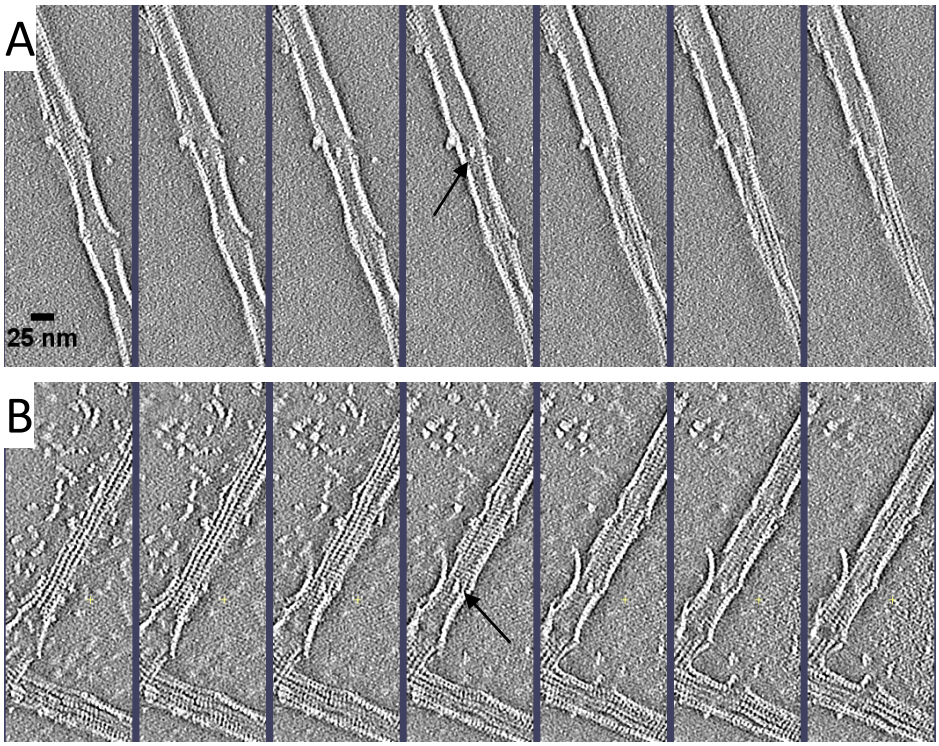

Figure 2-8 Slices from tomographic reconstructions of bound αTAT1
Serial slices of tubulin polymerized with αTAT1 at αTAT1:tubulin ratios of 3:1 **(A)** and 5:1 **(B)**. Densities are observed in the lumen of the microtubule (shown by arrows), however these cannot be unambiguously ascribed to αTAT1.

In order to directly visualize αTAT1 bound to the microtubule, we collected tomography data of microtubules assembled with taxol in the presence of αTAT1. Slices from the tomographic reconstructions are shown in Figure 2-8. These negatively stained samples again showed the numerous defects caused by steric hindrance of αTAT1. Enticingly we also observed densities within the lumen of the microtubule. However, due to the background of unassembled tubulin, it was not possible to exclude the possibility that some tubulin had been trapped in the lumen by chance.

Neither the dynamic nor the taxol-stabilized microtubule samples containing αTAT1 where amenable to 3D reconstruction preventing us from directly visualizing the binding site or sites of αTAT1 on microtubules. In order to further probe the possible interaction of αTAT1 with the outside surface of the microtubule, hinted at by the bundling effect of the enzyme, we used co-sedimentation assays with microtubules treated with subtilisin, a protease that removes the acidic C-terminal tails of tubulin that extend from the microtubule surface (see section 7.5 for details of the preparation of subtilisin-treated microtubules). Indeed, we observed a clear decrease in the amount of αTAT1 that co-sediments with subtilisin-treated microtubules (Figure 2-9). Consistent with αTAT1 interacting with microtubules through this charged region, we also observed that the

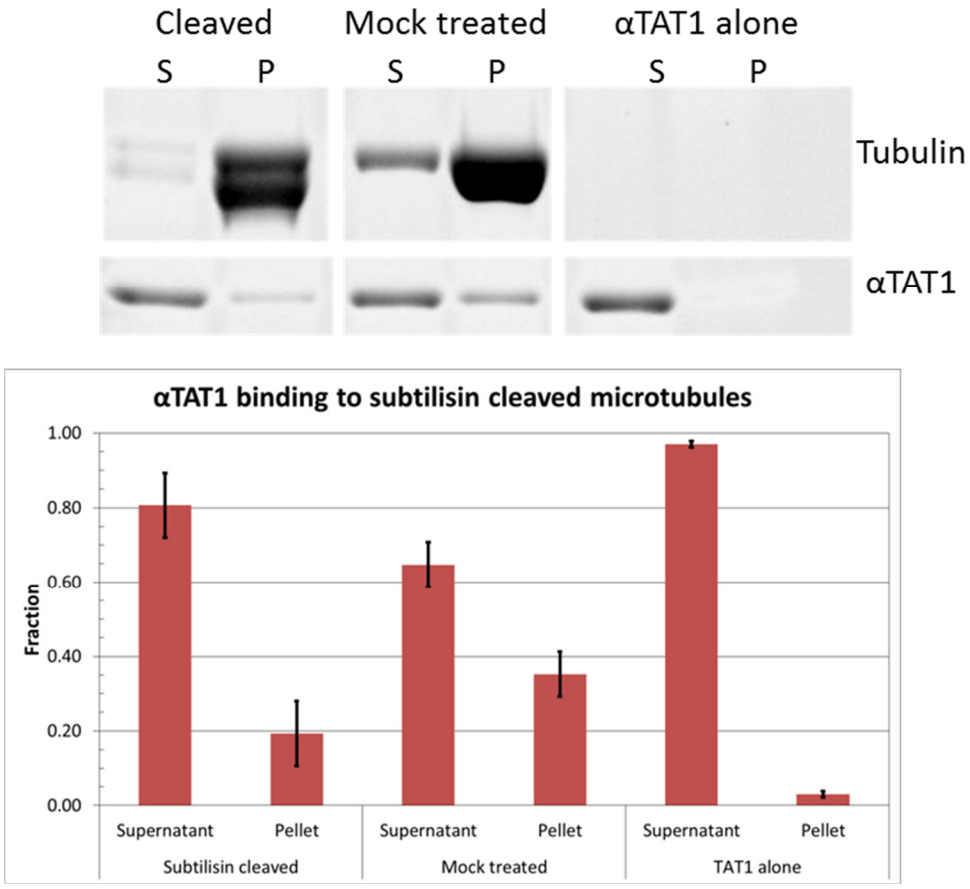

Figure 2-9 αTAT1 binding to microtubules is affected by the absence of the C-terminal tails of tubulin.
SDS gel (top) and quantitation (bottom) of pelleting assays showing that αTAT1 co-sediments less with subtilisin treated microtubules than with untreated tubulin. Data from three independent co-sedimentation assays. Error bars show standard deviation. Adapted from Howes, 2014.

binding of αTAT1 decreases with increasing salt concentrations. This result lends further support to the idea that αTAT1 binds tubulin at additional site(s) from its site of action on the microtubule luminal surface.

Interaction of αTAT1 with the external surface of the microtubule may help target the enzyme. This exterior binding event may serve to concentrate the enzyme, which could then be used to funnel it to the ends and/or make use of lattice fluctuations/defects to gain access to its luminal site. The size of the pores between protofilaments obtained in this study and previous work (H. Li et al., 2002; Meurer-Grob, Kasparian, & Wade, 2001) are approximately 20 Å in diameter. This is smaller than the smallest dimension of the αTAT1 monomer, which can be approximated by an ellipsoid with major and minor axes of 60 Å and 30 Å respectively (Kormendi et al., 2012; Taschner et al., 2012). Defects at changes in protofilament numbers and lattice fluctuations have been used to explain the fast binding of taxol (Díaz, Barasoain, & Andreu, 2003) and the ability of the anti-acetylated tubulin antibody to gain access to the lumen (Odde, 1998). Based on the importance of the tubulin C-terminal tails for αTAT1 association with microtubules, we speculate that αTAT1 could be responsive to other PTMs which also occur on the tails. This may be a mechanism for coordinating acetylation with other tubulin PTMs. Future studies could test the possibility that the N-terminal catalytic domain of αTAT1 binds to the luminal surface of the microtubule, while other regions of the protein mediate binding to the outside.

2.3.2 The affinity of αTAT1 for microtubules is not significantly affected by the tubulin acetylation state

Histone acetyltransferases associate with transcriptional cofactors containing bromodomains that bind acetylated histones, thus allowing for epigenetic spreading of this modification in chromatin (Filippakopoulos & Knapp, 2012). Although no such cofactors have been discovered that would "spread" tubulin acetylation inside microtubules, and although no classical bromodomain exists within αTAT1, we decided to test whether αTAT1 would bind preferentially to modified αK40. Tubulin was acetylated using 100-fold less αTAT1 compared to the treatments performed for the cryo-EM studies, in order to minimize any possible residual binding to undetectable levels. Acetylation levels were approximately 80% of the level obtained using previous concentrations of αTAT1**.** Deacetylase levels were kept the same, as residual enzyme is not observed after the microtubule pellet is resuspended. Catalytically inactive αTAT1 (D157N mutation) was then added after microtubules were assembled in the presence of taxol. Our pelleting results show that αTAT1 does not bind differently to microtubules with different tubulin acetylation states (Figure 2-10). This result suggest that αTAT1 is not sufficient to spread the Ac-αK40 mark.

Several groups have now reported the structure of αTAT1 (Friedmann et al., 2012; Kormendi et al., 2012; W. Li et al., 2012; Taschner et al., 2012), but none of these structures was solved with a bound tubulin peptide. Interestingly, while HATs are fully active on histone tail peptides, αTAT1 has no activity on a 19-residue peptide corresponding to the loop where K40 resides (W. Li et al., 2012). Contrary to histone tails, the H1-S2 loop in α-tubulin is structured, and recognition of the site by αTAT1 may require the proper secondary structure. Furthermore, αTAT1 is more active on microtubules than on soluble tubulin heterodimers due to a higher K_{cat} rather than increased

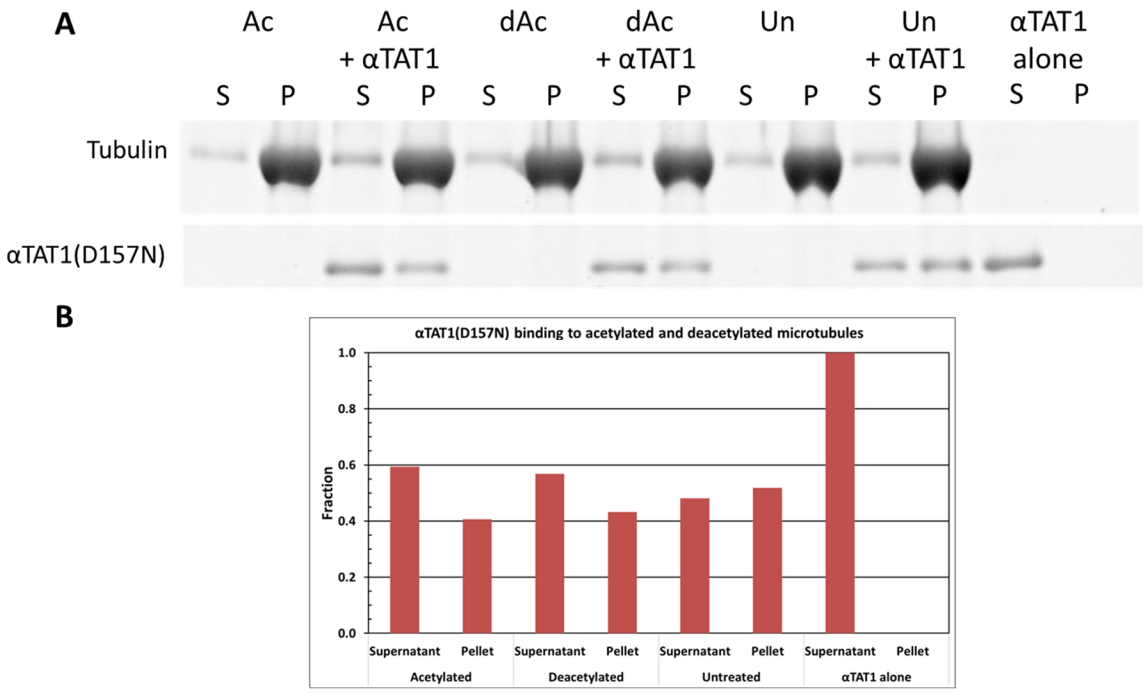

Figure 2-10 αTAT1 binding to microtubules is not affected by the acetylation state of tubulin
αTAT1(D157N) co-sedimented similarly with microtubules polymerized from tubulin that was previously acetylated or deacetylated. Un = untreated, Ac = acetylated, dAc = deacetylated. Adapted from Howes, 2014.

affinity, suggesting that the loop containing αK40 requires the context of the tubulin heterodimer or microtubule to be an optimal substrate for αTAT1.

Our studies demonstrate that the acetylation of αK40 has no significant effect on microtubule structure or tubulin conformation. Obviously, the biological role of tubulin acetylation does not require that this modification produce a direct effect on microtubule structure, stability or other intrinsic properties. Rather, it could operate to alter the binding of proteins that access the luminal surface of the microtubule. While the identity of these proteins remains unknown, the presence of luminal particles has been confirmed for many cell types (Bouchet-Marquis et al., 2007; Burton, 1984; Garvalov et al., 2006). Furthermore, the abundance of luminal particles appears to positively correlate with the degree of acetylation reported for these cells types (Garvalov et al., 2006). Interestingly, our *in vitro* studies indicate that the enzyme carrying out this tubulin modification, αTAT1, itself has the potential to affect microtubule structure and stability. Our attempts to decorate microtubules with αTAT1 to directly visualize its binding were unsuccessful. This was due to αTAT1 interfering with the assembly of microtubules and/or having multiple tubulin binding sites. Our *in vitro* observation of αTAT1 effect on microtubule stability is in good agreement with what has been seen in *in vivo* overexpression experiments, which showed that the effect is not dependent on the enzymatic activity of αTAT1. Instead, our study shows that the effect involves either the incorporation of the enzyme into the microtubule lumen, or its interaction with the microtubule surface. We believe that the later precedes luminal access, and may serve as a funneling mechanism to take advantage of protofilament breathing and/or lattice defects.

3 Chapter 3: Visualization of engineered kinesin motors

My work on engineered kinesins was a collaboration with the Bryant laboratory at Stanford University in the department of Bioengineering. Their research group is interested in directly testing structure-function relationships of biological motors and in the design of new motors with altered functional parameters (i.e. velocity, directionality, processivity). They have reported several modifications to myosin motors that allow for control of these functional parameters through external signals such as calcium ion concentration or photoactivation. We set out to explore the possibility of applying their myosin modifications to kinesin-based motors and wanted to obtain structural information about the engineered domains. Here I report the results of this collaboration.

3.1 Design principles of engineered motors

Cytoskeletal motors perform critical force generation and transport functions in eukaryotic cells (Sellers, 2000; Vale, 2003). Protein engineering has been used to modify cytoskeletal motors for dynamic control of activity (Cochran, Zhao, Wilcox, & Kull, 2012; K. Konishi, Uyeda, & Kubo, 2006; Tomishige & Vale, 2000) and directionality (Chen, Nakamura, Schindler, Parker, & Bryant, 2012), providing direct tests of structure-function relationships and potential tools for controlling cellular processes or for harnessing molecular transport in artificial systems (Goel & Vogel, 2008; Goodman, Derr, & Reck-Peterson, 2012). In these cases, the motor domain is left intact, but the lever arm is modified. An example of a motor that is modified to change direction is shown in Figure 3-1. By altering the effective angle at which the lever arm extends from the catalytic domain the directionality of the motor may be modified. The velocity of a motor may be modified by altering the length of the lever arm.

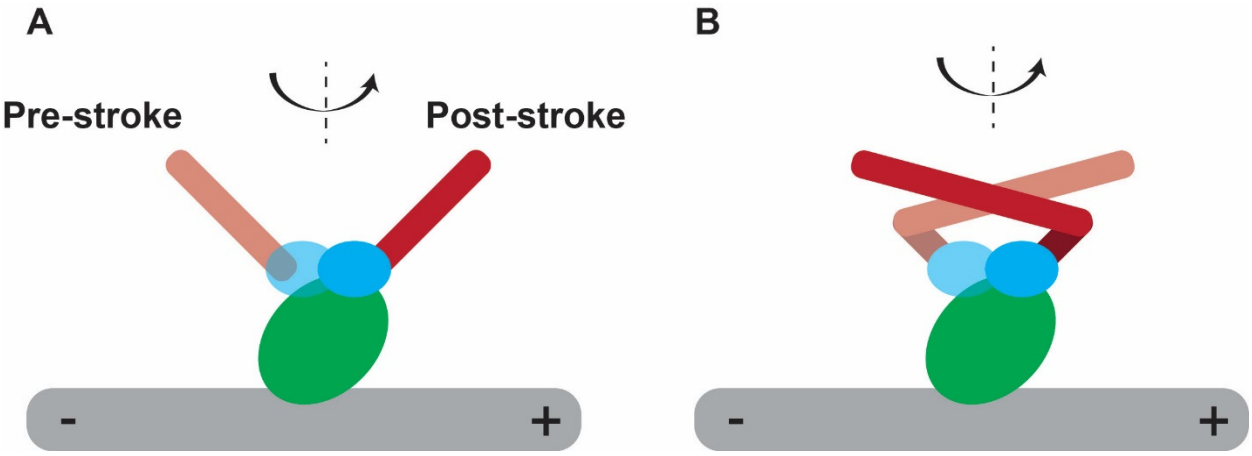

Figure 3-1 Design of a synthetic motor
A) The pre- and post-stroke states of a plus-end directed motor is shown, such as conventional kinesin.
B) An engineered kinesin using the same motor domain with an altered lever arm to produce motion in the opposite direction.

Previous work has created synthetic myosin motors that can be signaled to switch directions in response to changes in calcium ion concentration (Chen et al., 2012). Light is a more versatile control signal (Goodman et al., 2012) because it can be precisely modulated in space and time, and

is generally orthogonal to cellular signaling (Toettcher, Voigt, Weiner, & Lim, 2011). Here we report the design and characterization of a kinesin motor that changes direction when exposed to blue light. The structural designs incorporate a photoactive protein domain to enable light-dependent conformational changes in the engineered lever arm. We have used *in vitro* motility assays to confirm robust spatiotemporal control over Ncd function. The structure of these designs was confirmed by cryo-EM to verify the position of the engineered elements with respect to the catalytic domain.

The light, oxygen or voltage (LOV) protein domain, found in plant phototropins (Crosson, Rajagopal, & Moffat, 2003), responds to blue light with a structural transition that involves undocking of a C-terminal α-helix (Harper, Neil, & Gardner, 2003) as shown in Figure 3-2A & B. The LOV2 domain from *A. sativa* has been used in a variety of chimeric fusions to generate novel optical control of protein function (J. Lee et al., 2008; Lungu et al., 2012; Möglich & Moffat, 2010; Strickland et al., 2012; Strickland, Moffat, & Sosnick, 2008; Wu et al., 2009). We hypothesized that conformational changes in the LOV2 domain could provide a basis for optical control of lever

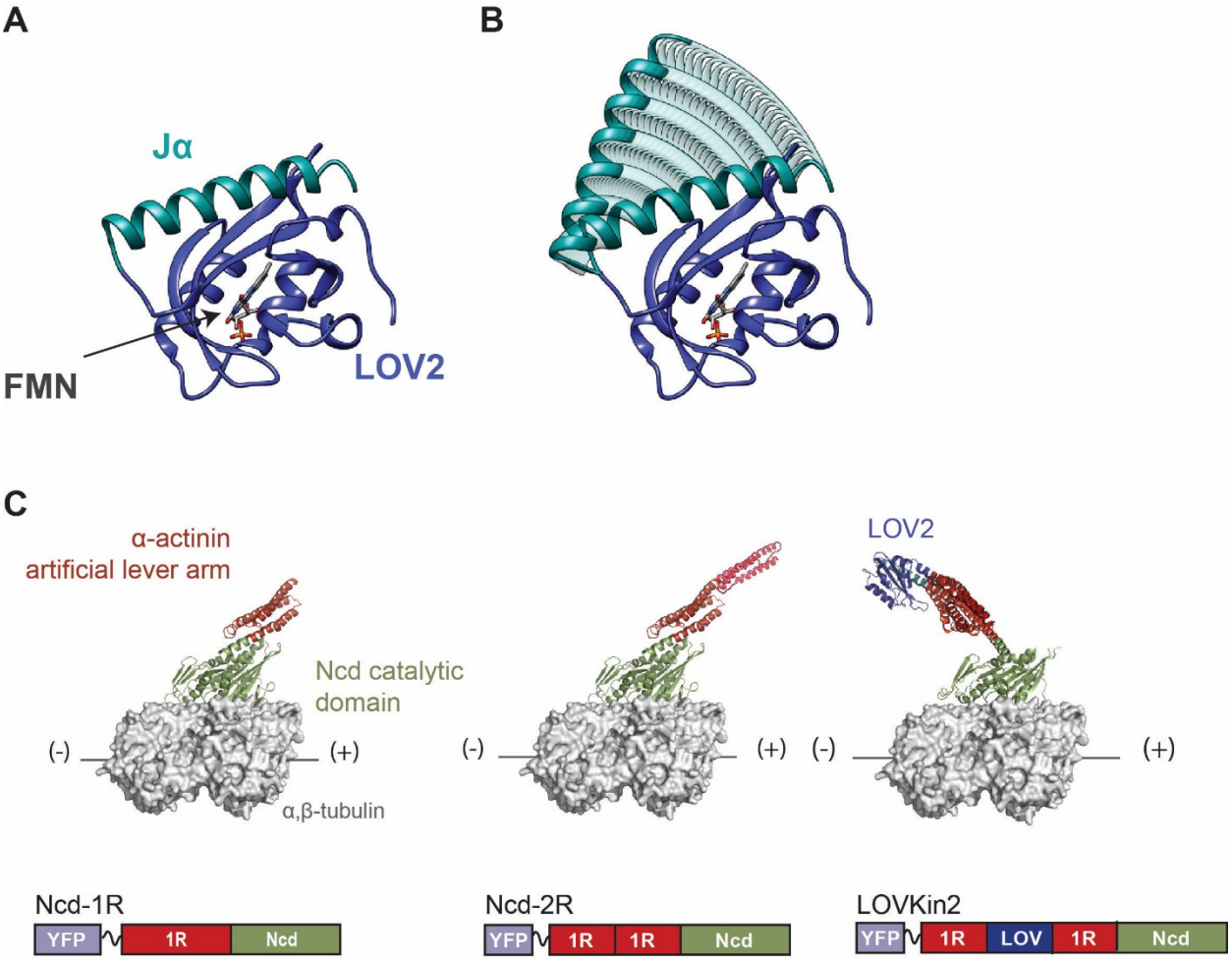

Figure 3-2 LOV domain response to light and motor designs
A) LOV domain in the dark state with docked Jα helix. **B)** Upon exposure to light and absorbtion of photons by the FMN molecule, interactions between Jα and the rest of the domain are disrupted, resulting in an undocking of the Jα helix. **C)** Synthetic Ncd-based kinesin motors showing designs of Ncd-1R, Ncd-2R and LOVKin2. Adpated from Nakamura, 2014.

arm structure, and was chosen as the light responsive element to be incorporated into the synthetic motor.

3.2 Structure of engineered kinesins on microtubules

The Ncd motor and other members of the kinesin-14 family have been proposed to use a swinging lever arm mechanism reminiscent of myosin, where the coiled-coil domain of the Ncd dimer is thought to act as an extended lever arm structure (Endres et al., 2006; Wendt et al., 2002; Yun et al., 2003). As a step toward adapting our design to Ncd, we first sought to create monomeric Ncd motors in which the coiled-coil is functionally replaced with an artificial lever arm. We created Ncd-1R by fusing an α-actinin spectrin repeat to the catalytic head of Ncd (Figure 3-2C). As expected Ncd-1R is a minus-end-directed kinesin, similar to WT Ncd. The velocity of this motor is faster than the catalytic domain alone and similar to an Ncd construct with a truncated native coiled-coil level (Nakamura et al., 2014), although slower than the > 100 nm s^{-1} velocities typical of intact Ncd motors (Endres et al., 2006).

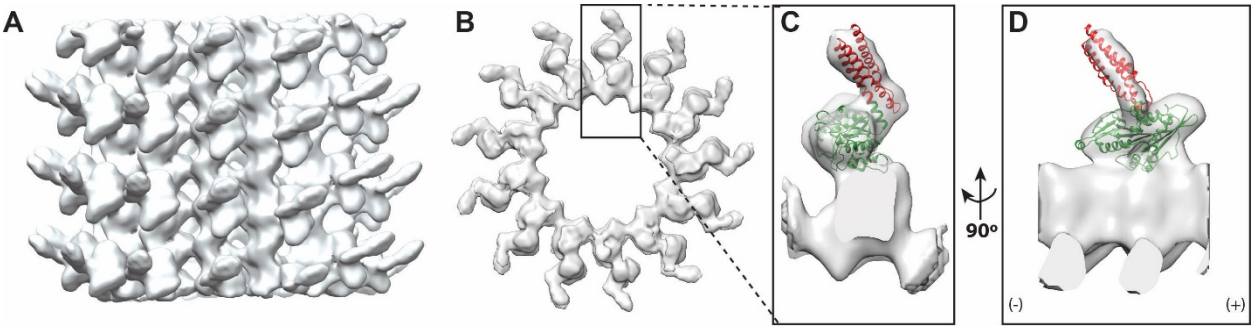

Figure 3-3 Reconstruction of Ncd-1R
Reconstruction of AMPPNP-bound Ncd-1R on taxol microtubules shown from side (**A**) and top (**B**) views. Docked atomic model for predicted Ncd-1R structure shown from top (**C**) and side views (**D**). Ncd catalytic domain shown in gree, and engineered lever arm using spectrin-like repeats from α-actinin shown in red. Adpated from Nakamura, 2014.

To validate that the engineered lever arm is in the expected orientation, we used cryo-EM to visualize the Ncd-1R motor. We used taxol stabilized microtubules because they allowed us to wash extensively without risking depolymerization of the microtubules. Attempts were made to see the lever arm in the pre- and post-stroke states. However, decorating microtubules with ADP-bound Ncd-1R was unsuccessful, preventing us from visualizing the pre-stroke state. We believe this is due to a greater propensity for Ncd-1R to aggregate without bound ATP. Incubating Ncd-1R with AMPPNP on ice before adding it to the microtubules was successful. The reconstruction and docking of the predicted atomic model is shown in Figure 3-3. We observed the lever arm in the expected orientation with respect to the catalytic domain.

We then sought to alter the velocity of this motor by increasing the length of the lever arm and created Ncd-2R. This motor incorporates two α-actinin spectrin-like repeats resulting in a longer lever arm than Ncd-1R. Using the same strategy to visualize the motor, we observed density for the lever arm in the expected position (see Figure 3-5), but at lower resolution for the lever arm itself. The density for this lever arm is also significantly weaker. We believe this is due to greater alignment inaccuracies at larger distances from the catalytic domain, where slight changes of angle at the base of the lever arm results in greater motion at the tip of the lever arm. This resulted in a

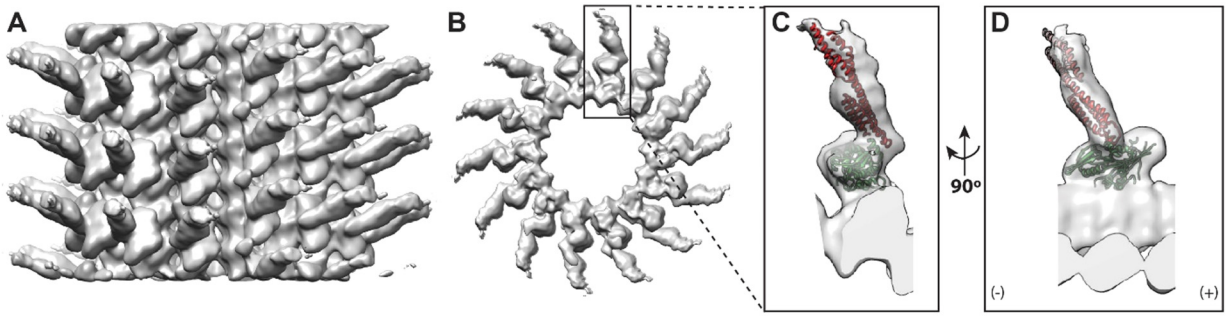

Figure 3-5 Reconstruction of Ncd-2R
Reconstruction of AMPPNP-bound Ncd-2R on taxol microtubules shown from side (**A**) and top (**B**) views. Docked atomic model for predicted Ncd-2R structure shown from top (**C**) and side views (**D**). Ncd catalytic domain shown in green, and engineered lever arm using two spectrin-like repeats from α-actinin shown in red. Electron density threshold chosen to show full lever arm.

blurring of the density and a reduction of resolution. However, we could confirm the position and size of the lever arm. The resolution of the tubulin subunits and the catalytic domain were similar to the Ncd-1R reconstruction.

We next created an optically controllable motor, LOVKin2, by fusing the catalytic domain of Ncd to a compound lever arm that included the two α-actinin spectrin-like repeats from Ncd-2R, but had the LOV2 domain inserted in between (see Figure 3-2C). In the dark state, the LOV2 domain folds the second α-actinin repeat back over the first α-actinin repeat, reducing the total length of the lever arm. Exposure to blue light reorients the second α-actinin spectrin repeat to create a longer lever arm. This reorientation upon photoactivation increased the velocity of the

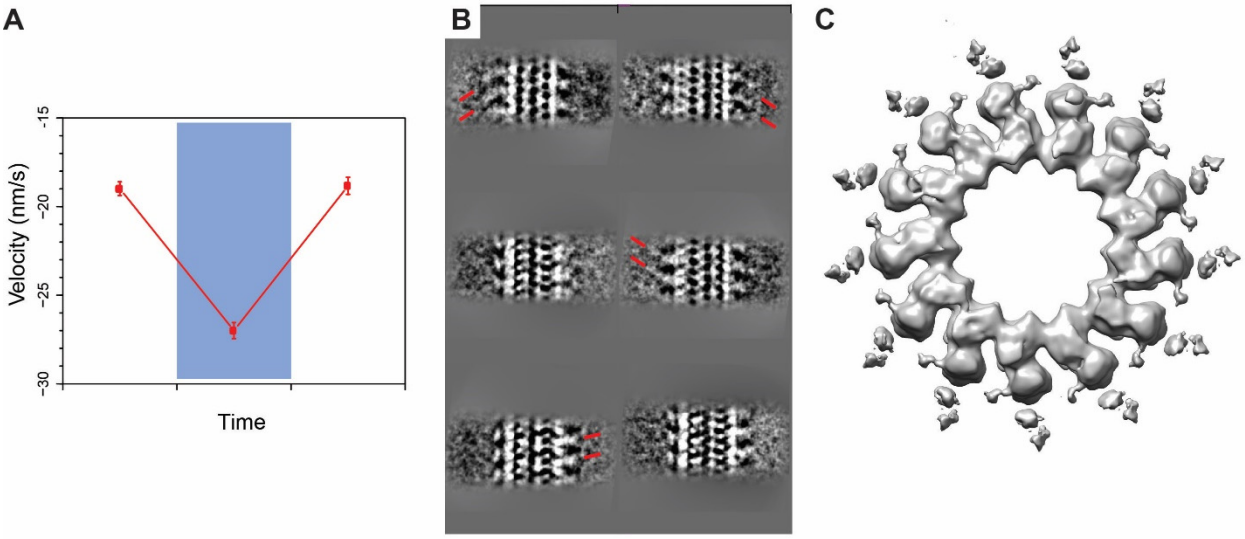

Figure 3-4 LOVKin2 function and visualization
A) Velocity for LOV2 in the dark (short lever arm, white regions) and blue light (long lever arm, blue region) showing increase in velocity. **B**) Class averages for microtubules decorated with LOVKin2. Red lines show lever arm extensions, which are not present in all class averages. **C**) Top view of the 3D reconstruction of a LOVKin2 decorated microtubule. Heterogeneity in the lever arm conformation resulted in blurred desenties for the lever arm. Adpated from Nakamura, 2014.

motor (Figure 3-4A). While the velocity measurements confirm the motor design functions as anticipated, we were unable to confirm the position of the lever arm. Attempts to look at the pre-stroke state were unsuccessful, similar to the Ncd-1R and Ncd-2R. Class averages of microtubules decorated with LOVKin2 in the post-stroke, dark state are shown in Figure 3-4. These class averages do not show the lever arm in a consistent position, suggesting that it is more flexible than the Ncd-1R or Ncd-2R constructs. In the 3D reconstruction, the tubulin and Ncd catalytic domain appear normal, but there is extra density surrounding the Ncd catalytic domain. This is mostly likely due to the lever arm adopting numerous conformations on the microtubule. However, the motor remains productive and performs as designed.

In future applications of this work, genetically encoded light-responsive motors may expand the optogenetics toolkit, complementing precise perturbations of ion channels (Boyden, Zhang, Bamberg, Nagel, & Deisseroth, 2005) and intracellular signaling (Toettcher et al., 2011) with spatiotemporal control of cytoskeletal transport and contractility. Light-activated control of molecular motors will also enable new synthetic approaches in cell biology (Goodman et al., 2012).

4 Chapter 4: Structural and functional differences between yeast and mammalian microtubules

During my graduate work, direct electron detectors became available, resulting in a dramatic resolution improvement for all reconstructions. The resolution for microtubule reconstructions went from 8-9 Å to better than 4 Å, allowing for descriptions of the atomic interactions within microtubules. The improved resolution motivated in part the decision to study yeast tubulin because it became possible to study tubulin mutants at near atomic resolution within the microtubule lattice. This allows for directly testing of molecular mechanisms related to dynamic instability and drug binding.

In addition to the wild type yeast tubulin, the yeast mutants we investigated have a single amino acid substitution on helix H7 of β-tubulin near the core of the protein. The wild-type threonine at residue position 238 is replaced with an alanine or valine. The T238A/V mutants were supplied by the Rice research group, who has performed extensive biochemical characterization of these tubulins (Geyer et al., 2015). They reported increased stability of microtubules assembled from this tubulin, consistent previous reports (Machin et al., 1995), and found that this stability arose from a reduced catastrophe frequency and slower depolymerization rate. The increased stability is thought to result from a disconnection between the GTP hydrolysis and the normal structural changes that accompany this hydrolysis. The T238A/V mutants have no changes in their hydrolysis rates, but the αβ-tubulin heterodimer does not respond to hydrolysis in the same manner as WT, and is thought to retain the GTP conformation inside the lattice. Importantly, these mutations have been shown not to alter the assembly pathway, only the disassembly of microtubules. A T238V mutation results in a milder phenotype than T238A, but alters αβ-tubulin conformational dynamics in a similar manner.

Another characteristic of WT yeast tubulin is that it does not bind taxol, a drug commonly used to stabilize mammalian microtubules. To investigate differences in drug binding we used a yeast mutant harboring five mutations that conferred taxol binding (Gupta, Bode, Georg, & Himes, 2003). We also assembled WT yeast tubulin with epothilone-B, a drug that binds the same site as taxol and is thought to work through a conserved mechanism to stabilize microtubules (Bollag et al., 1995). Here I report the results of our comparisons between yeast and mammalian microtubules.

We performed reconstructions of yeast microtubules under various polymerization conditions. This included assembly into dynamic microtubules, microtubules stabilized using the slowly hydrolysable analogues GMPCPP and GTPγS, and drug stabilized microtubules. Remarkably, GTPγS yeast tubulin readily polymerized using standard polymerization conditions. In contrast, mammalian tubulin polymerizes very poorly when bound to GTPγS and additional protein cofactors, such as EB, or changes in polymerization buffer are necessary to achieve robust polymerization. We also decorated the dynamic and GTPγS microtubules with Bim1 (the EB homolog in budding yeast) to investigate differences in plus-end tracking.

4.1 Yeast tubulin forms microtubules with protofilament distributions different to mammalian tubulin

The first parameter that we investigated under the different assembly conditions was the protofilament distribution, shown in Figure 4-1. We observed that the distribution for dynamic (GDP) yeast microtubules was different than that of mammalian microtubules. In the absence of a template or MAPs that would influence the polymerization process (as would be the normal case *in vivo*) mammalian microtubules form mostly 13 and some 14 protofilament microtubules when polymerized *in vitro* (Meurer-Grob et al., 2001; Wade, Chrétien, & Job, 1990). In contrast, the yeast tubulin formed mostly 12 protofilament microtubules. Interestingly, the yeast GMPCPP microtubules were mostly 13 protofilaments, also one protofilament less for the dominant number compared to mammalian microtubules that form mostly 14 protofilaments in this state. However, this trend is not consistent, particularly for the T238A mutant dynamic microtubules, which gave a distribution more like the mammalian distribution. This mutant has identical residues at the lateral contacts to the WT, so it is unlikely that specific amino acid differences at the lateral contacts explain the differences in protofilament numbers. The addition of Bim1 to the dynamic and GTPγS microtubules, which were also mostly 12 protofilaments, moved the distribution to 13 protofilaments. Previous studies have indicated a preference of plus-tip tracking proteins for a 13 protofilament lattice (des Georges et al., 2008; Maurer, Fourniol, Bohner, Moores, & Surrey, 2012; Zhang et al., 2015). However, these previous experiments were done under co-assembly conditions where the plus-tip tracking protein was present during microtubule assembly. Here, for the GTPγS state, the microtubules were first polymerized, then placed on the grid and washed with Bim1, giving the same end result. The observation that the microtubule lattice could rearrange relatively quickly (around 1 minute between first exposure to Bim1 and vitrification) to accommodate the Bim1 in these experiments suggests that the 12 protofilament GTPγS lattice is robust to transient

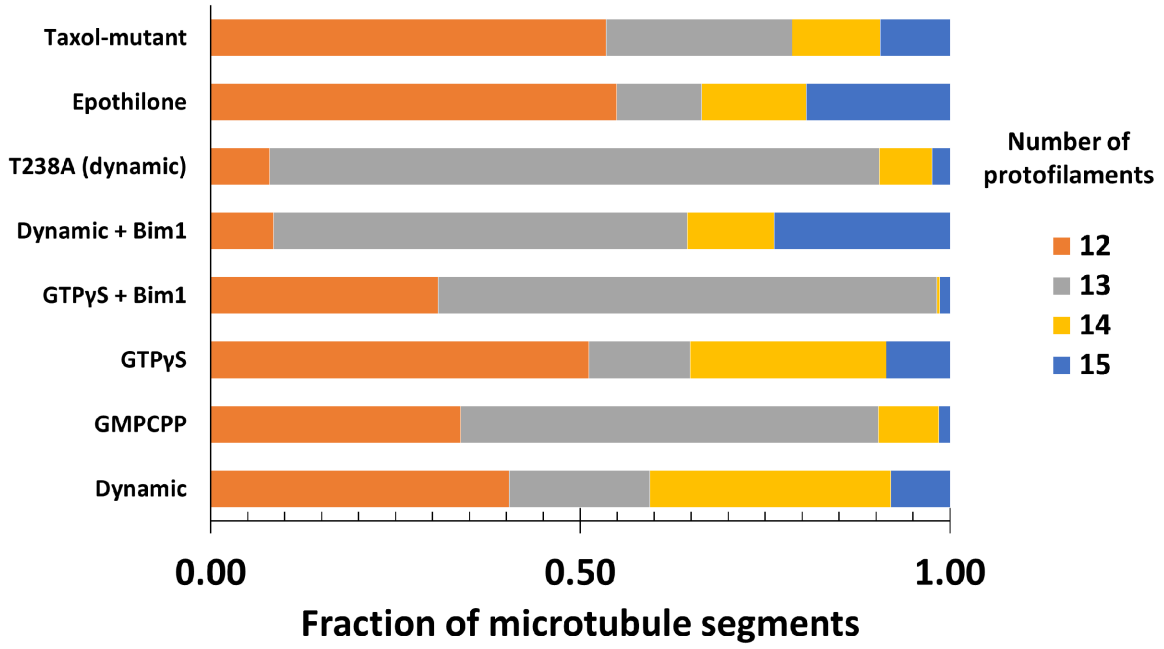

Figure 4-1 Protofilament distribution of yeast microtubules.
Fraction of microtubule segments for each number of possible protofilaments after sorting raw particles using multi-model refinement.

defects that must occur during the transition from 12 to 13 protofilaments, It is unlikely that the microtubules underwent a cycle of depolymerization and polymerization to change the protofilament number, as the tubulin concentration drops below the critical concentration immediately upon addition of Bim1. However, for dynamic microtubules, it is necessary to always keep the tubulin concentration above the critical concentration, so it is likely that some fraction of the microtubules we observed were polymerized in the presence of Bim1. The addition of drug, either taxol or epothilone, biased the protofilament distribution further towards 12 protofilament microtubules. This effect is consistent with previous observations of mammalian microtubules (Andreu et al., 1992; Meurer-Grob et al., 2001) and in the acetylation studies (see section 2.1).

We then looked more in detail at the lattices and measured their helical parameters. Microtubule lattices may be characterized by the following set of parameters.

- Rise: translation along the microtubule axis between protofilaments, or the offset between protofilaments
- Twist: angular spacing between protofilaments
- Dimer twist: the angular spacing between αβ-tubulin heterodimers along a single protofilament, or supertwist
- Dimer size: length of the tubulin heterodimer size measured parallel to the microtubule axis

The results are shown in Table 2.

Table 2 Summary of the lattice states and resolution for each reconstruction

Tubulin State	Rise (Å)	Twist (°)	Dimer twist (°)	Dimer size (Å)	Res. (Å)[b]
12 protofilaments					
Dynamic	10.427	-29.856	1.156	83.310	3.6
GTPγS	10.297	-29.883	0.939	82.110	5.7
GTPγS + Bim1[a]	10.311	-29.895	0.854	81.921	~7.5
Epothilone	10.432	-29.873	1.011	83.348	4.0
Taxol-mutant	10.409	-29.870	1.028	83.112	3.9
13 protofilaments					
Dynamic	9.651	-27.644	0.432	83.325	4.1
Dynamic + Bim1[a]	9.651	-27.696	0.070	82.290	~15
GMPCPP	9.651	-27.658	0.340	83.230	4.0
GTPγS + Bim1[a]	9.432	-27.694	-0.009	82.030	~5.0
T238A	9.550	-27.643	0.423	82.510	3.7

[a] These data did not have a dimer marker, resulting in the averaging of α- and β-tubulin.
[b] Resolution estimated from FSC curves at 0.143 correlation coefficient

Remarkably, the dynamic reconstruction revealed that the yeast heterodimer was approximately 83 Å in length (see Table 2), a size associated with an extended tubulin heterodimer (Alushin et al., 2014; Hyman, Chrétien, Arnal, & Wade, 1995; Zhang et al., 2015) previously observed in stabilized lattices. The T238A dynamic lattice had a similar, expanded heterodimer size as did the drug-stabilized lattices and those with the slowly hydrolysable analogue GMPCPP. This is different than what has been observed for the mammalian microtubules, where the GMPCPP-bound tubulin is extended by approximately 1.5 Å with respect to the GDP bound tubulin (Zhang et al., 2015). The addition of Bim1 results in lattice compaction, resembling the EB-bound mammalian lattice (Zhang et al., 2015). The GTPγS lattice is compacted by

approximately 1.2 Å with respect to the dynamic lattice. Difficulties in assembling the GTPγS mammalian microtubule without the addition of EB made it difficult to discern if the compacted GTPγS lattice observed was due to the nucleotide or the bound EB. Here we can confirm that the compaction is due to the nucleotide. Addition of Bim1 further compacts the lattice slightly, but most of the compaction comes from the nucleotide.

A general feature of 12 protofilament microtubules is the greater twist of the protofilaments, as measured by dimer twist, to accommodate microtubule closure. This results in the seam location not running parallel to the axis of the microtubule. A dimer twist value of zero would mean all the protofilaments run parallel to each other. 13 protofilament microtubules have much less dimer twist than 12 protofilament microtubules regardless of the lattice state. Comparing the dynamic (unstabilized) lattice to GTPγS or GMPCPP lattices of the same protofilament number, we observe a reduction in dimer twist, with the protofilaments adopting a straighter conformation in the stabilized states. Addition of Bim1 results in a dramatic reduction in dimer twist for the 13 protofilament microtubules, for both the GTPγS and the GDP. For mammalian microtubules, the addition of EB introduces a modest dimer twist (Zhang et al., 2015), a change in the opposite direction to what is observed here. However, the binding pattern of Bim1 to yeast microtubules is different (see section 4.3) precluding direct interpretation of this result. The addition of either drug relieves some of the dimer twist compared to the dynamic state, but not to the same extent as the GTP analogues.

4.2 Hydrolysis in the yeast microtubule lattice is slower

Given the striking result that the yeast lattice is not compacted, we performed a high resolution reconstruction of the yeast dynamic lattice to investigate the structural origins of this feature. The final resolution for this reconstruction is 3.6 Å. Close inspection of the density revealed extra density for the nucleotide in the E-site of the yeast tubulin heterodimer when compared to a mammalian heterodimer (see Figure 4-2). This density indicates that there is likely a mixture of GDP and GTP at the E-site. The residual GTP may account for the lattice remaining expanded. The fact that the lattice remains expanded when there is a mixture of hydrolyzed and non-hydrolyzed GTP nucleotide could indicate that lattice compaction is a cooperative event. The accommodation and rearrangements within the lattice may require neighboring tubulin heterodimers to also conform, and that resistance to compaction by a minority of tubulin heterodimers is sufficient to prevent the surrounding lattice from compacting. Residual GTP has been reported in the MT lattice assembled from mammalian tubulin (Dimitrov et al., 2008). This fraction is higher in yeast (Dougherty, Himes, Wilson, & Farrell, 1998) and would be consistent with reports of less GTPase activity and slower depolymerization of yeast MTs (Davis et al., 1993). Another possibility is that the yeast compacted lattice is much less stable than the mammalian lattice, and that the lifetime of this lattice is too short for us to capture on the EM grid. The T238A mutant also shows similar GTP/GDP mixture in the lattice based on the similarity between the densities for the nucleotide at the N- and E-sites. However, the expanded lattice and density that we observe are not consistent with direct measurements of the GTP content of the lattice which shows that it was significantly lower than for WT MTs (Geyer et al., 2015). It may be that the density observed in our reconstructions is from two molecules, GDP and inorganic phosphate, rather than a single GTP molecule. This would be consistent with the hydrolysis occurring, but the amount of material remaining in the nucleotide pocket staying constant.

We also investigated whether there were specific sequence differences around the nucleotide binding site that may explain the slower hydrolysis in yeast (see Figure 4-3). While there are many

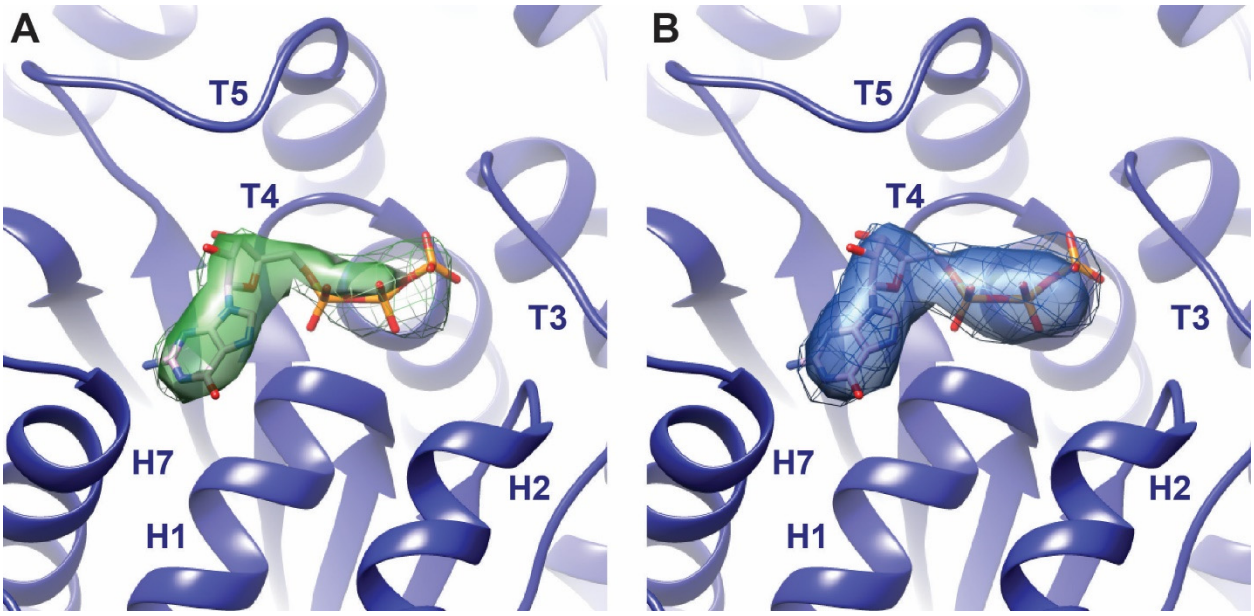

Figure 4-2 Extra density observed in the E-site of yeast microtubules
Segmented densities for the nucleotides in the (A) mammalian (Zhang, 2015) and (B) yeast WT dynamic reconstructions. The density for GDP in the yeast reconstruction is larger than expected, and appears to be a mixture of GTP and GDP.

differences most are conservative mutations. However, two substitutions may be significantly contributing to the observed behavior. A serine at position 98 on the T3 loop of β-tubulin is replaced by a glycine in mammalian, resulting in a slight enlarging of the binding pocket. Similarly, an asparagine at position 253 on H8 of α-tubulin is replaced by a threonine in mammalian tubulin, also creating more space for the nucleotide. Both of these residues are closest to the γ-phosphate. Together these mutations may allow for greater movement of the nucleotide, such that fluctuations between the proposed catalytic glutamic acid at position 254 on H8 of α-tubulin and the nucleotide lead to more efficient hydrolysis and inorganic phosphate release. However, further experiments would be needed to confirm this idea.

The resolution of our reconstruction allows for tracing the main chain of αβ-tubulin and for placing large side chains. However, it is not sufficient to unambiguously assign all rotamers, and there is still some error in the placement of the main chain. To incorporate previous knowledge about protein structure and to build the best possible atomic models we used Rosetta (DiMaio et al., 2015). Rosetta uses information from the Protein Data Bank (Berman et al., 2000) to predict likely conformations of amino acids fragments and then refines these conformations in the context of the atomic model and electron density using a highly developed scoring function. This scoring function ensures that only conformations with reasonable stereochemistry and hydrogen bonding networks are selected, while optimizing agreement with the density. An initial atomic model of an expanded mammalian tubulin heterodimer (Zhang et al., 2015) was first manually fitted into the dynamic density using Coot (Emsley, Lohkamp, Scott, & Cowtan, 2010). Residues were mutated to match the yeast sequence and regions of poor fit for the main chain were manually adjusted. To capture interactions between neighboring tubulin heterodimers, nine copies of this starting model were fit into the density to form a 3x3 lattice of heterodimers. This results in the central heterodimer having all the appropriate neighbors for forming contacts. The central heterodimer, and the eight copies, were then refined using Rosetta (DiMaio et al., 2015) keeping each copy

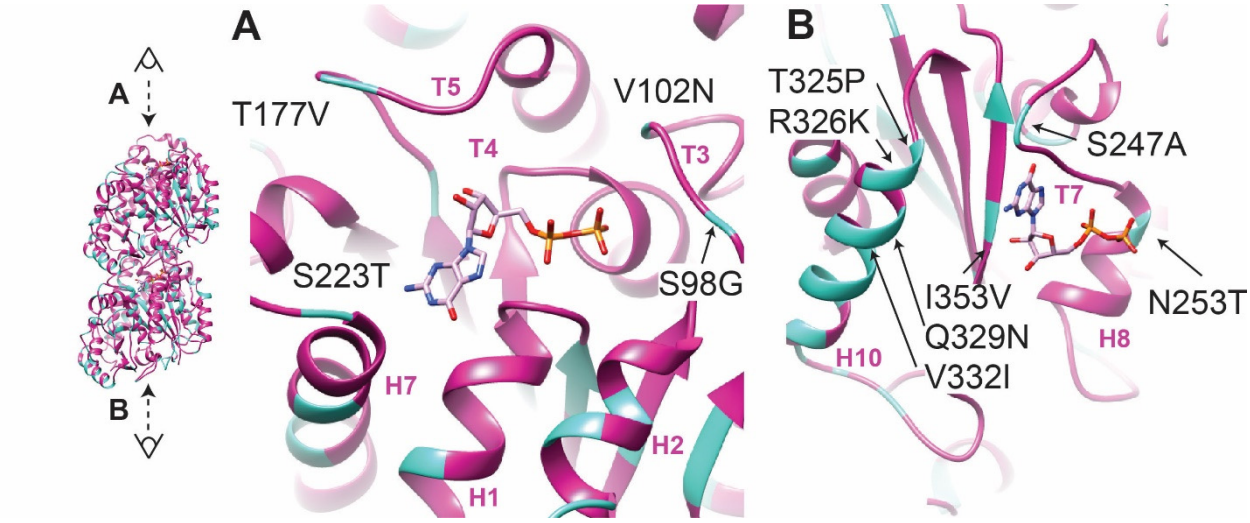

Figure 4-3 Conservation of residues around E-site
View of GDP-binding site from the plus-end (**A**) and minus-end (**B**) of the microtubule. Residues conserved between yeast and mammalian are shown in purple, mutated residues shown in torquise. Mutated residues within 7 Å of the nucleotide are labeled with the yeast amino acid identity, sequence position, and mammalian amino acid identity left-to-right.

identical. An ensemble of structures was generated to ensure sufficient sampling of possible solutions by Rosetta, which uses Monte Carlo sampling. The best structure from the ensemble of models was then subjected to minor refinements with Refmac (Brown et al., 2015) and minimization with Phenix (Adams et al., 2011) to ensure proper geometry of all amino acids and ligands.

To compare the atomic model of yeast αβ-tubulin with the mammalian αβ-tubulin, we aligned the models locally on the N-terminal domain of α- or β-tubulin and compared changes between residues only within the aligned monomer. This ensures that differences due to the refinement against a 12 (yeast) or 13 (mammalian) protofilament reconstruction do not account for the differences in the final models, but rather changes within the tubulin structure. Previous analyses of αβ-tubulin structures have demonstrated that the structure of the tubulin heterodimer itself does not vary greatly between microtubules of different protofilament numbers when comparing heterodimers taken from 13 of 14 protofilament reconstructions (Alushin et al., 2014; Zhang et al., 2015). We do not observe any significant differences between the expanded yeast αβ-tubulin and the expanded (GMPCPP) mammalian αβ-tubulin. The presence of both drugs slightly decreased the amount of twist within the heterodimer (see Table 1). This twist occurs around α-tubulin H8, as reported for previous mammalian reconstructions (Zhang et al., 2015), however the difference is more modest here. Given the high degree of sequence conservation between yeast and mammalian tubulin as well as the conservation of structural elements, it would be expected that motions within the molecule would use similar structural elements. We also refined an atomic model of the yeast tubulin mutant T238A in the dynamic state. Again, comparison of the atomic model with the WT model or with the mammalian model does not reveal any significant differences.

4.3 Bim1 binds microtubules within and between tubulin heterodimers

Plus-tip tracking in microtubules is thought to rely on differences in affinity of the end-binding (EB) protein for the different types of binding sites available on the microtubule lattice (Maurer, Bieling, Cope, Hoenger, & Surrey, 2011). Particularly, the GTP-cap of the microtubule is the favored binding site for EB proteins *in vivo*. Given that the dynamic lattice for yeast is still expanded and more closely resembles the tip, we reasoned that plus-tip recognition and tracking in yeast might have features that are distinct from the mammalian system. To investigate this, we assembled microtubules from GTPγS bound tubulin, and decorated them with a monomer construct of Bim1 that included only the N-terminal calponin homology (CH) domain that interacts with microtubules. A striking observation was that Bim1 bound to a noncanonical site within the tubulin heterodimer adjacent to the N-site, as well as to the canonical site adjacent to the E-site

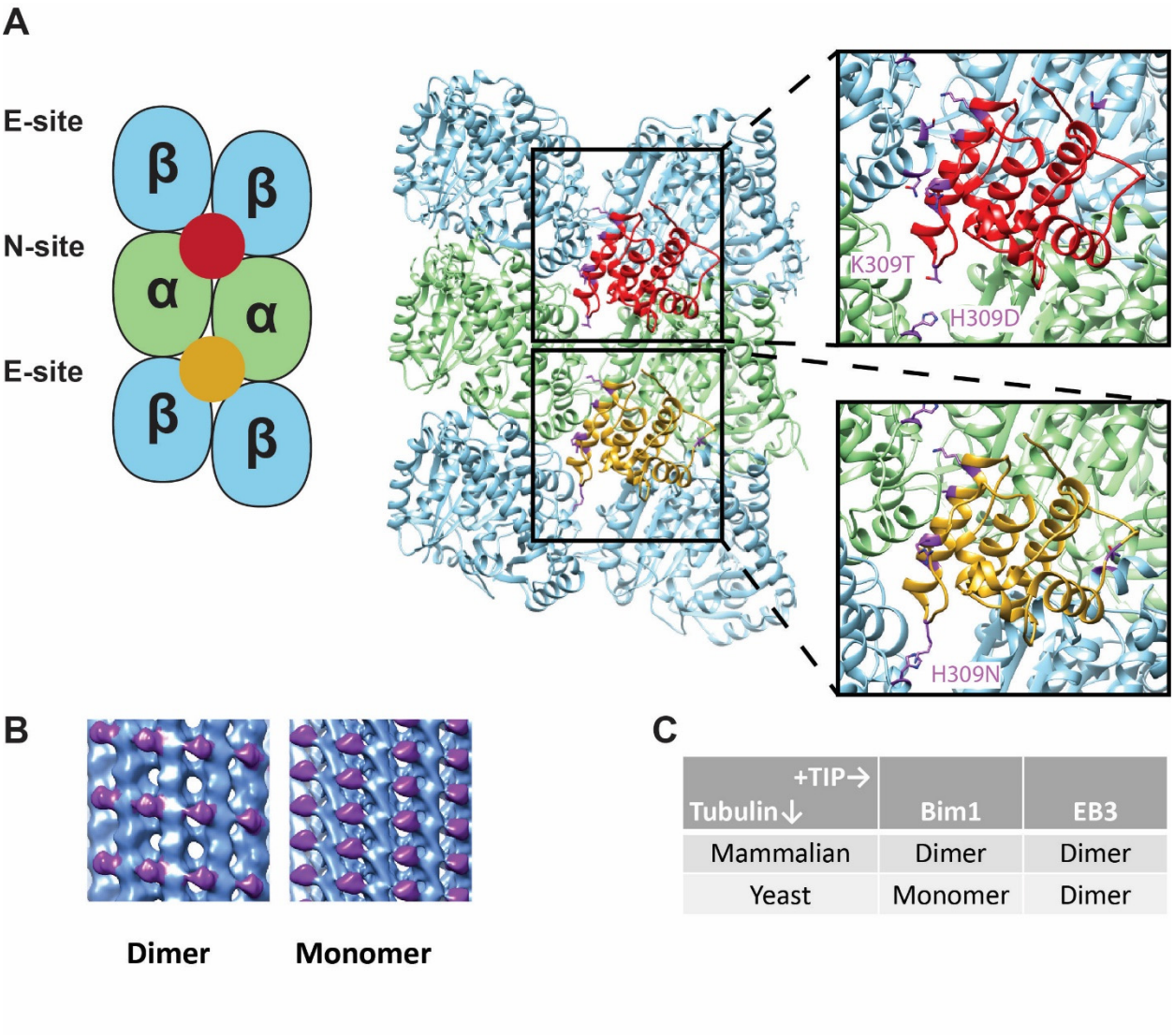

Figure 4-4 Bim1 binds to a noncanonical site
(A) Comparison between the canonical (gold) and noncanonical (red) sites. All mutated residues shown in purple, major mutations labeled. B) Possible decoration patterns for +TIP tracking protein on MT lattice. C) Observed decoration patterns for combinations of +TIP and tubulin sources.

(see Figure 4-4B). Previous studies using Mal3 (the plus-tip tracking protein from fission yeast) or EB3 on mammalian microtubules, had not resulted in any detectable binding to the noncanonical site. The previous studies and ours both used an excess of the plus-tip tracking protein to maximize the occupancy of Bim1 on the lattice (Maurer et al., 2012; Zhang et al., 2015).

To investigate whether binding at this second site was the result of sequence differences between the tubulins or the plus-tip tracking proteins, we prepared grids of mammalian microtubules decorated with Bim1 and yeast microtubules decorated with EB3, all with GTPγS lattices (see Figure 4-4B-C). We find that only Bim1 on yeast microtubules binds at the noncanonical site. Using the mammalian atomic model of EB3 bound to tubulin (Zhang et al., 2015), we compared the canonical and noncanonical sites by aligning β-tubulin with α-tubulin to place the CH domain at the noncanonical site. Using a 4 Å distance cutoff between tubulin and the CH domain, we then identified residues at the noncanonical site that might participate in binding

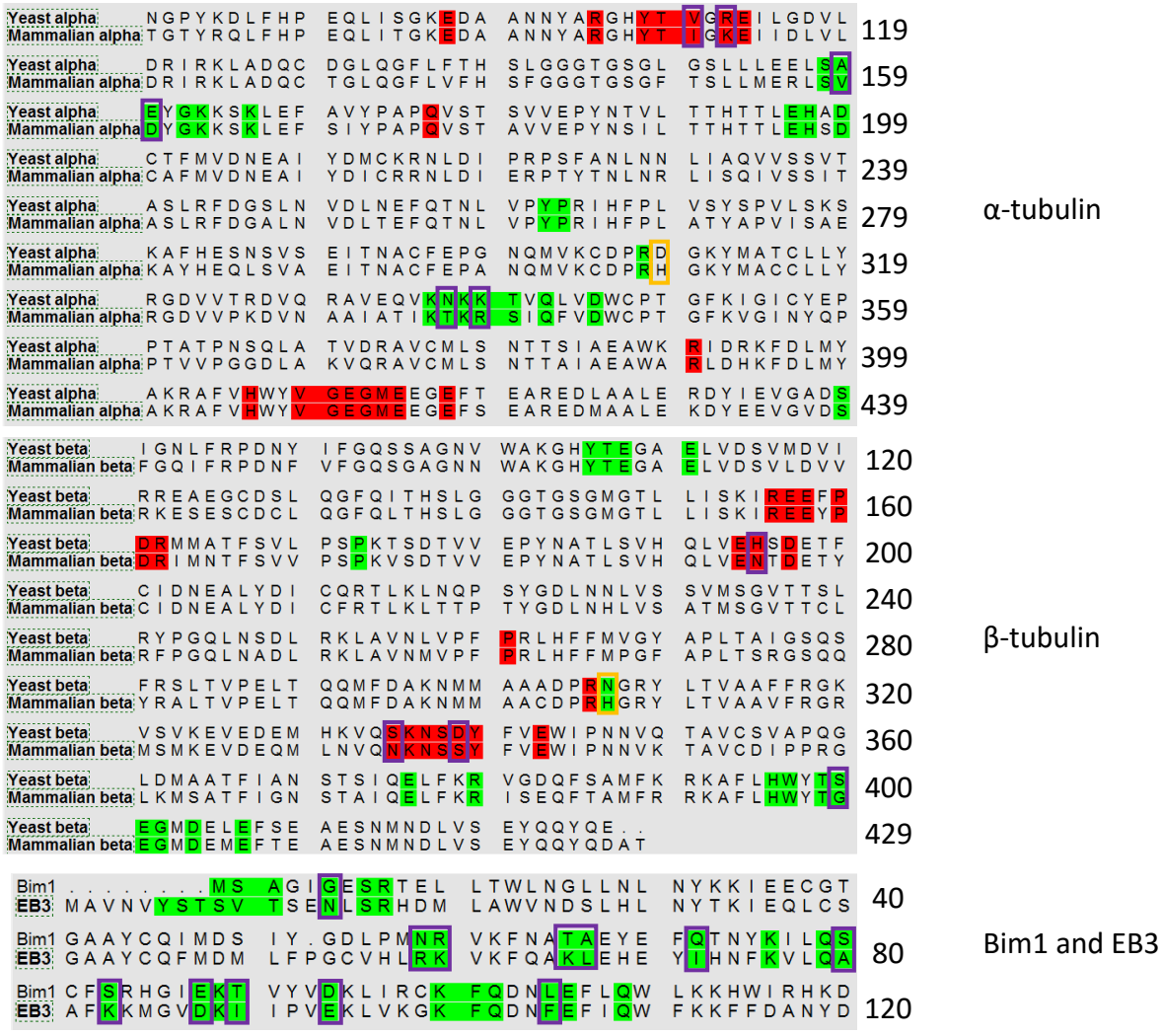

Figure 4-5 Sequence alignments for yeast & mammalian tubulin and Bim1 & EB3
Residues involved in canonical site binding shown in green, noncanonical site in red. Mutations are shown with purple boxes. The two histidine residues that are lost in yeast and thought to contribute significantly to noncanonical site binding are boxed in yellow.

to the CH domain. Looking at the sequence differences between yeast and mammalian tubulin surrounding the two binding sites, we observed that there are only minor changes on α-tubulin (see Figure 4-5) and that most of the differences are in β-tubulin. There is a replacement of a histidine residue on β-tubulin at residue 309 in mammals with asparagine in yeast that is mirrored on α-tubulin by the replacement of H309 in mammals with aspartic acid in yeast. However, given that EB3 does not bind at the noncanonical site on yeast microtubules, the changes in tubulin sequence alone are not sufficient to explain the additional binding. In EB3, K66 would interact with β-tubulin H309, however in Bim1 this position is a threonine. This, and other sequence differences between Bim1 and EB3 must also contribute to the additional binding. The extra binding at the noncanonical site results in a loss of the αβ-tubulin heterodimer marker, making it difficult to separate α- and β-tubulin during the reconstruction process. Consequently, in our final density map, α- and β-tubulin are averaged together making it impossible to distinguish the two Bim1 binding sites and visualize which residues on Bim1 are in fact making contacts at the noncanonical site.

Binding at a noncanonical site may be the result of using an unnatural nucleotide that altered the available binding sites in an unexpected way. To more closely replicate the *in vivo* state, we decorated dynamic yeast lattices with Bim1. Trapping this state for visualization was challenging due to the lack of dynamic microtubules in the presence of Bim1 when following standard protocols. We interpret this as Bim1 promoting rapid depolymerization of the microtubules. Sample preparation had to be extensively optimized to capture decorated microtubules in vitreous ice on the EM grid. By decreasing the molar ratio of Bim1:tubulin from 5:1 to 2:1, and vitrifying the sample with one minute allowed us to capture some decorated microtubules. The relatively small dataset for this state caused by the difficulty in preparing these samples contributed to the lower resolution. However, we still observed binding at the noncanonical site and compacted lattice in the presence of Bim1.

The fact that the dynamic yeast lattice is normally expanded, but compacts in the presence of Bim1, supports the idea that this protein promotes hydrolysis (Zhang et al., 2015). This also fits with the rapid depolymerization of the dynamic microtubules observed when preparing these samples. It would be interesting to test if the T238A mutant compacts with the addition of Bim1, and if it also exhibits the same rapid depolymerization. This would provide information about whether the mutation directly inhibits compaction or disrupts the allosteric network within tubulin.

The grids of Bim1 decorated microtubules were prepared with a molar excess Bim1 which is the reverse of the ratio found *in vivo*, where tubulin is roughly 2-fold excess of Bim1 for yeast (Ghaemmaghami et al., 2003). In mammalian cells, the excess of tubulin over end-binding proteins is even greater (Ingolia, Lareau, & Weissman, 2011; Schwanhäusser et al., 2011), reflecting the broader range of microtubule functions in mammalian cells and that much of the tubulin would be stabilized in non-dynamic microtubule assemblies. The ability of plus-tip tracking proteins to recognize the growing end of a microtubule relies on a greater affinity of the plus-tip tracker for the end of the microtubule than the rest of the lattice. However, a reduced differential in affinity for the different possible binding sites on the lattice may improve the ability of Bim1 to remain associated with the tip of the microtubule. Depending on what other cellular factors are also recruited to the plus-tip, increased lifetime at the tip may be more important than errors from recruiting a protein to the lattice instead of the tip for yeast.

4.4 Yeast tubulin oligomers in solution are longer and straighter than mammalian tubulin oligomers

The dynamic instability behavior of microtubules depends on fluctuations and transitions of αβ-tubulin both within the lattice and in the solution state. Based on our results, the lattices for yeast and mammalian microtubules are quite similar and do not explain the differences in dynamic instability, or the increased stability of the T238A mutant. We hypothesized that the differences may therefore be a result of changes outside of the lattice.

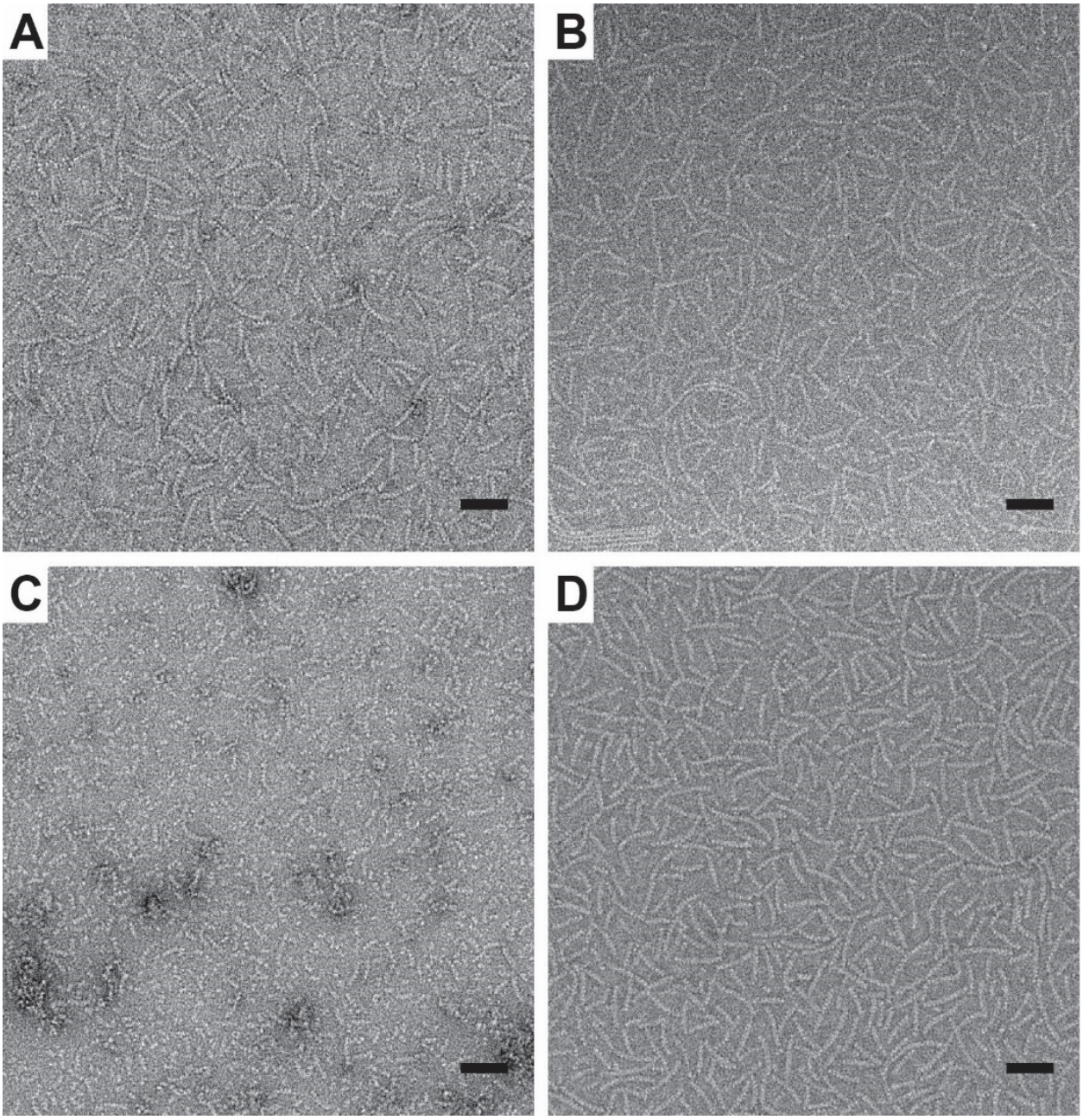

Figure 4-6 Oligomers formed by tubulin before polymerization
(**A**)Yeast WT, (**B**) T238A, (**C**) mammalian WT, and (**D**) T238V oligomers. Scale bar in A-D is 50 nm.

To investigate the behavior of soluble tubulin, we visualized tubulin oligomers under conditions favorable for polymerization, i.e., excess GTP and at tubulin concentrations above the critical concentration, but kept the temperature low to inhibit polymerization. These oligomers were visualized by negative stain and are shown in Figure 4-6. The WT yeast oligomers appeared straighter and longer than the mammalian oligomers. The differences between WT and T238A or T238V mutant tubulin were less dramatic. The mutant yeast tubulin looked similar to the WT yeast tubulin oligomers, but were even longer and straighter, and were more likely to self-associate.

To quantify these differences we manually traced oligomers from the micrographs and measured their length and curvature. We find that the mammalian oligomers are generally shorter than the yeast, and most frequently have 5 heterodimers bound together. WT yeast tubulin has 6

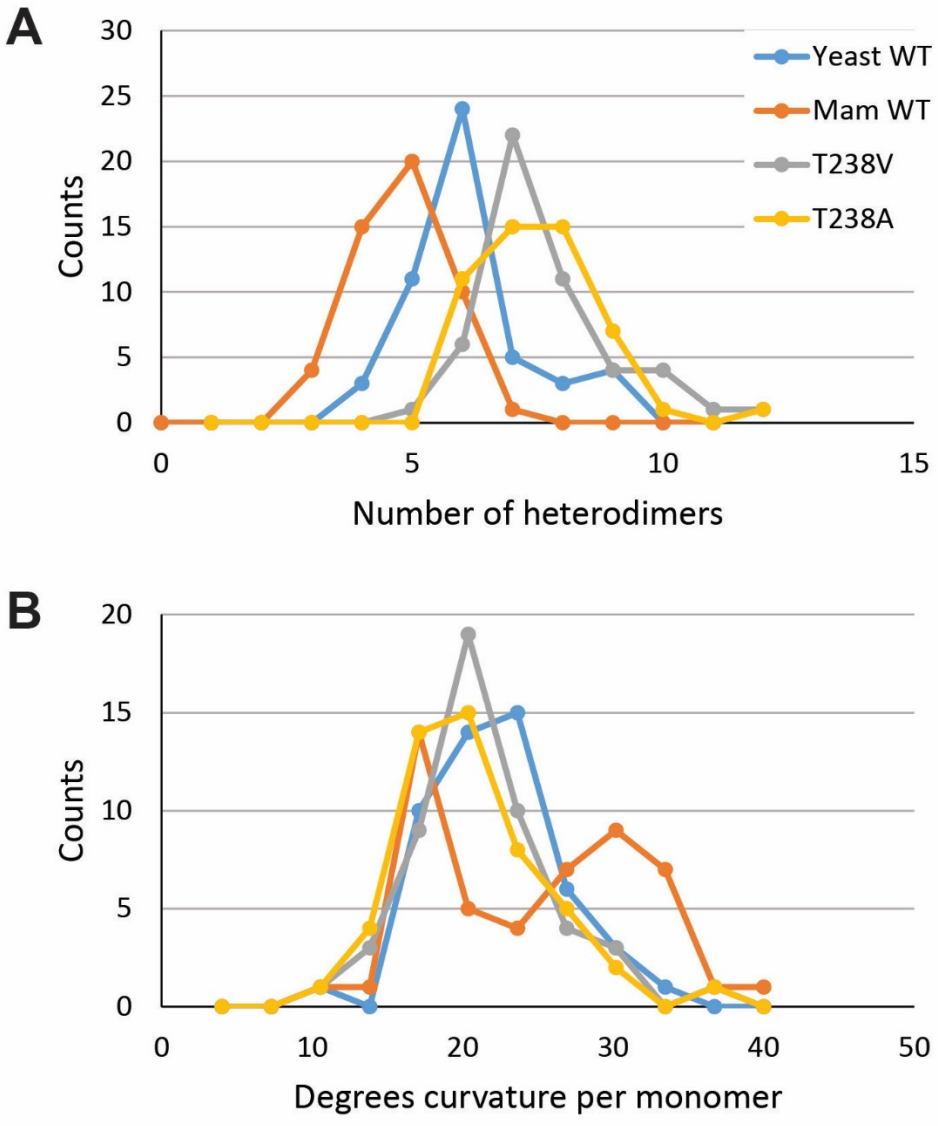

Figure 4-7 Quantification of tubulin oligomers
Quantification of the oligomer length (A) and curvature (B) show that yeast oliogmers are longer and straighter than mammalian. Interestingly, the mammalian oligomers show a second peak with higher curvature.

heterodimers most often, and the yeast mutants T238A/V have 7 (see Figure 4-7A). The curvature for the yeast oligomers has a single peak that is similar to what we observed for the mammalian oligomers, around 20°. Intriguingly, the mammalian oligomers have an additional peak near 30° which constitutes a significant portion of the oligomer population (see Figure 4-7B). This second peak may correspond to oligomers that have hydrolyzed the GTP.

There have been conflicting reports about what the functional unit of soluble tubulin is, both for nucleating and elongating a microtubule. Nucleation is energetically less favorable than elongation, as demonstrated by the lag phase during microtubule polymerization. However, once a nucleus exists, it is still not clear what is actually added to the growing tip of a microtubule. Data

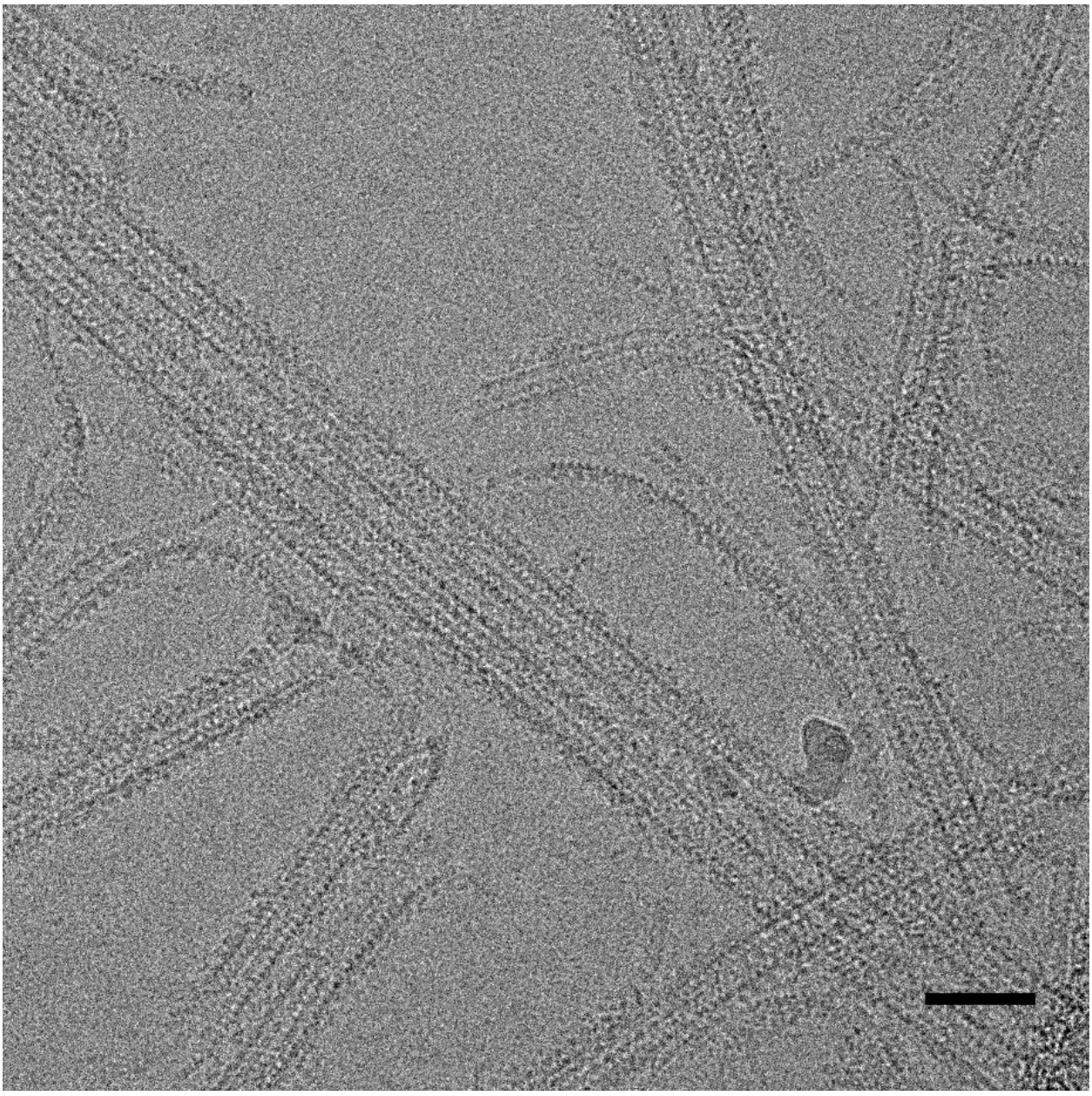

Figure 4-8 Long extensions observed with dynamic yeast microtubules
Examples of long extensions of tubulin from the ends of microtubules and free in solution. Many of these appear to be more than one protofilament. Scale bar 50nm.

exists for adding multiple tubulin heterodimers (Kerssemakers et al., 2006) and single heterodimers (Schek, Gardner, Cheng, Odde, & Hunt, 2007). Given that yeast oligomers are longer and straighter than mammalian oligomers, and that the critical concentration for these microtubules is lower, our data would support the idea that larger oligomers support the nucleation of microtubules. These larger oligomers would also account for the slower the elongation rates measured for yeast microtubules due to increased diffusion time to the tip of the microtubule (Davis et al., 1993). These stable oligomers would also explain the slower depolymerization rates, as heterodimers are less likely to dissociate from the microtubule. Consistent with this we frequently observe long extensions off the ends of dynamic yeast microtubules (see Figure 4-8) that are extremely rare when imaging mammalian dynamic microtubules.

The GTPase activity of unassembled tubulin is not zero and depends on tubulin concentration (Heusèle & Carlier, 1981; Wang, Cormier, Gigant, & Knossow, 2007). Previous reports of GTPase activity of non-assembled tubulin have shown yeast and mammalian tubulin to have similar rates (Davis et al., 1993). However, these experiments were carried out at tubulin concentrations much lower (0.2-0.7 μM) than used here (3-5 μM). At higher concentrations, it is expected that there is greater oligomerization and an increased opportunity to hydrolyze the GTP. The lack of a structural transition between non-hydrolyzed and hydrolyzed states of the yeast microtubule lattice parallels the single curvature peak for the oligomers of yeast tubulin. In contrast, the mammalian oligomers show two distinct curvature states where it is likely that the straighter oligomers have not hydrolyzed the GTP, and the more curved oligomers have hydrolyzed but not exchanged the GDP for GTP yet. Previous reports have indicated that near limiting concentrations of tubulin, GMPCPP bound yeast tubulin elongates less readily than GTPγS bound tubulin (Geyer et al., 2015). Future studies may look at the effect on nucleotide state on the length and curvature distribution of oligomers as a function of nucleotide state.

The high level of conservation between yeast and mammalian tubulin (amino acid sequences approximately 75% identical and 81% similar between yeast and mammals) and their conserved structural folds leads to the prediction that these proteins would have very similar behaviors. This prediction is strengthen by noting that most of this variation occurs on the unstructured C-terminal tails of tubulin where it would impact binding to MAPs, rather than contributing to changes within the microtubule. However, we find that these modest residue changes in the structural parts of the protein lead to important differences in the microtubule. In the absence of cellular factors, the yeast dynamic lattice remains expanded and forms mostly 12 protofilament microtubules. We also find that Bim1 binds within heterodimers. It is also likely that these amino acid changes alter the conformational fluctuations available to tubulin. This may explain why hydrolysis is slower in the yeast lattice.

5 Chapter 5: Structure of PRC1 bound to the microtubule

A collaboration between our laboratory and the Kapoor research group at Rockefeller University was started to look at mammalian tubulin mutants that had altered dynamic instability parameters. It was observed that these mutants bound PRC1 with much reduced affinity. Previous reports from the Kapoor laboratory had identified the approximate binding location (Subramanian et al., 2010) for PRC1 on microtubules. To better understand this interaction we decided to pursue a high resolution reconstruction of PRC1 bound to microtubules. This work was done with Elizabeth Kellogg, a postdoctoral researcher in the Nogales group.

The function of PRC1 is to crosslink and stabilize anti-parallel microtubule arrays to help form the mitotic spindle. The need to bind two microtubules is achieved by PRC1 being a homodimer with a single microtubule binding region. Previous studies have identified the dimerization domain of PRC1 to be in the N-terminal domain, and the primary microtubule binding region to rely on a set of conserved residues within the spectrin domain in the middle of the protein (Mollinari et al., 2002; Subramanian et al., 2010; Subramanian, Ti, Tan, Darst, & Kapoor, 2013). The C-terminal domain, which is predicted to be unstructured, was also found to contribute to the microtubule binding activity (Subramanian et al., 2010). The specific contacts made between the microtubule and PRC1 were unclear. Here we report a cryo-EM reconstruction of a PRC1 construct containing the spectrin domain and the full C-terminal domain bound to microtubules at near atomic resolution. The quality of the resulting cryo-EM reconstruction allows us to explain, in atomic detail, the key interactions between PRC1 and the microtubule surface.

5.1 PRC1-tubulin interactions

Full-length PRC1 consists of three domains: a dimerization domain, a spectrin domain, and a C-terminal domain (Figure 5-1A). We chose to focus on a construct consisting of only the spectrin and C-terminal domains (PRC1-SC) (see Figure 5-1A) in order to elucidate the binding mode of PRC1 on the microtubule surface. Eliminating the dimerization domain reduced the formation of microtubule bundles that would have precluded high-resolution cryo-EM analysis. Class averages display clear density corresponding to PRC1-SC extending from the microtubule surface on every tubulin heterodimer (Figure 5-1D). We generated a reconstruction with an overall resolution of 4 Å. The final density map, shown in Figure 5-1B and E, clearly shows high-resolution features corresponding to α-helical register (Figure 5-2A), β-strand separation (Figure 5-2B), and sidechain densities for larger amino acids (Figure 5-2C), as expected for a near-atomic resolution cryo-EM map. However, local resolution estimates (Figure 5-1C) indicate that while the resolution of tubulin is between 3-4 Å, the resolution for the SC-PRC1 molecule is in the range of 3.8-5 Å. This lower resolution is likely due to two contributing factors: (1) PRC1 does not appear to fully decorate the microtubule lattice in our images (i.e. it is substoichiometric with respect to tubulin), as our layer-line analysis estimates PRC1 occupancy to be about ~57% of all possible microtubule binding sites (see Figure 5-3); and (2), PRC1 appears to be flexible. While the local resolution for PRC1 is highest at the point of interaction with tubulin (3.8 Å), it is noticeably lower near the N and C-termini (5-6 Å).

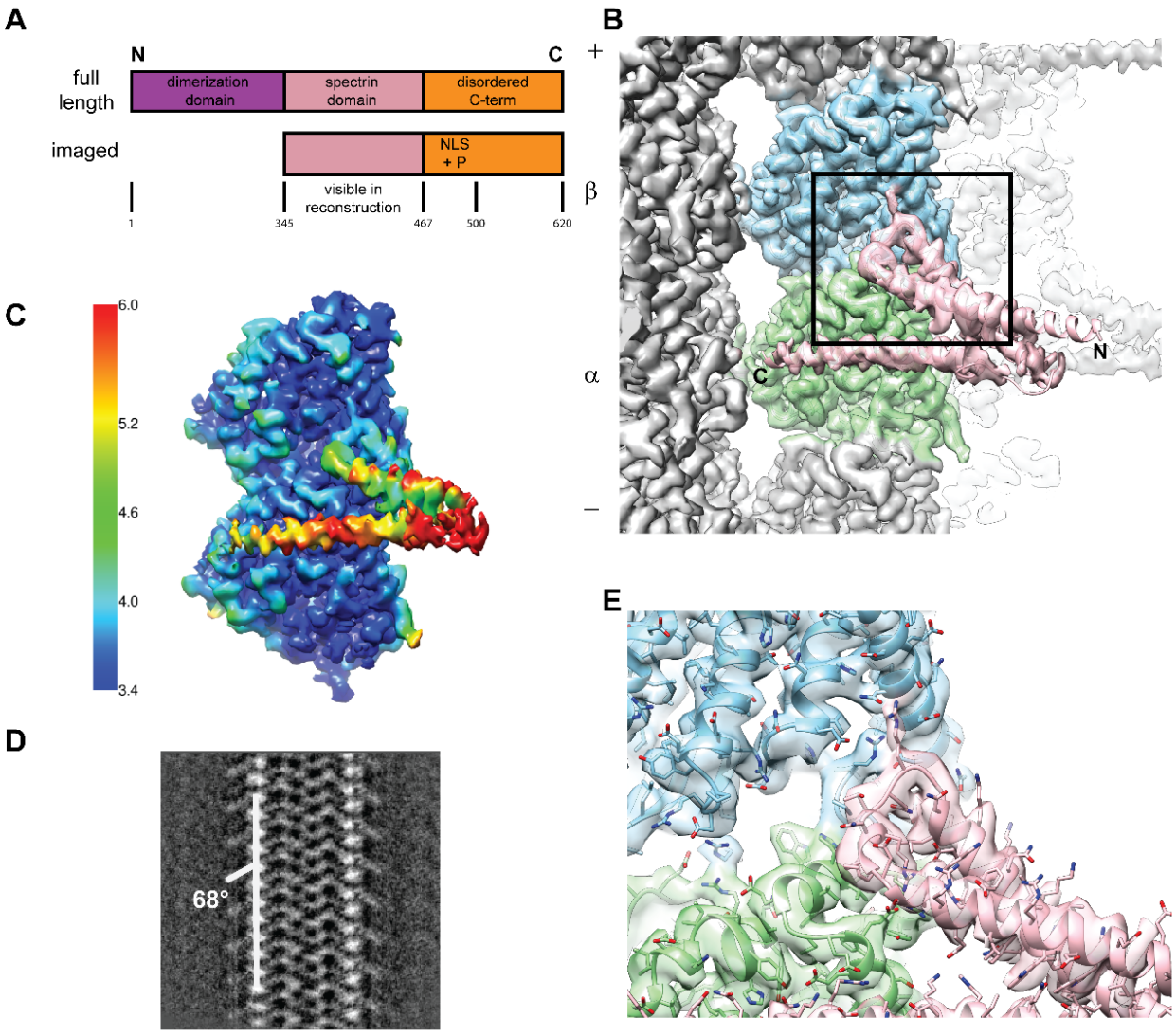

Figure 5-1 The spectrin domain of PRC1 is resolved to 4 Å

A) Domain structure of PRC1. Residues 470-500 contain the nuclear localization signals (NLS) and phosphorylation sites (P). (**B**) Side view of the MT showing bound PRC1. Although the construct used contains both the spectrin-domain and C-terminal domain, only the spectrin (residues 377-464) is visible in the cryo-EM reconstruction. (**C**) Local resolution estimation for the PRC1 and tubulin dimer. (**D**) 2D class average showing the angle between the spectrin domain and the MT wall. The spectrin domain makes a ~70 degree angle with respect to the microtubule surface. (**E**) Close-up of box in (**B**) The spectrin domain itself is well-resolved, showing clear density for large sidechains as well as backbone traces.

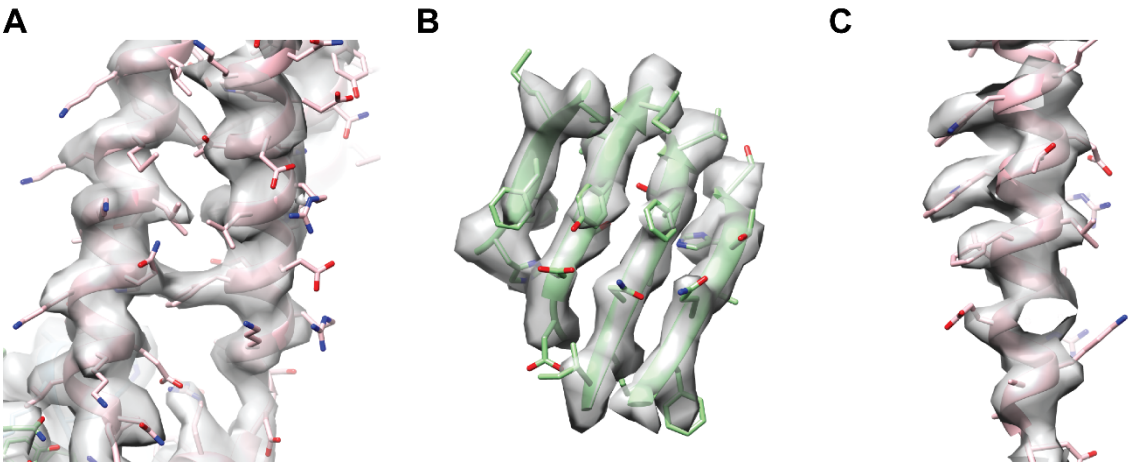

Figure 5-2 High-resolution features of the cryo-EM reconstruction
A & **C**) Helix 7 of PRC1 shows clear density for large aromatic sidechains as well as smaller hydrophobic sidechains **B**) β-strands are clearly separated and sidechain density is clearly visible.

The spectrin domain of PRC1 (PRC1-S) consists of a bundle of three helices, which we refer to as helices S-H7, S-H8, and S-H9, following previous nomenclature (Subramanian et al., 2013). The conformation of PRC1-S in our cryo-EM study corresponds very closely with previously reported crystal structures (Subramanian et al., 2010, 2013). The density for the C-terminal domain beyond residue 467 is not visible in our high-resolution map, even when low pass filtered to 10-20 Å, confirming previous predictions that PRC1's C-terminus is disordered even when bound to microtubules (Figure 5-1A). PRC1-SC adopts a well-defined binding-orientation on the microtubule; 2D class averages as well as the 3D reconstruction itself reveal that PRC1-SC makes an approximately 70 degree angle with the microtubule surface (68 +/- 2.5 based on the 3D reconstruction, see Figure 5-1D). Previous studies reported a 70 degree cross-bridge angle between antiparallel microtubules crosslinked by PRC1, however the resolution of the cryo-EM reconstruction was insufficient to assign this characteristic solely to the binding orientation of PRC1-S (Subramanian et al., 2010). Our present work at higher resolution indicates that the cross-bridge angle is defined by the orientation of the spectrin domain with respect to the microtubule lattice.

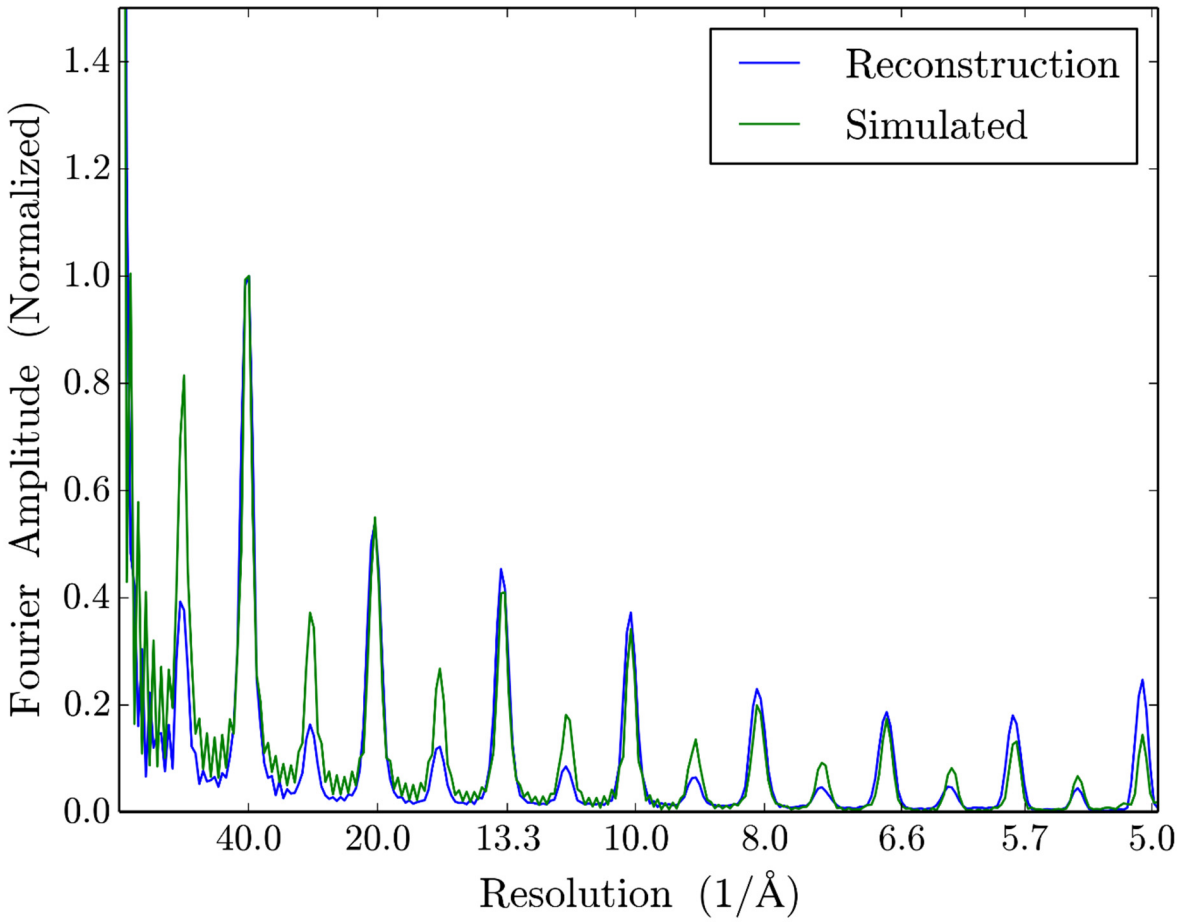

Figure 5-3 PRC1 occupancy estimation
Fourier amplitudes of the final reconstruction (blue) and the simulated map (green) used to estimate the PCR1 occupancy percentage. The simulated map was generated by docking the atomic model for tubulin-PRC1 into the final reconstruction for the whole microtubule. A simulated electron density map was then calculated using those atoms to compare with the final reconstruction. The PRC1 contributes primarily to the peak at 80Å, which is significantly lower for our reconstruction than the simulated map.

Our structure shows how the spectrin domain of PRC1 binds at the intra-dimer interface (between α- and β-tubulin within a single heterodimer) of tubulin on the microtubule surface. The main contacts involve the loop connecting the S-H7 and S-H8 helices (Figure 5-4A-B], but additional, crucial contacts are also made through S-H9 (Figure 5-4C). The loop between S-H7 and S-H8 was absent in previously determined crystal structures (Subramanian et al., 2010, 2013), suggesting that it only becomes ordered upon binding to the microtubule-lattice. This loop makes a number of contacts with the H12 helix in β-tubulin. Noticeably, R381 in PRC1-S interacts with

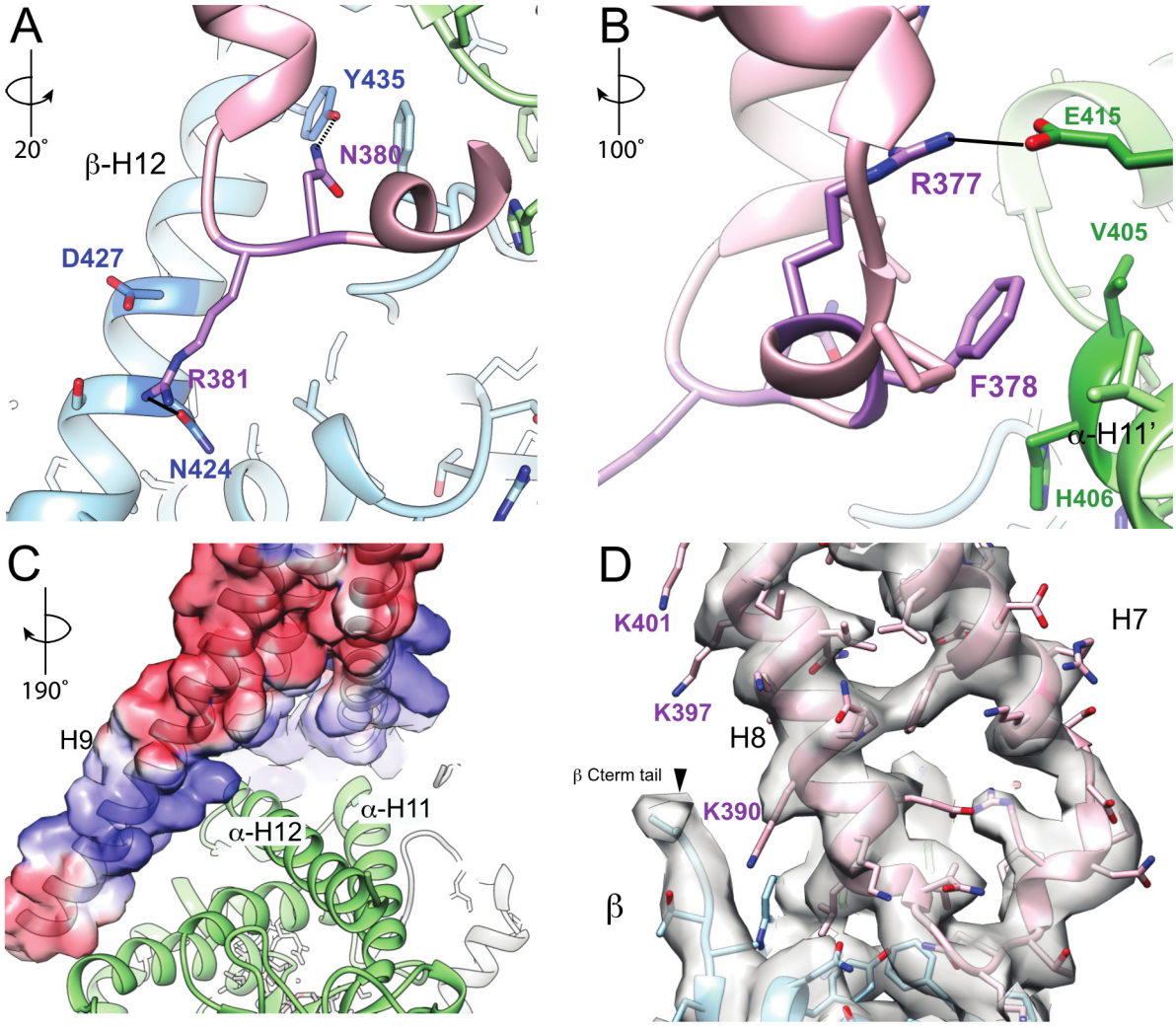

Figure 5-4 The PRC1-tubulin model detailing specific PRC1-tubulin contacts
A) R381 and N380 in loop H7-H8 of PRC1 (pink) contacts N424, potentially D427, and Y435 in β-tubulin (blue). **B**) F378 of PRC1-S nestles into a hydrophobic pocket formed by V405 and H406 in α-tubulin (green), and R377 of PRC1 forms contacts with E415 of α-tubulin. **C**). Helix H9 of PRC1-S forms a complementary electrostatic surface with tubulin; H9 is largely composed of positively charged residues whereas tubulin has a relatively negatively charged surface. **D**) The structured β-tubulin tail can clearly be seen in our reconstruction, the negative charges of the tail favorably interacts with the multiple lysines (K390, 397, 401) of PRC1-S. All rotations (**A-C**) are reported relative to the orientation shown in panel **D**, which corresponds to an approximately 90° in-plane rotation with respect to the orientation shown in Figure 5-1.

N424 and potentially with D427, both within H12 of β-tubulin. Additionally, N380 in PRC1-S is well-positioned (3 Å distance between donor and acceptor atoms) to hydrogen bond with β-tubulin's Y435 (Figure 5-4A), located further down the H12 helix. On the other end of the loop connecting S-H7 and S-H8, closer to H7, F378 in PRC1 nestles into a hydrophobic pocket in α-tubulin formed by V405, H406 and V409 (within the loop connecting α-H11 and α-H12). Additionally, R377 in PRC1-S appears to hydrogen bond (2.9 Å distance) with E415 in α-tubulin (within H11) (Figure 5-4B). Although S-H9 is draped over the surface of the α-tubulin subunit, it makes surprisingly few defined contacts, only its C-terminal portion interacts with α-H12. The position of S-H9 suggests that it interacts with the negative charge of the nearby microtubule surface (formed by α-tubulin) through electrostatic interactions (Figure 5-4C). Finally, although the acidic C-terminal tails of tubulin are generally unstructured, we can clearly trace up to five extra amino acids from the last residue seen in crystallographic studies in our reconstruction for both α- and β-subunits, indicating that the tubulin tails become partially structured upon PRC1-SC binding. The β-tubulin tail (sequence DATAEEGEFEEEAEEEVA) is near lysines K390, K397 and K401 on the surface of S-H8 (Figure 5-4D). The α-tubulin tail, in contrast, has no structured PRC1-SC density in close proximity. However, the C-terminus of PRC1-S is approximately ~30 Å from the C-terminal tail of α-tubulin, placing it easily within appropriate range to interact with the disordered C-terminal domain of PRC1-SC (which comprises >100 disordered amino acids that are not visualized). Together, these features suggest that PRC1-SC-binding is in part mediated by the tubulin tails of both subunits.

5.2 Molecular basis of PRC1's specificity for the intra-dimer interface

PRC1 specifically recognizes and binds the microtubule surface at the intra-dimer interface (within an αβ-tubulin heterodimer) rather than that between heterodimers, at a site that is only available on an assembled form of tubulin. The tubulin region contacted by PRC1-S is generally similar at the inter-dimer interface (i.e. the residues involved are conserved in α- and β-tubulin). However, a number of notable exceptions account for the specificity. Firstly, R381 in PRC1-S is close enough to interact with β-D427, which at an identical position at the inter-dimer interface is substituted by α-A427, incapable of hydrogen bonding to R381 (Figure 5-5A). Secondly, β-Y435, which hydrogen bonds with N380 in PRC1-S, corresponds to V435 in α-tubulin at the inter-dimer interface (Figure 5-5A). Thirdly, the hydrophobic pocket filled by F378 at the intra-dimer interface is disrupted at the inter-dimer interface by the presence of a polar residue, β-T409, instead of a valine at the intra-dimer interface. (Figure 5-5B). Finally, α-G416, whose small size allows PRC1-S R450 to interact with neighboring charged amino acids (α-E414 and α-E420), is substituted by β-M416 at the inter-dimer interface, sterically occluding PRC1S-R450 from interacting with these glutamic acid residues (Figure 5-5C). Thus, critical sequence changes between α- and β-tubulin both sterically and chemically confer PRC1's selectivity for the tubulin intra-dimer interface.

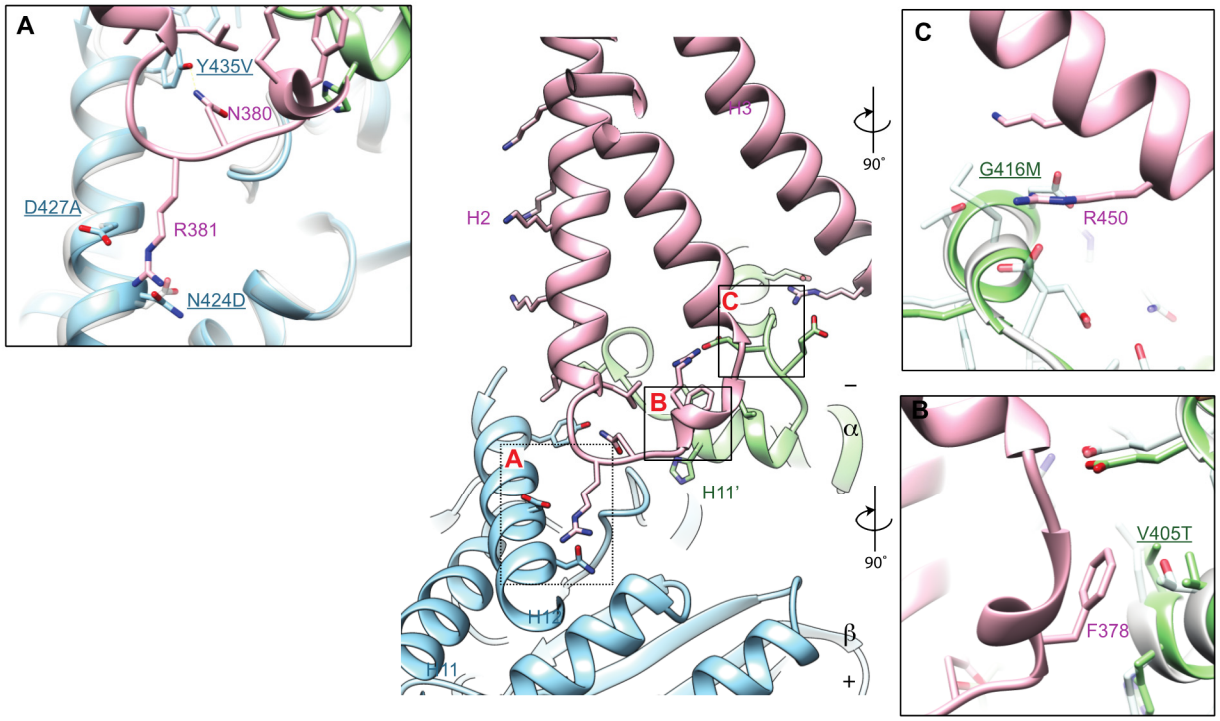

Figure 5-5 Molecular basis of PRC1's specificity for the intra-dimer interface
A number of critical PRC1-tubulin contacts are present only at the N-site. **A**) D417 at the intra-dimer site is mutated to A at the inter-dimer site, eliminating interactions between R381. Y425 is a V at the inter-dimer site, which eliminates hydrogen bonding to N380 in PRC1S. **B**) V409T reduces the hydrophobicity of the tubulin pocket which cradles PRC1S-F378. **C**) G416M occludes PRC1-R450 sterically from interacting with tubulin.

5.3 Disordered C-terminal domain contacts neighboring microtubule protofilaments

Cosedimentation assays, which measure the equilibrium binding of proteins of interest to larger complexes that can be separated by centrifugation, demonstrated that the spectrin domain alone has weak affinity for the microtubule lattice (Mollinari et al., 2002; Subramanian et al., 2010). A five-fold increase in binding affinity for microtubules is achieved by including the ARG/LYS rich C-terminal disordered domain (3.3 vs 0.6 μM) (Subramanian et al., 2010). In our reconstruction, the C-terminal domain of PRC1-SC beyond residue 467 is not traceable, verifying that it has no regular structure. However, the improved resolution of the reconstruction allows us to determine where the C-terminal domain is roughly localized on the microtubule-surface. The end of S-H9 is located close to H3 of α-tubulin (Figure 5-1B). This positions the C-terminal domain of PRC1-SC in an ideal position to interact with the neighboring α-subunit. Electrostatic maps, computed using the Adaptive Poisson-Boltzmann Server (APBS), (Baker, Sept, Joseph, Holst, & McCammon, 2001), reveal that the surface of the neighboring protofilament within the same microtubule, adjacent to the C-terminus of PRC1-SC, is relatively negatively charged, indicating that it forms a complementary electrostatic surface for the predominantly positively charged R/K rich C-terminal domain of PRC1 and may serve to increase the affinity of PRC1-SC. Indeed, as the interface between PRC1-S and tubulin is relatively small (~500 $Å^2$), the C-terminus may provide much needed favorable enthalpic interactions to both target PRC1 to the microtubule lattice, as well as increase the binding-affinity of PRC1-SC for the microtubule lattice. Consistent with the lack of specific contacts, S-H9 appears to be at lower resolution, potentially due to intrinsic flexibility, and adopting multiple conformations on the surface of the microtubule. We interpret this as evidence of non-specific electrostatic interactions between PRC1 and tubulin. Indeed, the electrostatic map demonstrates strong positive charge on the PRC1 binding surface of S-H9 and strong negative charge on the interacting surface of tubulin.

Despite the presence of more than 100 residues beyond S-H9 in our construct, we do not see density for any of these residues, consistent with previous proposals that the C-terminal domain of PRC1 is disordered. Due to the orientation of PRC1's H9, pointing its C-terminal end towards the center of the microtubule very near the lateral contacts between protofilaments, we predict that the disordered C-terminus is interacting with the neighboring protofilament. This prediction is, again, supported by electrostatic calculations which identify the microtubule surface of the neighboring protofilament as relatively negatively charged. This would complement the rich positive charge (R/K) of the C-terminal domain. Additionally, the negatively charged tubulin-tails become structured in our cryo-EM reconstruction, allowing us to trace 5 additional residues beyond the C-terminus of α- and β-tubulin. While PRC1-S seems to clearly interact with the β-tubulin C-terminus, none of the traced PRC1-SC density is sufficiently close to interact with the α-tubulin tail. Instead, we believe the disordered C-terminal domain is within range (~30 Å) to interact with the α-tubulin tail. The C-terminal domain of PRC1 contains phosphorylation sites at T470 and T481 that are known substrates for cyclin-CDK complexes and whose phosphorylation state is tightly coupled to the cell cycle (W. Jiang et al., 1998; Mollinari et al., 2002). When PRC1 is phosphorylated, its microtubule bundling activity is reduced, consistent with our model where the negative charge of a phosphate group would disrupt the electrostatic interactions between tubulin and PRC1, though it is not possible to exclude other models. The presence of a disordered region under phospho-regulation is commonly observed for other microtubule binding proteins such as Ndc80 (Alushin et al., 2012).

5.4 Kinesin, Dynein, and PRC1 partially share a tubulin binding site

The ridge on α-tubulin between α-H11 and α-H12 was previously identified as a binding site for the kinesin motor domain (Sindelar & Downing, 2007) and the dynein microtubule binding domain (Redwine et al., 2012), near to where we observe the loop connecting S-H7 to S-H8 binding to tubulin. We performed sequence and structural alignments to investigate whether specific residues on tubulin (T) are shared between kinesin (K), PRC1 (P) and dynein's microtubule binding domain (D). No atomic resolution information exists about the binding of dynein to microtubules, but pseudo-atomic models of this interaction have been generated by docking known crystal structures into lower resolution EM maps (Redwine et al., 2012; Uchimura et al., 2015). These models also incorporate biochemical and modeling data. Strikingly, K-R278 overlaps very near to P-R381, and forms very similar interactions with tubulin (Figure 5-6). The microtubule binding domain of dynein has two lysine residues (D-K3298 and D-K3299) very near to the position of K-R278 and P-R381, one of which is likely to interact with tubulin in a similar manner observed in this reconstruction and in previous x-ray crystal structures. Previous mutational analyses have also identified these lysine residues in dynein as critical to the D-tubulin interaction (Koonce & Tikhonenko, 2000). To identify other residues that may not have been investigated by mutagenesis and because no high resolution structure for dynein bound to microtubules exists, we investigated all residues within a 4.0 Å distance cut-off between tubulin and its binding partner. We observe that residues T-α-H406 (see Figure 5-5) and T-α-V409 of the same hydrophobic pocket are within range to potentially interact with kinesin and dynein as well, reinforcing this an important binding pocket at the intra-dimer interface on tubulin. T-α-G416 interacts with K237 of kinesin (Gigant et al., 2013) and R450 of PRC1 in our model. Furthermore,

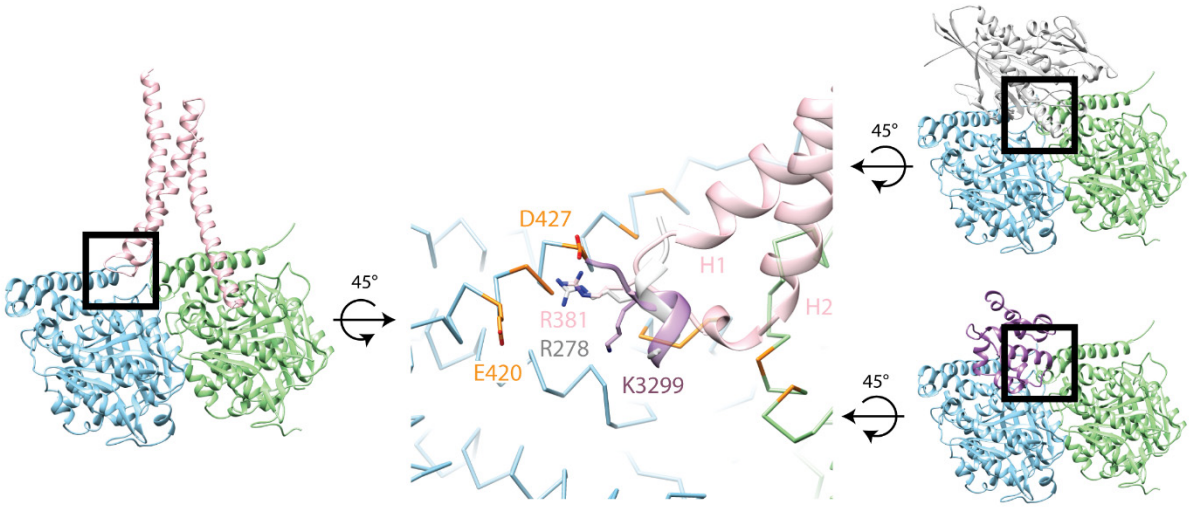

Figure 5-6 PRC1 binding site overlaps with kinesin and dynein's microtubule binding domain
The binding site for PRC1, kinesin and dynein are superimposed. Part of kinesin's structure near loop L12 shown in grey, dynein MTBD shown in purple, PRC1-S shown in pink, α-tubulin in light blue, and β-tubulin in light green. Tubulin residues common to PRC1-S, kinesin- and dynein-binding shown in orange. Side chains shown for tubulin residues (D427 and E420) that stimulate kinesin ATPase activity, the common arginine between kinesin and PRC1, and the two potential lysine residues on dynein that may occupy the same site.

we observed that residues T-β-R264 on the loop between β-H8 and S7 and T-β-Q434 on β-H12 are potentially shared between PRC1 and the loop L12 on kinesin that moves depending on the nucleotide state of kinesin (Atherton et al., 2014; Goulet et al., 2012; Shang et al., 2014; Uchimura, Oguchi, Hachikubo, Ishiwata, & Muto, 2010). In summary we find that G416 on H12 of α-tubulin is shared between kinesin and PRC1, and that N424 and D427 on β-tubulin (also on H12) are shared between kinesin, PRC1, and dynein. The ridge between H11 and H12 on α-tubulin that forms a hydrophobic pocket with residues α-V405 and α-H406 is also shared by all three binding partners.

In contrast to PRC1 and other MAPs that bind once per heterodimer, the NDC80 protein binds between heterodimers and within heterodimers, not discriminating between the intra- or inter-dimer interface (Alushin et al., 2010; Wilson-Kubalek, Cheeseman, Yoshioka, Desai, & Milligan, 2008). This protein does not have a lysine or arginine residue that might specifically interact with β-tubulin N424 like PRC1-R381 and kinesin-R278. Instead residues such as the conserved glutamic acid (T-α/β-E415) and lysine/arginine residues on the C-terminal end of H11 for α- and β-tubulin that are similar between the two sites mediate important interactions for NDC80. However, due to the limited resolution of this and previous studies, particularly those involving dynein, we cannot unambiguously identify all the common interacting residues. Given that multiple microtubule-binding proteins recognize tubulin in the same region and bind through H11 and H12, and the sheer number of microtubule-binding proteins, it is tempting to speculate that they bind via a limited number of binding motifs. This will be an important area for future cryo-EM based structural studies.

6 Chapter 6: Conclusions and future directions

By utilizing high resolution cryo-EM we have gained critical knowledge about microtubules and their binding proteins. We demonstrated that acetylation of α-tubulin at K40 has no effect on the structure of microtubules. This makes it unlikely that MAPs recognize the modification on the outside of the microtubule. Rather, the marker must be used by proteins that directly bind near or at this site. Our experiments using cell-extracts to try identify some of these proteins failed due to the robust acetylation activity of the extracts, but I believe they could work with some modifications. Identifying additional proteins beyond αTAT1 that bind the inside of microtubules would create a new classification for MAPs. The fact that luminal particles have been observed inside microtubules makes this possibility even more likely. Using cell extracts from different cell lines, or limiting the acetylation activity (by depleting acetyl-CoA or αTAT1), I believe it would be possible to identify one or more of these proteins. The identification of another protein that binds the inside would make the question of how proteins access the lumen even more pressing. Contrary to my own expectations, increasing the number of open ends did not improve the binding of αTAT1. Subsequent experiments have shown that the enzymatic activity for αTAT1 is also not increased for tubulin polymers with greater accessibility (Szyk et al., 2014). At that time we were able to visualize the microtubule lattice at subnanometer resolution confirming that there were no large scale effects. However, one cannot exclude the possibility that we did not have the resolution to visualize the changes that accompany acetylation. Now it is possible to see the lattice at near atomic resolution using the direct electron detector. It may be possible to resolve changes in the conformation of this loop as a result of acetylation. However, this loop is flexible, and consistently remains poorly resolved in our mammalian microtubules, and even in the yeast microtubule reconstructions that are not a mixture of acetylated and deacetylated states. Fungal tubulin lacks this lysine residue and searches of the genome do not reveal any obvious homolog to αTAT1.

The structural work on yeast tubulin using cryo-EM is just starting and offers many exciting possibilities. We have shown that the yeast lattice remains expanded when the microtubules are polymerized *in vitro*, suggesting that the GTPase activity of yeast tubulin itself is sufficiently slowed to prevent lattice compaction. We also showed that compaction occurs when a plus-tip tracking protein is added. However, yeast microtubules are still dynamic *in vitro*, without other protein cofactors. This likely means that the compacted yeast lattice is a very short lived state. Further investigations into why the compacted yeast lattice is significantly less stable than the mammalian lattice could reveal important properties about dynamic instability. A possible approach to address this could be to reexamine the huge number of yeast tubulin mutants have been characterized *in vivo*, and through low resolution structural screens of likely candidates find mutants that compact, but do not disassemble. Another exciting possibility for the yeast tubulin studies is to look at a catalytically dead tubulin with no GTPase activity. This would finally reveal the structure of the GTP cap of microtubules. Finally, our finding that Bim1 binds within and between heterodimers raises the question of how the full length Bim1 dimer actually interacts with microtubules and whether the geometry of the dimerization domain allows for both or only one of the CH domains to bind.

Our PRC1 work showed how it binds microtubules using its spectrin domain, and identified many of the atomic interactions. We also showed that the cross bridge angle observed in tomography studies is consistent with the angle we observed for the spectrin domain. The crystal structure of PRC1 that includes the N-terminal dimerization domain (Subramanian et al., 2013) includes the two spectrin domains, but the orientation of spectrin domains is incompatible with

binding anti-parallel microtubules. This raises the question of what rearrangements are necessary to make it compatible with our high resolution data and the tomography data. We also demonstrated that the C-terminal domain of PRC1 does not become ordered upon binding to microtubules. While it contributes to the binding affinity of PRC1, and contains sites for phospho-regulation and nuclear localization, it is much larger than either of these functions would require, suggesting there is still some unknown role for this domain. One possibility is that this domain is used to bind other spindle proteins. Identifying one of these proteins and co-decorating microtubules could provide important biological insights. Increasing the biological complexity of the structural targets will be a general trend for future cryo-EM studies. Further improvements to cryo-EM data collection and image processing will continue to provide even greater biological insight across a wide range of resolutions.

7 Chapter 7: Materials, methods and protocols

7.1 Kinesin purification

Protein and plasmid for monomeric kinesin (Kif5b), defective in ATP hydrolysis (E236A) was supplied by the Vale lab (Rice et al., 1999).

- BL21 (DE3) cells were transformed and colonies grown overnight on AMP plates.
- Stater cultures were
- BL21 (DE3) cells bearing k349 hydrolysis mutant plasmid were grown in 6 liters of 1x YT at 37ºC till the OD_{600} reaches 0.4-0.6
- The cells were induced with 0.2mM IPTG, temperature was lowered to 22ºC and the culture was shaken overnight.

Buffers used

Lyse	Wash A	Wash B	Elution	SEC Buffer
50mM Phosphate buffer pH 8.0 300mM KCl 2mM MgCl2 10% glycerol 1ul per 10ml of MTG 10mM Imidazole	50mM Phosphate buffer pH 8.0 300mM KCl 2mM MgCl2 10% glycerol 200uM ATP 1ul per 10ml of MTG 10mM Imidazole	50mM Phosphate buffer pH 8.0 150mM KCl 2mM MgCl2 10% glycerol 1ul per 10ml of MTG 30mM Imidazole	50mM Phosphate buffer pH 8.0 150mM KCl 2mM MgCl2 10% glycerol 1ul per 10ml of MTG 250mM Imidazole	25mM Tris pH 7.5 150mM KCl 10% glycerol 2mM MgCl2 2mM DTT

- The harvested cells were re-suspended in lyse (40ml/l **<u>with</u>** protease inhibitors, 1 tablet per liter culture) and lysed by sonication (3 x 45sec at power level 7.0).
- The lysate was clarified by centrifuging at 30K rpm for 60 minutes.
- Meantime the Ni beads (1ml beads per liter culture) were equilibrated with lyse buffer.
- The supernatant was applied to the Ni beads and allowed to bind for 2 hours while shaking in cold room.
- Beads combined into single tube and the following wash steps were used:
  - Two washes with 3 x bead volume of Wash A buffer
  - Two washes with 3 x bead volume of Wash B buffer
- The protein was then eluted using 2 x bead volume of elution buffer. *Samples were collected during each step and analyzed using SDS gel.*
- Protein was concentrated to final volume < 5ml using 10kD MWCO filter unit
- Loaded onto SEC column equilibrated in SEC buffer, run at 1 ml/min, 1 ml fractions collected.

7.2 SIRT2 Purification

Buffers

- 4XT: 80 mM Tris pH 7.4, 800 mM NaCl

- 2XT: 40 mM Tris pH 7.4, 400 mM NaCl

Check each step for reducing agent/protease inhibitor
Use 1-thiolglycerol (1 µl per 10 ml of buffer) or BME (2 mM β-ME) as reducing agent

- Perform transformation and plate on LB Amp plates and grow sufficient starter cultures for 1:200 inoculation of main culture.
- Grow cells to OD_{600} 0.8, induce with IPTG (0.2mM final), shake O/N at RT (20°C)
- Harvest cells and resuspend in 4XT with reducing agent and protease inhibitors (20 ml per 1l culture)
- Sonicate (3 x 45sec at power level 7.0)
- Spin at 30k x g for 30min
- While spinning, wash Ni-NTA beads (1 ml packed beads per 1l culture) in 2XT with reducing agent
- Dilute sup 1:1 with ddH_2O (now the buffer is 2XT).
- Add imidazole to 10mM
- Add beads to the supernatant and bind for 2 hours
- Wash twice with 10ml 2XT with 10 mM imidazole
- Elute with 200 mM imidazole in 2XT (5 x 0.5ml)
- Remove imidazole using PD-10 desalting columns and store in 20 mM Tris, pH 7.4, 150 mM NaCl, 1 mM $MgCl_2$

7.3 αTAT1 Purification

Buffers

- 4XT: 80 mM Tris pH 7.4, 800 mM NaCl
- 2XT: 40 mM Tris pH 7.4, 400 mM NaCl

Check each step for DTT/protease inhibitor

- Perform transformation for GST-αTAT1 and plate on LB plate o/n at 37º
- Grow a starter culture of GST- αTAT1 overnight. The next day inoculate starter culture at 1:200
- Shake media at 37° until OD_{600} is around 0.8
- Add IPTG to 0.2 mM final and shake the flask at 16° o/n
- Harvest cells and resuspend in 4XT (20ml per 1l, 1mM DTT)
- Sonicate 3 x 30 sec at power level 7.0 (approx. 70 W)
- Spin at 30k x g for 30 minutes
- Take supernatant and dilute 1:1 with water (now 2XT)
- Wash glutathione sepharose beads with 2XT
- Add beads to supernatant (2 ml for 1L culture) at 4º for 2 hours in 50 ml conical
- after 1 hour incubation, wash beads in batch mode
    - pellet the beads at 1K rpm for 3~4 minute
    - very carefully decant the sup; leave about 15 ml
    - transfer to 15 ml conical
    - wash with 15 ml (fill the tube) 2XT buffer with 5 mM DTT, four times
- Transfer beads to 5 ml tube with cap
    - add 2 ml wash buffer

- total volume = 4 ml (2 ml resin and 2 ml wash buffer)
- add 500 µg precision protease (kept in -80ºC)
- leave in 4ºC room from 4 hours to o/n

- Equilibrate S200 column in 2XT buffer
- Concentrate beads supernatant and remove aggregates by filtration through 0.2 µm filters.
- Load and run on S200, collect 0.5 ml fractions. Depending on final concentration, may need to re-concentrate before aliquoting and freezing.

7.4 Preparation of acetylated and deacetylated tubulin

Porcine tubulin was purchased from Cytoskeleton (Cat # T240), reconstituted to 10 mg/ml in BRB80 buffer (80 mM PIPES pH 6.9, 1 mM EGTA, 1 mM $MgCl_2$) with 10 % (v/v) glycerol, 1 mM GTP and 1 mM DTT, and flash frozen in 10 µl aliquots until needed. Acetylation and deacetylation reactions were carried out in ADE buffer (40 mM PIPES, pH 6.9, 0.8 mM EGTA, 0.5 mM $MgSO_4$) with 30 % glycerol, 0.5 mM GTP and 1 mM DTT. Tubulin concentrations were 40-50 µM for all acetylation and deacetylation reactions. αTAT1 and acetyl-CoA were used at final concentrations of 6-20 µM and 50 µM, respectively. SIRT2 and NADH were used at final concentrations of 5 µM and 1 mM, respectively. Acetylation levels were estimated using Western blots probed with an anti-acetylated tubulin antibody (Cat # T7451) and a fluorescent secondary antibody (GE Healthcare, Cat #PA43009). Quantification of the *in vitro* acetylation levels was estimated by normalizing the western blot signal to the amount of tubulin in the replicated lane, and using *Tetrahymena* ciliary tubulin as a standard for completely acetylated tubulin.

7.5 Preparation of subtilisin cleaved microtubules

Subtilisin cleaved microtubules were prepared by incubating preformed microtubules (approximately 2 mg/ml) with 0.05 mg / ml subtilisin (EMD Chemical, Cat # 572909) in BRB80 at 37 °C for 20 minutes. Digestion was halted by the addition of phenylmethanesulfonyl fluoride to 2 mM final. Attempts to digest tubulin further to completely remove the C-terminal tails of both

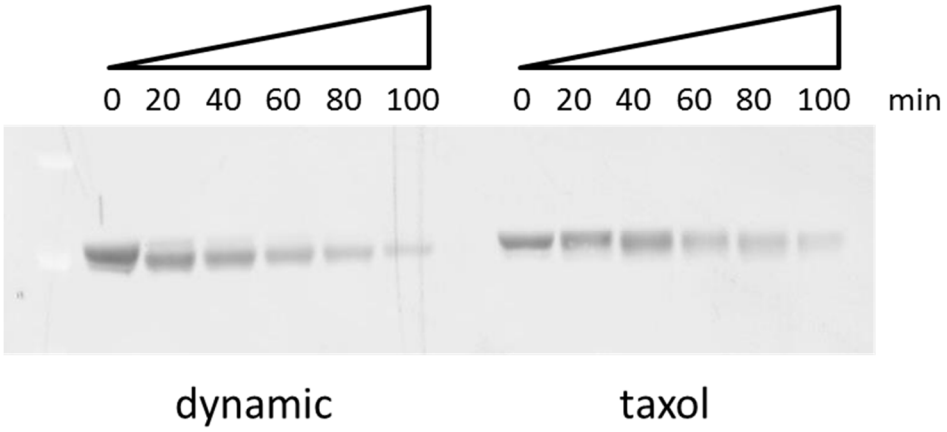

Figure 7-1 Subtilisin digestion cleaves N-terminal loop of α-tubulin.
Performed microtubules, dynamic (left) and stabilized with taxol (right) were incubated with subtilisin for the time indicated, and then probed with the anti-acetylated tubulin antibody. A decrease in signal at later time points suggests that the N-terminal loop of α-tubulin is nonspecifically cleaved along with the C-terminal tails.

monomers resulted in the cleavage of the N-terminal loop of α-tubulin, as judged by the signal obtained in a western blot of the tubulin preparations using the anti-acetylated tubulin antibody (Figure 7-1). This suggests that subtilisin can access the lumen of microtubules, where it can then cleave the flexible loop containing αK40.

7.6 Preparation of kinesin decorated microtubules

Kinesin was desalted into EM buffer, BRB80 with 0.05% (v/v) Nonidet P-40 (Roche, Cat # 11332473001) and 2 mM DTT, supplemented with 0.5 mM ATP, using a Zeba spin desalting column (Pierce, Cat # 89882) and diluted to 1 mg/ml in above buffer (sometimes supplemented with GTP or the appropriate stabilizer to preserve the microtubules). After dilution, kinesin was spun at 80,000 x g at 4 °C to remove any aggregates. Microtubules were diluted to 0.5 mg/ml and applied to a glow discharged C-flat grid (Protochips) in the chamber of a Virtrobot. Microtubules were allowed to adhere to the grid for 30 seconds. Kinesin was then applied to the grid twice, 4 µl each addition, briefly manually blotting after the first addition, to ensure complete decoration of the microtubules. The grid was then blotted for 4 s and plunged into ethane slush.

7.7 Taxol-stabilized microtubule preparation

Soluble tubulin was obtained from bovine brain (Cytoskeleton) at 10 mg/ml. Aliquots were thawed and polymerized in BRB80 buffer supplemented with 10% glycerol and 1 mM GTP at 37°C for 15 minutes, followed by addition of 160 µM taxol and an additional 30 minutes of incubation at 37°C. For biochemical experiments, taxol microtubules were first pelleted in a tabletop microcentrifuge for 20 minutes at room temperature at 17,000 x g. The pellet was then resuspended in binding buffer (BRB80, 5% sucrose, 1 mM DTT) containing 160 µM taxol. Microtubules were diluted in the presence of 20 µM taxol for all subsequent experiments.

7.8 Yeast tubulin purification and microtubule polymerization

A yeast strain that had been sensitized to taxol by mutating residues on β-tubulin (Gupta et al., 2003) was purified according to Drummond *et al.* (Drummond et al., 2011). Small quantities of yeast WT tubulin were prepared according to Widlund (Widlund et al., 2012). The bulk of wildtype and all of T238A were purified from strains of *Saccharomyces cerevisiae* with inducible overexpression of tubulin according to previous studies (Ayaz et al., 2014, 2012; Geyer et al., 2015; Johnson et al., 2011). Aliquots were stored at -80 °C until needed. Aggregates from the freeze-thaw cycle were removed by cold filtration using spin filters before polymerization. All tubulin was polymerized in BRB80 supplemented with 10% glycerol, 1 mM DTT and 1 mM GTP at 30°C. Taxol (Cytoskeleton, Cat # TXD01) and epothilone-B (Selleck Chemicals, Cat # S1364) were dissolved in DMSO to 2 mM and 5 mM respectively. Dynamic microtubules were polymerized for 15 minutes. For drug stabilized microtubules, (taxol and epothilone) dynamic microtubules were polymerized for 10 min as above, and approximately two-fold molar excess of drug was added and polymerized for another 20 minutes. All microtubules were pelleted at 17,000x *g* for 20 min. Dynamic microtubules were resuspended in a 1mg/ml kinesin monomer solution in warm EM buffer (BRB80 with 1 mM DTT, 1 mM GTP and 0.05% Nonidet-P 40). For GMPCPP and GTPγS microtubules the dynamic pellet was resuspended in cold BRB80 buffer with 2 mM of the desired nucleotide and left on ice for 20 minutes to fully depolymerize and exchange the nucleotide bound to β-tubulin. These were then warmed to 30 °C for 30 minutes to polymerize.

7.9 Imaging of cryo-EM samples

Micrographs used to generate near atomic resolution electron density maps were collected using a semi-automated data-collection pipeline (Suloway et al., 2005) coupled with a Titan electron microscope (FEI, Hillsboro, OR) operated at 300kV and equipped with a K2 direct detector (Gatan, Pleasanton, CA) to collect the raw micrographs. The micrographs were collected at a nominal magnification of 27,500x, resulting in a final pixel size of 1.32 Å per pixel. Twenty frames of 300ms each were collected at a dose rate of 8 e^{--} per pixel per s, with a total dose of 28 e^{-} per $Å^2$.

Micrographs were also collected on a Tecnai F20 transmission electron microscope (FEI, Hillsboro, OR) operating at 120 kV and equipped with a Gatan 4k Ultrascan charge-coupled device. Micrographs were collected using Leginon (Suloway et al., 2005) with a dose of 20 e^{-} per $Å^2$ and nominal magnification of 80,000×, giving a final size of 1.37 Å per pixel.

7.10 Image analysis and data processing

Cryo-EM images were generally processed using the Appion EM image processing pipeline (Lander et al., 2009), including individual frame alignment using MOTIONCORR (X. Li et al., 2013), CTF estimation using CTFFIND4 (Mindell & Grigorieff, 2003) and particle extraction. For 3D processing, overlapping square boxes of 675 Å, spaced 80 Å apart, were masked from the raw images. EMAN2 multi-model refinement (Tang et al., 2007) was performed using initial models of 12, 13, 14, and 15 protofilament microtubules (Sui & Downing, 2010) low-pass filtered to 20 Å resolution, followed by IHRSR (Egelman, 2007) to obtain initial 3D reconstructions. Frealign (Lyumkis, Brilot, Theobald, & Grigorieff, 2013) was used to further process the particles belonging to microtubules of a single protofilament number. Finally, we applied in-house scripts to verify seam location and enforce it for each microtubule (Zhang & Nogales, 2015) . The overall resolution of the resulting map after this last step was not significantly better, but the discrimination between α- and β-tubulin was improved.

7.11 Grid preparation, imaging and processing for tubulin oligomers

Tubulin was prepared in the polymerization buffer, but kept on ice. To obtain the appropriate density of oligomers on the EM grid, it was necessary to adjust the concentration of each tubulin type and the time it was incubated on the grid. All final solutions applied to the grid were above the critical concentration for that tubulin. 4 µl of cold tubulin was applied to a glow discharged continuous carbon grid and the drop incubated on the grid for 10-30 seconds. The grid was then rinsed in 3 droplets of 40 µl each of 2 % (w/v) uranyl acetate and blotted dry. Grids were imaged on an Tecnai F20 (FEI, Eindhoven) microscope equipped with a Ultrascan 4000 CCD (Gatan, Pleasanton, CA) under low dose conditions using Leginon (Suloway et al., 2005) at a nominal magnification of 80,000x, corresponding to a pixel size of 1.37 Å per pixel. Oligomers were manually traced using ImageJ (Schneider, Rasband, & Eliceiri, 2012). The length and curvature of the oligomers were measured using the "Measure Roi Curve" plugin (OptiNav, Bellevue, WA). The number of heterodimers within each oligomer was determined by rounding the length to the nearest integer multiple of the heterodimer length, 8nm.

8 References

Adams, P. D., Afonine, P. V, Bunkóczi, G., Chen, V. B., Echols, N., Headd, J. J., … Zwart, P. H. (2011). The Phenix software for automated determination of macromolecular structures. *Methods*, *55*(1), 94–106. doi:10.1016/j.ymeth.2011.07.005

Akella, J. S., Wloga, D., Kim, J., Starostina, N. G., Lyons-Abbott, S., Morrissette, N. S., … Gaertig, J. (2010). MEC-17 is an α-tubulin acetyltransferase. *Nature*, *467*(7312), 218–222. doi:10.1038/nature09324

Akhmanova, A., & Steinmetz, M. O. (2010). Microtubule +TIPs at a glance. *Journal of Cell Science*, *123*(Pt 20), 3415–3419. doi:10.1242/jcs.062414

Alushin, G. M., Lander, G. C., Kellogg, E. H., Zhang, R., Baker, D., & Nogales, E. (2014). High-resolution microtubule structures reveal the structural transitions in αβ-tubulin upon GTP hydrolysis. *Cell*, *157*(5), 1117–29. doi:10.1016/j.cell.2014.03.053

Alushin, G. M., Musinipally, V., Matson, D., Tooley, J., Stukenberg, P. T., & Nogales, E. (2012). Multimodal microtubule binding by the Ndc80 kinetochore complex. *Nature Structural & Molecular Biology*, *19*(11), 1161–7. doi:10.1038/nsmb.2411

Alushin, G. M., Ramey, V. H., Pasqualato, S., Ball, D. a., Grigorieff, N., Musacchio, A., & Nogales, E. (2010). The Ndc80 kinetochore complex forms oligomeric arrays along microtubules. *Nature*, *467*(7317), 805–810. doi:10.1038/nature09423

Andreu, J. M., Bordas, J., Diaz, J. F., García de Ancos, J., Gil, R., Medrano, F. J., … Towns-Andrews, E. (1992). Low resolution structure of microtubules in solution. Synchrotron X-ray scattering and electron microscopy of taxol-induced microtubules assembled from purified tubulin in comparison with glycerol and MAP-induced microtubules. *Journal of Molecular Biology*, *226*(1), 169–84.

Arnal, I., & Wade, R. H. (1995). How does taxol stabilize microtubules? *Current Biology*, *5*(8), 900–8.

Atherton, J., Farabella, I., Yu, I.-M., Rosenfeld, S. S., Houdusse, A., Topf, M., & Moores, C. A. (2014). Conserved mechanisms of microtubule-stimulated ADP release, ATP binding, and force generation in transport kinesins. *eLife*, *3*, e03680. doi:10.7554/eLife.03680

Ayaz, P., Munyoki, S., Geyer, E. A., Piedra, F.-A., Vu, E. S., Bromberg, R., … Rice, L. M. (2014). A tethered delivery mechanism explains the catalytic action of a microtubule polymerase. *eLife*, *3*, e03069. doi:10.7554/eLife.03069

Ayaz, P., Ye, X., Huddleston, P., Brautigam, C. A., & Rice, L. M. (2012). A TOG:αβ-tubulin complex structure reveals conformation-based mechanisms for a microtubule polymerase. *Science*, *337*(6096), 857–60. doi:10.1126/science.1221698

Baker, N. A., Sept, D., Joseph, S., Holst, M. J., & McCammon, J. A. (2001). Electrostatics of nanosystems: application to microtubules and the ribosome. *Proceedings of the National Academy of Sciences*, *98*(18), 10037–10041. doi:10.1073/pnas.181342398

Berman, H. M., Westbrook, J., Feng, Z., Gilliland, G., Bhat, T. N., Weissig, H., … Bourne, P. E. (2000). The Protein Data Bank. *Nucleic Acids Research*, *28*(1), 235–42.

Bieling, P., Telley, I. A., & Surrey, T. (2010). A minimal midzone protein module controls formation and length of antiparallel microtubule overlaps. *Cell*, *142*(3), 420–432. doi:10.1016/j.cell.2010.06.033

Blake-Hodek, K. a, Cassimeris, L., & Huffaker, T. C. (2010). Regulation of microtubule dynamics by Bim1 and Bik1, the budding yeast members of the EB1 and CLIP-170 families of plus-end tracking proteins. *Molecular Biology of the Cell*, *21*(12), 2013–23. doi:10.1091/mbc.E10-02-0083

Bollag, D. M., McQueney, P. A., Zhu, J., Hensens, O., Koupal, L., Liesch, J., … Woods, C. M. (1995). Epothilones, a new class of microtubule-stabilizing agents with a taxol-like mechanism of action. *Cancer Research*, *55*(11), 2325–33.

Bonnet, C., Boucher, D., Lazereg, S., Pedrotti, B., Islam, K., Denoulet, P., & Larcher, J. C. (2001). Differential binding regulation of microtubule-associated proteins MAP1A, MAP1B, and MAP2 by tubulin polyglutamylation. *The Journal of Biological Chemistry*, *276*(16), 12839–48. doi:10.1074/jbc.M011380200

Bouchet-Marquis, C., Zuber, B., Glynn, A.-M., Eltsov, M., Grabenbauer, M., Goldie, K. N., … Chrétien, D. (2007). Visualization of cell microtubules in their native state. *Biology of the Cell*, *99*(1), 45–53. doi:10.1042/BC20060081

Bowne-Anderson, H., Zanic, M., Kauer, M., & Howard, J. (2013). Microtubule dynamic instability: A new model with coupled GTP hydrolysis and multistep catastrophe. *BioEssays*, *35*(5), 452–461. doi:10.1002/bies.201200131

Boyden, E. S., Zhang, F., Bamberg, E., Nagel, G., & Deisseroth, K. (2005). Millisecond-timescale, genetically targeted optical control of neural activity. *Nature Neuroscience*, *8*(9), 1263–8. doi:10.1038/nn1525

Brangwynne, C. P., MacKintosh, F. C., Kumar, S., Geisse, N. A., Talbot, J., Mahadevan, L., … Weitz, D. a. (2006). Microtubules can bear enhanced compressive loads in living cells because of lateral reinforcement. *The Journal of Cell Biology*, *173*(5), 733–41. doi:10.1083/jcb.200601060

Brown, A., Long, F., Nicholls, R. a., Toots, J., Emsley, P., & Murshudov, G. (2015). Tools for macromolecular model building and refinement into electron cryo-microscopy reconstructions. *Acta Crystallographica. Section D, Biological Crystallography*, *71*(Pt 1), 136–53. doi:10.1107/S1399004714021683

Bulinski, J. C., Richards, J. E., & Piperno, G. (1988). Posttranslational modifications of alpha tubulin: detyrosination and acetylation differentiate populations of interphase microtubules in cultured cells. *The Journal of Cell Biology*, *106*(4), 1213–20.

Burton, P. R. (1984). Luminal material in microtubules of frog olfactory axons: structure and distribution. *The Journal of Cell Biology*, *99*(2), 520–8.

Cai, D., McEwen, D. P., Martens, J. R., Meyhofer, E., & Verhey, K. J. (2009). Single molecule imaging reveals differences in microtubule track selection between Kinesin motors. *PLoS Biology*, *7*(10), e1000216. doi:10.1371/journal.pbio.1000216

Chen, L., Nakamura, M., Schindler, T. D., Parker, D., & Bryant, Z. (2012). Engineering

controllable bidirectional molecular motors based on myosin. *Nature Nanotechnology*, *7*(4), 252–6. doi:10.1038/nnano.2012.19

Choudhary, C., Kumar, C., Gnad, F., Nielsen, M. L., Rehman, M., Walther, T. C., … Mann, M. (2009). Lysine acetylation targets protein complexes and co-regulates major cellular functions. *Science*, *325*(5942), 834–40. doi:10.1126/science.1175371

Chu, C.-W. W., Hou, F., Zhang, J., Phu, L., Loktev, A. V, Kirkpatrick, D. S., … Zou, H. (2011). A novel acetylation of β-tubulin by San modulates microtubule polymerization via down-regulating tubulin incorporation. *Molecular Biology of the Cell*, *22*(4), 448–56. doi:10.1091/mbc.E10-03-0203

Chuong, S. D. X., Good, A. G., Taylor, G. J., Freeman, M. C., Moorhead, G. B. G., & Muench, D. G. (2004). Large-scale identification of tubulin-binding proteins provides insight on subcellular trafficking, metabolic channeling, and signaling in plant cells. *Molecular & Cellular Proteomics*, *3*(10), 970–83. doi:10.1074/mcp.M400053-MCP200

Cochran, J. C., Zhao, Y. C., Wilcox, D. E., & Kull, F. J. (2012). A metal switch for controlling the activity of molecular motor proteins. *Nature Structural & Molecular Biology*, *19*(1), 122–7. doi:10.1038/nsmb.2190

Creppe, C., Malinouskaya, L., Volvert, M.-L., Gillard, M., Close, P., Malaise, O., … Nguyen, L. (2009). Elongator controls the migration and differentiation of cortical neurons through acetylation of alpha-tubulin. *Cell*, *136*(3), 551–64. doi:10.1016/j.cell.2008.11.043

Crosson, S., Rajagopal, S., & Moffat, K. (2003). The LOV domain family: photoresponsive signaling modules coupled to diverse output domains. *Biochemistry*, *42*(1), 2–10. doi:10.1021/bi026978l

Cueva, J. G., Hsin, J., Huang, K. C., & Goodman, M. B. (2012). Posttranslational Acetylation of α-Tubulin Constrains Protofilament Number in Native Microtubules. *Current Biology*, *22*(12), 1066–74. doi:10.1016/j.cub.2012.05.012

Danilchik, M. V, Funk, W. C., Brown, E. E., & Larkin, K. (1998). Requirement for microtubules in new membrane formation during cytokinesis of Xenopus embryos. *Developmental Biology*, *194*(1), 47–60. doi:10.1006/dbio.1997.8815

Davis, A., Sage, C. R., Wilson, L., & Farrell, K. W. (1993). Purification and biochemical characterization of tubulin from the budding yeast Saccharomyces cerevisiae. *Biochemistry*, *32*(34), 8823–8835. doi:10.1021/bi00085a013

De Brabander, M. J., Van de Veire, R. M., Aerts, F. E., Borgers, M., & Janssen, P. A. (1976). The effects of methyl (5-(2-thienylcarbonyl)-1H-benzimidazol-2-yl) carbamate, (R 17934; NSC 238159), a new synthetic antitumoral drug interfering with microtubules, on mammalian cells cultured in vitro. *Cancer Research*, *36*(3), 905–16.

de Forges, H., Bouissou, A., & Perez, F. (2012). Interplay between microtubule dynamics and intracellular organization. *The International Journal of Biochemistry & Cell Biology*, *44*(2), 266–74. doi:10.1016/j.biocel.2011.11.009

Dehmelt, L., & Halpain, S. (2005). The MAP2/Tau family of microtubule-associated proteins. *Genome Biology*, *6*(1), 204. doi:10.1186/gb-2004-6-1-204

des Georges, A., Katsuki, M., Drummond, D. R., Osei, M., Cross, R. A., & Amos, L. A. (2008). Mal3, the Schizosaccharomyces pombe homolog of EB1, changes the microtubule lattice. *Nature Structural & Molecular Biology*, *15*(10), 1102–8. doi:10.1038/nsmb.1482

Desai, A., & Mitchison, T. J. (1997). Microtubule polymerization dynamics. *Annual Review of Cell and Developmental Biology*, *13*, 83–117. doi:10.1146/annurev.cellbio.13.1.83

Díaz, J. F., Barasoain, I., & Andreu, J. M. (2003). Fast kinetics of Taxol binding to microtubules. Effects of solution variables and microtubule-associated proteins. *The Journal of Biological Chemistry*, *278*(10), 8407–19. doi:10.1074/jbc.M211163200

Díaz-Valencia, J. D., Morelli, M. M., Bailey, M., Zhang, D., Sharp, D. J., & Ross, J. L. (2011). Drosophila katanin-60 depolymerizes and severs at microtubule defects. *Biophysical Journal*, *100*(10), 2440–9. doi:10.1016/j.bpj.2011.03.062

DiMaio, F., Song, Y., Li, X., Brunner, M. J., Xu, C., Conticello, V., … Baker, D. (2015). Atomic-accuracy models from 4.5-Å cryo-electron microscopy data with density-guided iterative local refinement. *Nature Methods*, *12*(4). doi:10.1038/nmeth.3286

Dimitrov, A., Quesnoit, M., Moutel, S., Cantaloube, I., Poüs, C., & Perez, F. (2008). Detection of GTP-tubulin conformation in vivo reveals a role for GTP remnants in microtubule rescues. *Science*, *322*(5906), 1353–6. doi:10.1126/science.1165401

Dougherty, C. A., Himes, R. H., Wilson, L., & Farrell, K. W. (1998). Detection of GTP and Pi in wild-type and mutated yeast microtubules: implications for the role of the GTP/GDP-Pi cap in microtubule dynamics. *Biochemistry*, *37*(31), 10861–5. doi:10.1021/bi980677n

Drummond, D. R., Kain, S., Newcombe, A., Hoey, C., Katsuki, M., & Cross, R. A. (2011). Purification of Tubulin from the Fission Yeast Schizosaccharomyces pombe. *Methods in Molecular Biology*, *777*(3), 29–55. doi:10.1007/978-1-61779-252-6_3

Dunn, S., Morrison, E. E., Liverpool, T. B., Molina-París, C., Cross, R. A., Alonso, M. C., & Peckham, M. (2008). Differential trafficking of Kif5c on tyrosinated and detyrosinated microtubules in live cells. *Journal of Cell Science*, *121*(Pt 7), 1085–95. doi:10.1242/jcs.026492

Eddé, B., Rossier, J., Le Caer, J. P., Desbruyères, E., Gros, F., & Denoulet, P. (1990). Posttranslational glutamylation of alpha-tubulin. *Science*, *247*(4938), 83–5.

Egelman, E. H. (2007). The iterative helical real space reconstruction method: surmounting the problems posed by real polymers. *Journal of Structural Biology*, *157*(1), 83–94. doi:10.1016/j.jsb.2006.05.015

Emsley, P., Lohkamp, B., Scott, W. G., & Cowtan, K. (2010). Features and development of Coot. *Acta Crystallographica. Section D, Biological Crystallography*, *66*(Pt 4), 486–501. doi:10.1107/S0907444910007493

Endres, N. F., Yoshioka, C., Milligan, R. A., & Vale, R. D. (2006). A lever-arm rotation drives motility of the minus-end-directed kinesin Ncd. *Nature*, *439*(7078), 875–8. doi:10.1038/nature04320

Fackenthal, J. D., Hutchens, J. a, Turner, F. R., & Raff, E. C. (1995). Structural analysis of mutations in the Drosophila beta 2-tubulin isoform reveals regions in the beta-tubulin

molecular required for general and for tissue-specific microtubule functions. *Genetics*, *139*(1), 267–86.

Felgner, H., Frank, R., & Schliwa, M. (1996). Flexural rigidity of microtubules measured with the use of optical tweezers. *Journal of Cell Science*, *109 (Pt 2*, 509–16.

Filippakopoulos, P., & Knapp, S. (2012). The bromodomain interaction module. *FEBS Letters*, *586*(17), 2692–704. doi:10.1016/j.febslet.2012.04.045

Fink, G., Hajdo, L., Skowronek, K. J., Reuther, C., Kasprzak, A. A., & Diez, S. (2009). The mitotic kinesin-14 Ncd drives directional microtubule-microtubule sliding. *Nature Cell Biology*, *11*(6), 717–23. doi:10.1038/ncb1877

Fourniol, F. J., Li, T. De, Bieling, P., Mullins, R. D., Fletcher, D. A., & Surrey, T. (2014). *Micropattern-guided assembly of overlapping pairs of dynamic microtubules*. *Methods in Enzymology* (1st ed., Vol. 540). Elsevier Inc. doi:10.1016/B978-0-12-397924-7.00019-4

Friedman, J. R., Webster, B. M., Mastronarde, D. N., Verhey, K. J., & Voeltz, G. K. (2010). ER sliding dynamics and ER-mitochondrial contacts occur on acetylated microtubules. *The Journal of Cell Biology*, *190*(3), 363–375. doi:10.1083/jcb.200911024

Friedmann, D. R., Aguilar, A., Fan, J., Nachury, M. V, & Marmorstein, R. (2012). Structure of the α-tubulin acetyltransferase, αTAT1, and implications for tubulin-specific acetylation. *Proceedings of the National Academy of Sciences*, *109*(48), 19655–60. doi:10.1073/pnas.1209357109

Fulvio, S. Di, Azakir, B. A., Therrien, C., & Sinnreich, M. (2011). Dysferlin Interacts with Histone Deacetylase 6 and Increases alpha-Tubulin Acetylation. *PloS One*, *6*(12), e28563. doi:10.1371/journal.pone.0028563

Garvalov, B. K., Zuber, B., Bouchet-Marquis, C., Kudryashev, M., Gruska, M., Beck, M., … Cyrklaff, M. (2006). Luminal particles within cellular microtubules. *The Journal of Cell Biology*, *174*(6), 759–65. doi:10.1083/jcb.200606074

Geahlen, R. L., & Haley, B. E. (1979). Use of a GTP photoaffinity probe to resolve aspects of the mechanism of tubulin polymerization. *The Journal of Biological Chemistry*, *254*(23), 11982–7.

Geyer, E. A., Burns, A., Lalonde, B. A., Ye, X., Piedra, F.-A., Huffaker, T. C., & Rice, L. M. (2015). A mutation uncouples the tubulin conformational and GTPase cycles, revealing allosteric control of microtubule dynamics. *eLife*, *4*(October). doi:10.7554/eLife.10113

Ghaemmaghami, S., Huh, W.-K., Bower, K., Howson, R. W., Belle, a, Dephoure, N., … Weissman, J. S. (2003). Global analysis of protein expression in yeast. *Nature*, *425*(1997), 737–741. doi:10.1038/nature02046\nnature02046 [pii]

Gigant, B., Wang, C., Ravelli, R. B. G., Roussi, F., Steinmetz, M. O., Curmi, P. a, … Knossow, M. (2005). Structural basis for the regulation of tubulin by vinblastine. *Nature*, *435*(7041), 519–22. doi:10.1038/nature03566

Gigant, B., Wang, W., Dreier, B., Jiang, Q., Pecqueur, L., Plückthun, A., … Knossow, M. (2013). Structure of a kinesin-tubulin complex and implications for kinesin motility. *Nature Structural & Molecular Biology*, *20*(8), 1001–7. doi:10.1038/nsmb.2624

Goel, A., & Vogel, V. (2008). Harnessing biological motors to engineer systems for nanoscale transport and assembly. *Nature Nanotechnology*, *3*(8), 465–75. doi:10.1038/nnano.2008.190

Goodman, B. S., Derr, N. D., & Reck-Peterson, S. L. (2012). Engineered, harnessed, and hijacked: synthetic uses for cytoskeletal systems. *Trends in Cell Biology*, *22*(12), 644–52. doi:10.1016/j.tcb.2012.09.005

Goodwin, S. S., & Vale, R. D. (2010). Patronin Regulates the Microtubule Network by Protecting Microtubule Minus Ends. *Cell*, *143*(2), 263–274. doi:10.1016/j.cell.2010.09.022

Goulet, A., Behnke-Parks, W. M., Sindelar, C. V, Major, J., Rosenfeld, S. S., & Moores, C. A. (2012). The structural basis of force generation by the mitotic motor kinesin-5. *The Journal of Biological Chemistry*, *287*(53), 44654–66. doi:10.1074/jbc.M112.404228

Gupta, M. L., Bode, C. J., Georg, G. I., & Himes, R. H. (2003). Understanding tubulin-Taxol interactions: mutations that impart Taxol binding to yeast tubulin. *Proceedings of the National Academy of Sciences*, *100*(11), 6394–7. doi:10.1073/pnas.1131967100

Halpain, S., & Dehmelt, L. (2006). The MAP1 family of microtubule-associated proteins. *Genome Biology*, *7*(6), 224. doi:10.1186/gb-2006-7-6-224

Harper, S. M., Neil, L. C., & Gardner, K. H. (2003). Structural basis of a phototropin light switch. *Science (New York, N.Y.)*, *301*(5639), 1541–4. doi:10.1126/science.1086810

Heusèle, C., & Carlier, M. F. (1981). GTPase activity of the tubulin-colchicine in relation with tubulin-tubulin interactions. *Biochemical and Biophysical Research Communications*, *103*(1), 332–8.

Hiller, G., & Weber, K. (1978). Radioimmunoassay for tubulin: a quantitative comparison of the tubulin content of different established tissue culture cells and tissues. *Cell*, *14*(4), 795–804.

Hirokawa, N., Noda, Y., Tanaka, Y., & Niwa, S. (2009). Kinesin superfamily motor proteins and intracellular transport. *Nature Reviews. Molecular Cell Biology*, *10*(10), 682–96. doi:10.1038/nrm2774

Horio, T., & Murata, T. (2014). The role of dynamic instability in microtubule organization. *Frontiers in Plant Science*, *5*(October), 511. doi:10.3389/fpls.2014.00511

Howard, J., & Hyman, A. a. (2003). Dynamics and mechanics of the microtubule plus end. *Nature*, *422*(6933), 753–8. doi:10.1038/nature01600

Howes, S. C., Alushin, G. M., Shida, T., Nachury, M. V, & Nogales, E. (2014). Effects of tubulin acetylation and tubulin acetyltransferase binding on microtubule structure. *Molecular Biology of the Cell*, *25*(2), 257–66. doi:10.1091/mbc.E13-07-0387

Hubbert, C. C., Guardiola, A., Shao, R., Kawaguchi, Y., Ito, A., Nixon, A., … Yao, T.-P. (2002). HDAC6 is a microtubule-associated deacetylase. *Nature*, *417*(6887), 455–8. doi:10.1038/417455a

Hyman, A. a, Chrétien, D., Arnal, I., & Wade, R. H. (1995). Structural changes accompanying GTP hydrolysis in microtubules: information from a slowly hydrolyzable analogue guanylyl-(alpha,beta)-methylene-diphosphonate. *The Journal of Cell Biology*, *128*(1-2), 117–25.

Ingolia, N. T., Lareau, L. F., & Weissman, J. S. (2011). Ribosome profiling of mouse embryonic

stem cells reveals the complexity and dynamics of mammalian proteomes. *Cell*, *147*(4), 789–802. doi:10.1016/j.cell.2011.10.002

Janke, C., & Bulinski, J. C. (2011). Post-translational regulation of the microtubule cytoskeleton: mechanisms and functions. *Nature Reviews. Molecular Cell Biology*, *12*(12), 773–86. doi:10.1038/nrm3227

Jiang, K., Hua, S., Mohan, R., Grigoriev, I., Yau, K., Liu, Q., … Akhmanova, A. (2014). Microtubule Minus-End Stabilization by Polymerization-Driven CAMSAP Deposition. *Developmental Cell*, *28*(3), 295–309. doi:10.1016/j.devcel.2014.01.001

Jiang, W., Jimenez, G., Wells, N. J., Hope, T. J., Wahl, G. M., Hunter, T., & Fukunaga, R. (1998). PRC1: a human mitotic spindle-associated CDK substrate protein required for cytokinesis. *Molecular Cell*, *2*(6), 877–885. doi:S1097-2765(00)80302-0 [pii]

Johnson, V., Ayaz, P., Huddleston, P., & Rice, L. M. (2011). Design, overexpression, and purification of polymerization-blocked yeast αβ-tubulin mutants. *Biochemistry*, *50*(40), 8636–44. doi:10.1021/bi2005174

Kalebic, N., Martinez, C., Perlas, E., Hublitz, P., Bilbao-Cortes, D., Fiedorczuk, K., … Heppenstall, P. A. (2013). Tubulin acetyltransferase αTAT1 destabilizes microtubules independently of its acetylation activity. *Molecular and Cellular Biology*, *33*(6), 1114–23. doi:10.1128/MCB.01044-12

Kerssemakers, J. W. J., Munteanu, E. L., Laan, L., Noetzel, T. L., Janson, M. E., & Dogterom, M. (2006). Assembly dynamics of microtubules at molecular resolution. *Nature*, *442*(7103), 709–712. doi:10.1038/nature04928

Konishi, K., Uyeda, T. Q. P., & Kubo, T. (2006). Genetic engineering of a Ca(2+) dependent chemical switch into the linear biomotor kinesin. *FEBS Letters*, *580*(15), 3589–94. doi:10.1016/j.febslet.2006.05.037

Konishi, Y., & Setou, M. (2009). Tubulin tyrosination navigates the kinesin-1 motor domain to axons. *Nature Neuroscience*, *12*(5), 559–67. doi:10.1038/nn.2314

Koonce, M. P., & Tikhonenko, I. (2000). Functional elements within the dynein microtubule-binding domain. *Molecular Biology of the Cell*, *11*(2), 523–9.

Kormendi, V., Szyk, A., Piszczek, G., & Roll-Mecak, A. (2012). Crystal structures of tubulin acetyltransferase reveal a conserved catalytic core and the plasticity of the essential N terminus. *The Journal of Biological Chemistry*, *287*(50), 41569–75. doi:10.1074/jbc.C112.421222

Kosetsu, K., de Keijzer, J., Janson, M. E., & Goshima, G. (2013). MICROTUBULE-ASSOCIATED PROTEIN65 is essential for maintenance of phragmoplast bipolarity and formation of the cell plate in Physcomitrella patens. *The Plant Cell*, *25*(11), 4479–92. doi:10.1105/tpc.113.117432

Kumar, P., & Wittmann, T. (2012). +TIPs: SxIPping along microtubule ends. *Trends in Cell Biology*, *22*(8), 418–28. doi:10.1016/j.tcb.2012.05.005

L'Hernault, S. W., & Rosenbaum, J. L. (1983). Chlamydomonas alpha-tubulin is posttranslationally modified in the flagella during flagellar assembly. *The Journal of Cell*

Biology, *97*(1), 258–63.

L'Hernault, S. W., & Rosenbaum, J. L. (1985). Chlamydomonas alpha-tubulin is posttranslationally modified by acetylation on the epsilon-amino group of a lysine. *Biochemistry*, *24*(2), 473–8.

Lakämper, S., & Meyhöfer, E. (2006). Back on track - on the role of the microtubule for kinesin motility and cellular function. *Journal of Muscle Research and Cell Motility*, *27*(2), 161–71. doi:10.1007/s10974-005-9052-3

Lander, G. C., Stagg, S. M., Voss, N. R., Cheng, A., Fellmann, D., Pulokas, J., … Carragher, B. (2009). Appion: an integrated, database-driven pipeline to facilitate EM image processing. *Journal of Structural Biology*, *166*(1), 95–102.

LeDizet, M., & Piperno, G. (1986). Cytoplasmic microtubules containing acetylated alpha-tubulin in Chlamydomonas reinhardtii: spatial arrangement and properties. *The Journal of Cell Biology*, *103*(1), 13–22.

LeDizet, M., & Piperno, G. (1987). Identification of an acetylation site of Chlamydomonas alpha-tubulin. *Proceedings of the National Academy of Sciences*, *84*(16), 5720–4.

Lee, J., Natarajan, M., Nashine, V. C., Socolich, M., Vo, T., Russ, W. P., … Ranganathan, R. (2008). Surface sites for engineering allosteric control in proteins. *Science (New York, N.Y.)*, *322*(5900), 438–42. doi:10.1126/science.1159052

Lee, K.-Y., Esmaeili, B., Zealley, B., & Mishima, M. (2015). Direct interaction between centralspindlin and PRC1 reinforces mechanical resilience of the central spindle. *Nature Communications*, *6*, 7290. doi:10.1038/ncomms8290

Levy, J. R., Sumner, C. J., Caviston, J. P., Tokito, M. K., Ranganathan, S., Ligon, L. A., … Holzbaur, E. L. F. (2006). A motor neuron disease-associated mutation in p150Glued perturbs dynactin function and induces protein aggregation. *The Journal of Cell Biology*, *172*(5), 733–45. doi:10.1083/jcb.200511068

Li, H., DeRosier, D. J., Nicholson, W. V, Nogales, E., & Downing, K. H. (2002). Microtubule structure at 8 A resolution. *Structure*, *10*(10), 1317–28.

Li, W., Zhong, C., Li, L., Sun, B., Wang, W., Xu, S., … Ding, J. (2012). Molecular basis of the acetyltransferase activity of MEC-17 towards α-tubulin. *Cell Research*, *22*(12), 1707–11. doi:10.1038/cr.2012.154

Li, X., Mooney, P., Zheng, S., Booth, C. R., Braunfeld, M. B., Gubbens, S., … Cheng, Y. (2013). Electron counting and beam-induced motion correction enable near-atomic-resolution single-particle cryo-EM. *Nature Methods*, *10*(6), 584–90. doi:10.1038/nmeth.2472

Löwe, J., Li, H., Downing, K. H., & Nogales, E. (2001). Refined structure of alpha beta-tubulin at 3.5 A resolution. *Journal of Molecular Biology*, *313*(5), 1045–57. doi:10.1006/jmbi.2001.5077

Lungu, O. I., Hallett, R. A., Choi, E. J., Aiken, M. J., Hahn, K. M., & Kuhlman, B. (2012). Designing photoswitchable peptides using the AsLOV2 domain. *Chemistry & Biology*, *19*(4), 507–17. doi:10.1016/j.chembiol.2012.02.006

Lyumkis, D., Brilot, A. F., Theobald, D. L., & Grigorieff, N. (2013). Likelihood-based classification of cryo-EM images using FREALIGN. *Journal of Structural Biology*, *183*(3), 377–388. doi:10.1016/j.jsb.2013.07.005

Machin, N. A., Lee, J. M., & Barnes, G. (1995). Microtubule stability in budding yeast: characterization and dosage suppression of a benomyl-dependent tubulin mutant. *Molecular Biology of the Cell*, *6*(9), 1241–59.

Maruta, H., Greer, K., & Rosenbaum, J. L. (1986). The acetylation of alpha-tubulin and its relationship to the assembly and disassembly of microtubules. *The Journal of Cell Biology*, *103*(2), 571–9.

Maurer, S. P., Bieling, P., Cope, J., Hoenger, A., & Surrey, T. (2011). GTPgammaS microtubules mimic the growing microtubule end structure recognized by end-binding proteins (EBs). *Proceedings of the National Academy of Sciences of the United States of America*, *108*(10), 3988–3993. doi:10.1073/pnas.1014758108

Maurer, S. P., Fourniol, F. J., Bohner, G., Moores, C. A., & Surrey, T. (2012). EBs recognize a nucleotide-dependent structural cap at growing microtubule ends. *Cell*, *149*(2), 371–82. doi:10.1016/j.cell.2012.02.049

Meurer-Grob, P., Kasparian, J., & Wade, R. H. (2001). Microtubule structure at improved resolution. *Biochemistry*, *40*(27), 8000–8008. doi:10.1021/bi010343p

Mimori-Kiyosue, Y., Shiina, N., & Tsukita, S. (2000). The dynamic behavior of the APC-binding protein EB1 on the distal ends of microtubules. *Current Biology*, *10*(14), 865–8.

Mindell, J. a., & Grigorieff, N. (2003). Accurate determination of local defocus and specimen tilt in electron microscopy. *Journal of Structural Biology*, *142*, 334–347. doi:10.1016/S1047-8477(03)00069-8

Minoura, I., Hachikubo, Y., Yamakita, Y., Takazaki, H., Ayukawa, R., Uchimura, S., & Muto, E. (2013). Overexpression, purification, and functional analysis of recombinant human tubulin dimer. *FEBS Letters*, *587*(21), 3450–5. doi:10.1016/j.febslet.2013.08.032

Mitchison, T., & Kirschner, M. (1984). Dynamic instability of microtubule growth. *Nature*, *312*(5991), 237–42. doi:10.1038/312237a0

Möglich, A., & Moffat, K. (2010). Engineered photoreceptors as novel optogenetic tools. *Photochemical & Photobiological Sciences*, *9*(10), 1286–300. doi:10.1039/c0pp00167h

Mollinari, C., Kleman, J. P., Jiang, W., Schoehn, G., Hunter, T., & Margolis, R. L. (2002). PRC1 is a microtubule binding and bundling protein essential to maintain the mitotic spindle midzone. *Journal of Cell Biology*, *157*(7), 1175–1186. doi:10.1083/jcb.200111052

Nakamura, M., Chen, L., Howes, S. C., Schindler, T. D., Nogales, E., & Bryant, Z. (2014). Remote control of myosin and kinesin motors using light-activated gearshifting. *Nature Nanotechnology*, *9*(August), 1–5. doi:10.1038/nnano.2014.147

Nakano, A., Kato, H., Watanabe, T., Min, K.-D., Yamazaki, S., Asano, Y., … Takashima, S. (2010). AMPK controls the speed of microtubule polymerization and directional cell migration through CLIP-170 phosphorylation. *Nature Cell Biology*, *12*(6), 583–90. doi:10.1038/ncb2060

Nédélec, F., Surrey, T., & Karsenti, E. (2003). Self-organisation and forces in the microtubule cytoskeleton. *Current Opinion in Cell Biology*, *15*(1), 118–24. doi:10.1016/S0955-0674(02)00014-5

Nogales, E., Medrano, F. J., Diakun, G. P., Mant, G. R., Towns-Andrews, E., & Bordas, J. (1995). The effect of temperature on the structure of vinblastine-induced polymers of purified tubulin: detection of a reversible conformational change. *Journal of Molecular Biology*, *254*(3), 416–30. doi:10.1006/jmbi.1995.0628

Nogales, E., Whittaker, M., Milligan, R. A., & Downing, K. H. (1999). High-resolution model of the microtubule. *Cell*, *96*(1), 79–88.

Nogales, E., Wolf, S. G., & Downing, K. H. (1998). Structure of the alpha beta tubulin dimer by electron crystallography. *Nature*, *391*(6663), 199–203. doi:10.1038/34465

North, B. J., Marshall, B. L., Borra, M. T., Denu, J. M., & Verdin, E. (2003). The human Sir2 ortholog, SIRT2, is an NAD+-dependent tubulin deacetylase. *Molecular Cell*, *11*(2), 437–44. doi:10.1016/S1097-2765(03)00038-8

Odde, D. (1998). Diffusion inside microtubules. *European Biophysics Journal*, *27*(5), 514–20.

Perez, F., Diamantopoulos, G. S., Stalder, R., & Kreis, T. E. (1999). CLIP-170 highlights growing microtubule ends in vivo. *Cell*, *96*(4), 517–27.

Peris, L., Wagenbach, M., Lafanechère, L., Brocard, J., Moore, A. T., Kozielski, F., … Andrieux, A. (2009). Motor-dependent microtubule disassembly driven by tubulin tyrosination. *The Journal of Cell Biology*, *185*(7), 1159–66. doi:10.1083/jcb.200902142

Piperno, G., & Fuller, M. T. (1985). Monoclonal antibodies specific for an acetylated form of alpha-tubulin recognize the antigen in cilia and flagella from a variety of organisms. *The Journal of Cell Biology*, *101*(6), 2085–94.

Piperno, G., LeDizet, M., & Chang, X. J. (1987). Microtubules containing acetylated alpha-tubulin in mammalian cells in culture. *The Journal of Cell Biology*, *104*(2), 289–302.

Portran, D., Zoccoler, M., Gaillard, J., Stoppin-Mellet, V., Neumann, E., Arnal, I., … Vantard, M. (2013). MAP65/Ase1 promote microtubule flexibility. *Molecular Biology of the Cell*, *24*, 1964–73. doi:10.1091/mbc.E13-03-0141

Quinones, G. B., Danowski, B. A., Devaraj, A., Singh, V., & Ligon, L. A. (2011). The posttranslational modification of tubulin undergoes a switch from detyrosination to acetylation as epithelial cells become polarized. *Molecular Biology of the Cell*, *22*(7), 1045–57. doi:10.1091/mbc.E10-06-0519

Redwine, W. B., Hernández-López, R., Zou, S., Huang, J., Reck-Peterson, S. L., & Leschziner, A. E. (2012). Structural basis for microtubule binding and release by dynein. *Science*, *337*(6101), 1532–6. doi:10.1126/science.1224151

Reed, N. A., Cai, D., Blasius, T. L., Jih, G. T., Meyhofer, E., Gaertig, J., & Verhey, K. J. (2006). Microtubule acetylation promotes kinesin-1 binding and transport. *Current Biology*, *16*(21), 2166–72. doi:10.1016/j.cub.2006.09.014

Rice, S., Lin, A. W., Safer, D., Hart, C. L., Naber, N., Carragher, B. O., … Vale, R. D. (1999). A

structural change in the kinesin motor protein that drives motility. *Nature*, *402*(6763), 778–84. doi:10.1038/45483

Sackett, D. L., Werbovetz, K. a, & Morrissette, N. S. (2010). *Isolating tubulin from nonneural sources. Methods in cell biology* (First edit., Vol. 95). Elsevier. doi:10.1016/S0091-679X(10)95002-4

Sakamoto, T., Uezu, A., Kawauchi, S., Kuramoto, T., Makino, K., Umeda, K., … Nakanishi, H. (2008). Mass spectrometric analysis of microtubule co-sedimented proteins from rat brain. *Genes to Cells*, *13*(4), 295–312. doi:10.1111/j.1365-2443.2008.01175.x

Schatz, P. J., Solomon, F., & Botstein, D. (1988). Isolation and characterization of conditional-lethal mutations in the TUB1 alpha-tubulin gene of the yeast Saccharomyces cerevisiae. *Genetics*, *120*(3), 681–95.

Scheffler, K., Minnes, R., Fraisier, V., Paoletti, A., & Tran, P. T. (2015). Microtubule minus end motors kinesin-14 and dynein drive nuclear congression in parallel pathways. *The Journal of Cell Biology*, *209*(1), 47–58. doi:10.1083/jcb.201409087

Schek, H. T., Gardner, M. K., Cheng, J., Odde, D. J., & Hunt, A. J. (2007). Microtubule assembly dynamics at the nanoscale. *Current Biology*, *17*(17), 1445–55. doi:10.1016/j.cub.2007.07.011

Schneider, C. A., Rasband, W. S., & Eliceiri, K. W. (2012). NIH Image to ImageJ: 25 years of image analysis. *Nature Methods*, *9*(7), 671–5. doi:10.1038/nmeth.2089

Schwanhäusser, B., Busse, D., Li, N., Dittmar, G., Schuchhardt, J., Wolf, J., … Selbach, M. (2011). Global quantification of mammalian gene expression control. *Nature*, *473*(7347), 337–42. doi:10.1038/nature10098

Sellers, J. R. (2000). Myosins: a diverse superfamily. *Biochimica et Biophysica Acta*, *1496*(1), 3–22. doi:10.1016/S0167-4889(00)00005-7

Serrador, J. M., Cabrero, J. R., Sancho, D., Mittelbrunn, M., Urzainqui, A., & Sánchez-Madrid, F. (2004). HDAC6 deacetylase activity links the tubulin cytoskeleton with immune synapse organization. *Immunity*, *20*(4), 417–28.

Shang, Z., Zhou, K., Xu, C., Csencsits, R., Cochran, J. C., & Sindelar, C. V. (2014). High-resolution structures of kinesin on microtubules provide a basis for nucleotide-gated force-generation. *eLife*, *3*, 1–27. doi:10.7554/eLife.04686

Shida, T., Cueva, J. G., Xu, Z., Goodman, M. B., & Nachury, M. V. (2010). The major alpha-tubulin K40 acetyltransferase alphaTAT1 promotes rapid ciliogenesis and efficient mechanosensation. *Proceedings of the National Academy of Sciences*, *107*(50), 21517–22. doi:10.1073/pnas.1013728107

Sindelar, C. V., & Downing, K. H. (2007). The beginning of kinesin's force-generating cycle visualized at 9-A resolution. *The Journal of Cell Biology*, *177*(3), 377–85. doi:10.1083/jcb.200612090

Stephens, R. E. (1992). Tubulin in sea urchin embryonic cilia: post-translational modifications during regeneration. *Journal of Cell Science*, *101*, 837–45.

Stoppin-Mellet, V., Fache, V., Portran, D., Martiel, J.-L., & Vantard, M. (2013). MAP65

coordinate microtubule growth during bundle formation. *PloS One*, *8*(2), e56808. doi:10.1371/journal.pone.0056808

Strickland, D., Lin, Y., Wagner, E., Hope, C. M., Zayner, J., Antoniou, C., … Glotzer, M. (2012). TULIPs: tunable, light-controlled interacting protein tags for cell biology. *Nature Methods*, *9*(4), 379–84. doi:10.1038/nmeth.1904

Strickland, D., Moffat, K., & Sosnick, T. R. (2008). Light-activated DNA binding in a designed allosteric protein. *Proceedings of the National Academy of Sciences of the United States of America*, *105*(31), 10709–14. doi:10.1073/pnas.0709610105

Subramanian, R., Ti, S., Tan, L., Darst, S. A., & Kapoor, T. M. (2013). Marking and Measuring Single Microtubules by PRC1 and Kinesin-4.pdf. *Cell*, *154*(2), 377–390. doi:10.1016/j.cell.2013.06.021

Subramanian, R., Wilson-Kubalek, E. M., Arthur, C. P., Bick, M. J., Campbell, E. A., Darst, S. A., … Kapoor, T. M. (2010). Insights into antiparallel microtubule crosslinking by PRC1, a conserved nonmotor microtubule binding protein. *Cell*, *142*(3), 433–443. doi:10.1016/j.cell.2010.07.012

Sudo, H., & Baas, P. W. (2010). Acetylation of microtubules influences their sensitivity to severing by katanin in neurons and fibroblasts. *The Journal of Neuroscience*, *30*(21), 7215–26. doi:10.1523/JNEUROSCI.0048-10.2010

Sui, H., & Downing, K. H. (2010). Structural basis of interprotofilament interaction and lateral deformation of microtubules. *Structure*, *18*(8), 1022–31. doi:10.1016/j.str.2010.05.010

Suloway, C., Pulokas, J., Fellmann, D., Cheng, A., Guerra, F., Quispe, J., … Carragher, B. (2005). Automated molecular microscopy: the new Leginon system. *Journal of Structural Biology*, *151*(1), 41–60. doi:10.1016/j.jsb.2005.03.010

Szyk, A., Deaconescu, A. M., Spector, J., Goodman, B., Valenstein, M. L., Ziolkowska, N. E., … Roll-Mecak, A. (2014). Molecular basis for age-dependent microtubule acetylation by tubulin acetyltransferase. *Cell*, *157*(6), 1405–1415. doi:10.1016/j.cell.2014.03.061

Tan, D., Asenjo, A. B., Mennella, V., Sharp, D. J., & Sosa, H. (2006). Kinesin-13s form rings around microtubules. *The Journal of Cell Biology*, *175*(1), 25–31. doi:10.1083/jcb.200605194

Tang, G., Peng, L., Baldwin, P. R., Mann, D. S., Jiang, W., Rees, I., & Ludtke, S. J. (2007). EMAN2: an extensible image processing suite for electron microscopy. *Journal of Structural Biology*, *157*(1), 38–46. doi:10.1016/j.jsb.2006.05.009

Taschner, M., Vetter, M., & Lorentzen, E. (2012). Atomic resolution structure of human α-tubulin acetyltransferase bound to acetyl-CoA. *Proceedings of the National Academy of Sciences*, *109*(48), 19649–54. doi:10.1073/pnas.1209343109

Thomas, J. H., Neff, N. F., & Botstein, D. (1985). Isolation and characterization of mutations in the beta-tubulin gene of Saccharomyces cerevisiae. *Genetics*, *111*(4), 715–34.

Thyberg, J., & Moskalewski, S. (1993). Relationship between the Golgi complex and microtubules enriched in detyrosinated or acetylated alpha-tubulin: studies on cells recovering from nocodazole and cells in the terminal phase of cytokinesis. *Cell and Tissue Research*, *273*(3),

457–66.

Toettcher, J. E., Voigt, C. A., Weiner, O. D., & Lim, W. A. (2011). The promise of optogenetics in cell biology: interrogating molecular circuits in space and time. *Nature Methods*, *8*(1), 35–8. doi:10.1038/nmeth.f.326

Tomishige, M., & Vale, R. D. (2000). Controlling kinesin by reversible disulfide cross-linking. Identifying the motility-producing conformational change. *The Journal of Cell Biology*, *151*(5), 1081–92. doi:10.1083/jcb.151.5.1081

Topalidou, I., Keller, C., Kalebic, N., Nguyen, K. C. Q., Somhegyi, H., Politi, K. A., … Chalfie, M. (2012). Genetically separable functions of the MEC-17 tubulin acetyltransferase affect microtubule organization. *Current Biology*, *22*(12), 1057–65. doi:10.1016/j.cub.2012.03.066

Uchimura, S., Fujii, T., Takazaki, H., Ayukawa, R., Nishikawa, Y., Minoura, I., … Muto, E. (2015). A flipped ion pair at the dynein-microtubule interface is critical for dynein motility and ATPase activation. *The Journal of Cell Biology*, *208*(2), 211–22. doi:10.1083/jcb.201407039

Uchimura, S., Oguchi, Y., Hachikubo, Y., Ishiwata, S., & Muto, E. (2010). Key residues on microtubule responsible for activation of kinesin ATPase. *The EMBO Journal*, *29*(7), 1167–75. doi:10.1038/emboj.2010.25

Vale, R. D. (2003). The molecular motor toolbox for intracellular transport. *Cell*, *112*(4), 467–80. doi:10.1016/S0092-8674(03)00111-9

van Heel, M., Harauz, G., Orlova, E. V, Schmidt, R., & Schatz, M. (1996). A new generation of the IMAGIC image processing system. *Journal of Structural Biology*, *116*(1), 17–24. doi:10.1006/jsbi.1996.0004

Wade, R. H., Chrétien, D., & Job, D. (1990). Characterization of microtubule protofilament numbers. How does the surface lattice accommodate? *Journal of Molecular Biology*, *212*(4), 775–86. doi:10.1016/0022-2836(90)90236-F

Walczak, C. E., & Heald, R. (2008). Mechanisms of mitotic spindle assembly and function. *International Review of Cytology*, *265*(07), 111–58. doi:10.1016/S0074-7696(07)65003-7

Wang, C., Cormier, A., Gigant, B., & Knossow, M. (2007). Insight into the GTPase activity of tubulin from complexes with stathmin-like domains. *Biochemistry*, *46*, 10595–10602. doi:10.1021/bi701147f

Ward, J. J., Roque, H., Antony, C., & Nédélec, F. (2014). Mechanical design principles of a mitotic spindle. *eLife*, *3*, e03398. doi:10.7554/eLife.03398

Wendt, T. G., Volkmann, N., Skiniotis, G., Goldie, K. N., Müller, J., Mandelkow, E., & Hoenger, A. (2002). Microscopic evidence for a minus-end-directed power stroke in the kinesin motor ncd. *The EMBO Journal*, *21*(22), 5969–78. doi:10.1093/emboj/cdf622

Widlund, P. O., Podolski, M., Reber, S., Alper, J., Storch, M., Hyman, A. a, … Drechsel, D. N. (2012). One-step purification of assembly competent tubulin from diverse eukaryotic sources. *Molecular Biology of the Cell*, *23*, 4393–4401. doi:10.1091/mbc.E12-06-0444

Wilson-Kubalek, E. M., Cheeseman, I. M., Yoshioka, C., Desai, A., & Milligan, R. A. (2008).

Orientation and structure of the Ndc80 complex on the microtubule lattice. *The Journal of Cell Biology*, *182*(6), 1055–61. doi:10.1083/jcb.200804170

Wu, Y. I., Frey, D., Lungu, O. I., Jaehrig, A., Schlichting, I., Kuhlman, B., & Hahn, K. M. (2009). A genetically encoded photoactivatable Rac controls the motility of living cells. *Nature*, *461*(7260), 104–8. doi:10.1038/nature08241

Yun, M., Bronner, C. E., Park, C.-G., Cha, S.-S., Park, H.-W., & Endow, S. A. (2003). Rotation of the stalk/neck and one head in a new crystal structure of the kinesin motor protein, Ncd. *The EMBO Journal*, *22*(20), 5382–9. doi:10.1093/emboj/cdg531

Zhang, R., Alushin, G. M., Brown, A., & Nogales, E. (2015). Mechanistic Origin of Microtubule Dynamic Instability and Its Modulation by EB Proteins. *Cell*, *162*(4), 849–59. doi:10.1016/j.cell.2015.07.012

Zhang, R., & Nogales, E. (2015). A new protocol to accurately determine microtubule lattice seam location. *Journal of Structural Biology*. doi:10.1016/j.jsb.2015.09.015